

J. L. Arsuaga,
I. Martínez, A. Gracia
& C. Lorenzo

*Departamento de Paleontología, U.A. de
Paleoantropología UCM-CSIC,
Instituto de Geología Económica
UCM-CSIC; Facultad de Ciencias
Geológicas, Universidad Complutense de
Madrid, Ciudad Universitaria,
28040 Madrid, Spain*

Received 16 April 1996
Revision received 11 October
1996 and accepted 19 January
1997

Keywords: Sima de los Huesos,
Atapuerca, Middle Pleistocene,
morphometrics, crania.

The Sima de los Huesos crania (Sierra de Atapuerca, Spain). A comparative study

The Sima de los Huesos (Sierra de Atapuerca) cranial remains found up to and including the 1995 field season are described and compared with other fossils in order to assess their evolutionary relationships. The phenetic affinities of the Sima de los Huesos crania and a large sample of *Homo* fossils are investigated through principal component analyses. Metrical comparisons of the Sima de los Huesos and other European and African Middle Pleistocene fossils with Neandertals are performed using Z-scores relative to the Neandertal sample statistics. The most relevant cranial traits are metrically and morphologically analyzed and cladistically evaluated. The Sima de los Huesos crania exhibit a number of primitive traits lost in Upper Pleistocene Neandertals (especially in the braincase, but also in the facial skeleton), as well as other traits that are transitional to the Neandertal morphology (particularly in the occipital bone), and features close to what is found in Neandertals (as the supraorbital morphology and midfacial prognathism). Different combinations of primitive and derived traits (shared with Neandertals) are also displayed by the other European Middle Pleistocene fossils. In conclusion, the Sima de los Huesos sample is evolutionarily related to Neandertals as well as to the other European Middle Pleistocene fossils. In our opinion, all the European Middle Pleistocene fossils belong to the Neandertal lineage, and none can be included in an Afro-European common ancestor of Neandertals and modern humans.

© 1997 Academic Press Limited

Journal of Human Evolution (1997) **33**, 219–281

Antecedents and inventory

The first cranial remains were discovered in the Sima de los Huesos (Pit of the Bones) of the Cueva Mayor (Sierra de Atapuerca, Burgos, Spain) in 1976, and consisted of the parietal fragments AT-17 and AT-18 (Aguirre *et al.*, 1976; Aguirre & Lumley, 1977). More cranial remains were found in the 1984 field season and subsequent campaigns. An inventory comprising all the fossils recovered up to and including the 1986 season was published by Aguirre *et al.* (1986), a new one by Aguirre & Bermúdez de Castro (1991), and an updated inventory up to and including the 1989 field season by Aguirre *et al.* (1991). Studies on the first (and still very fragmentary) cranial fossils were accomplished by Martínez & Arsuaga (1985, 1987) and Aguirre *et al.* (1989). An extensive article with detailed descriptions of cranial material (and long bones) found up to and including the 1988 campaign was published by Arsuaga *et al.* (1991). Three well-preserved crania were discovered in the 1992 field season, and preliminarily described and evaluated (together with the rest of the cranial sample and postcranial remains) in Arsuaga (1993) and Arsuaga *et al.* (1993, 1995).

A sample of human and bear bones from Sima de los Huesos has been directly dated by Bischoff *et al.* (1997) by U-series and ESR, indicating a minimum age of about 200 ka and a probable age of >300 ka for the human fossils. These dates are compatible with the faunal content of the site, in terms of large mammals (García *et al.*, 1997) and micromammals (Cuenca-Bescós *et al.*, 1997).

In the present article we will study only the best preserved (more complete) Sima de los Huesos cranial remains found up to and including the 1995 campaign.

Skulls

We use the term “cranium” when significant parts of a calvaria (including different bones) are represented (with or without face).

Cranium 1. (AT-40, AT-63a–b, AT-65, AT-86, AT-122, AT-177a–e, AT-206, AT-216, AT-223, AT-472, AT-937) [Figure 1(a)]. This adult specimen consists of a large portion of occipital bone preserving most of the occipital plane with both lambdoidal borders, a segment of the nuchal torus and parts of the nuchal plane plus the posterior inferior quadrant of a right parietal bone and two small fragments that complete the parietal side of the right lambdoidal border plus a large fragment of the right temporal bone (petromastoid region and tympanic plate). This skull includes Occipital III, described as an isolated cranial bone in [Arsuaga *et al.* \(1991\)](#).

Cranium 2. (AT-18, AT-33a–c, AT-36, AT-61, AT-66a–b, AT-76, AT-105, AT-106a–b, AT-126, AT-132, AT-211, AT-215, AT-225, AT-1621) [Figure 1(b)]. An incomplete calvarium of an adult individual, composed of seven fragments representing most of a left parietal bone articulated with a fragment of frontal bone and a very small fragment of right parietal bone plus a large rhomboidal lambdatic bone plus eight fragments of an occipital bone, with the left lambdoidal suture completely preserved, as well as the occipitomastoid border. Parietal II and Occipital I, described as isolated cranial bones in [Arsuaga *et al.* \(1991\)](#), belong to this skull.

Cranium 3. (AT-188a–c, AT-441, AT-444, AT-452, AT-573a–b, AT-582, AT-627, AT-773, AT-774, AT-775, AT-1177, AT-1190, AT-1596) [Figures 1(c) and (d)]. A juvenile calvarium, preserving most of the parietal arch plus both lateral sides of the frontal bone lacking the central region plus most of the right side of the occipital bone. Based on the supraorbital torus and occipital bone morphology, this specimen is considered adolescent (see below). In this paper adolescence is defined as post-M2 emergence and pre-M3 emergence. The beginning of adulthood is defined by the third molar emergence, although complete fusion of all skeletal epiphyses is not yet completed at this time ([Smith, 1993](#)).

Cranium 4. (AT-600) [Figures 2 and 3]. A complete adult calvarium, only lacking a small part of the glabellar region. The cranial capacity of this specimen has been measured three times using millet seed, giving a figure of 1390 cc (± 10 cc). Given its large dimensions in calvaria and cranial base, this individual is very likely a male.

Cranium 5. (AT-700) [Figures 4 and 5]. A complete adult cranium, articulated with mandible AT-888+AT-721. It corresponds to the individual dentition XXI ([Bermúdez de Castro & Nicolás, 1997](#)). The cranial capacity was measured as for Cranium 4, yielding a value of 1125 cc (± 10 cc). Braincase dimensions are substantially smaller than in Cranium 4. When calvarial and cranial base measures are compared with other Middle Pleistocene fossils or to Neandertals, Cranium 5 appears as a small male or a female (see below), but on the other hand the facial skeleton and mandible are quite large. [Rosas \(1997\)](#) assigns the mandible to a male. In this specimen tooth sizes are not conclusive for sex diagnosis ([Bermúdez de Castro, 1995](#); [Bermúdez de Castro & Nicolás, 1997](#)). Cranium 5 age at death has been estimated between 30–40 years by [Bermúdez de Castro & Nicolás \(1997\)](#) based on tooth wear. Although cranial



Figure 1. (a) Atapuerca SH Cranium 1. (b) Atapuerca SH Cranium 2. (c) and (d) Atapuerca SH Cranium 3. Scale bar represents 2 cm.



Figure 2. Atapuerca SH Cranium 4. In posterior view, the cranial side walls are convergent upwards. Note also the sagittal keeling. Scale bar represents 2 cm.

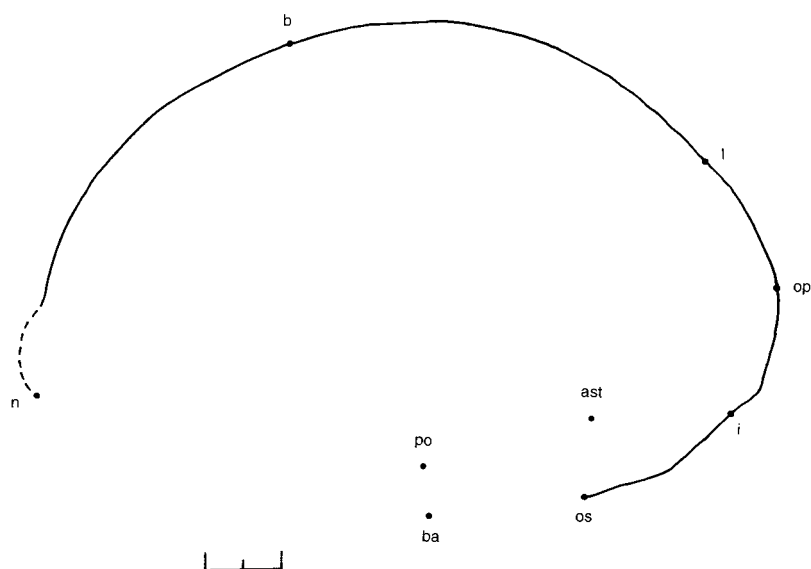


Figure 3. Sagittal profile of Atapuerca SH Cranium 4. This profile was drawn with the dioptograph and later checked with sagittal tomographic images. Scale bar represents 2 cm.

suture closure is not a satisfactory age indicator (Bocquet-Appel & Masset, 1995), it is interesting to note that in Cranium 5 the coronal, sagittal and lambdoidal sutures are open (in fact, the braincase was found disarticulated) whereas in Cranium 4 the process of exocranial suture closure is advanced.

Cranium 6. (AT-405, AT-412, AT-418, AT-419, AT-426, AT-450, AT-572, AT-581, AT-584a–c, AT-622, AT-623, AT-631, AT-633, AT-634, AT-637, AT-640, AT-642, AT-733, AT-734, AT-735, AT-736, AT-737, AT-739, AT-781, AT-925, AT-929, AT-1164) (Figures 6 and 7). Most of the cranium of a male individual based on dental evidence (Bermúdez de Castro & Nicolás, 1997). Based on standards for modern humans this individual would be around 14 years old (Bermúdez de Castro & Nicolás, 1997). Since this cranium represents a well-preserved specimen with dentition, it can be used to ascertain the developmental stage of other, more fragmentary, cranial remains. Individual dentition XX (Bermúdez de Castro & Nicolás, 1997).

Cranium 7. (AT-240, AT-242, AT-244, AT-245, AT-786, AT-804, AT-1541, AT-1542, AT-1546) [Figures 8(a) and (e)]. Composed of most of a right parietal bone (lacking the sagittal and bregmatic regions), connected through a large lambdoidal extra-sutural bone to a small fragment of the left parietal bone, and to four fragments of the occipital bone, preserving the left lambdoidal and occipito-mastoid sutures, as well as a large portion of the occipital plane. The complete left temporal bone is also preserved, and it is articulated with the occipital bone, as well as with the antero-inferior corner of the left parietal bone. Based on the state of development of the temporal bone (Martínez & Arsuaga, 1997) and on the occipital bone morphology (see below) this specimen is considered adolescent.

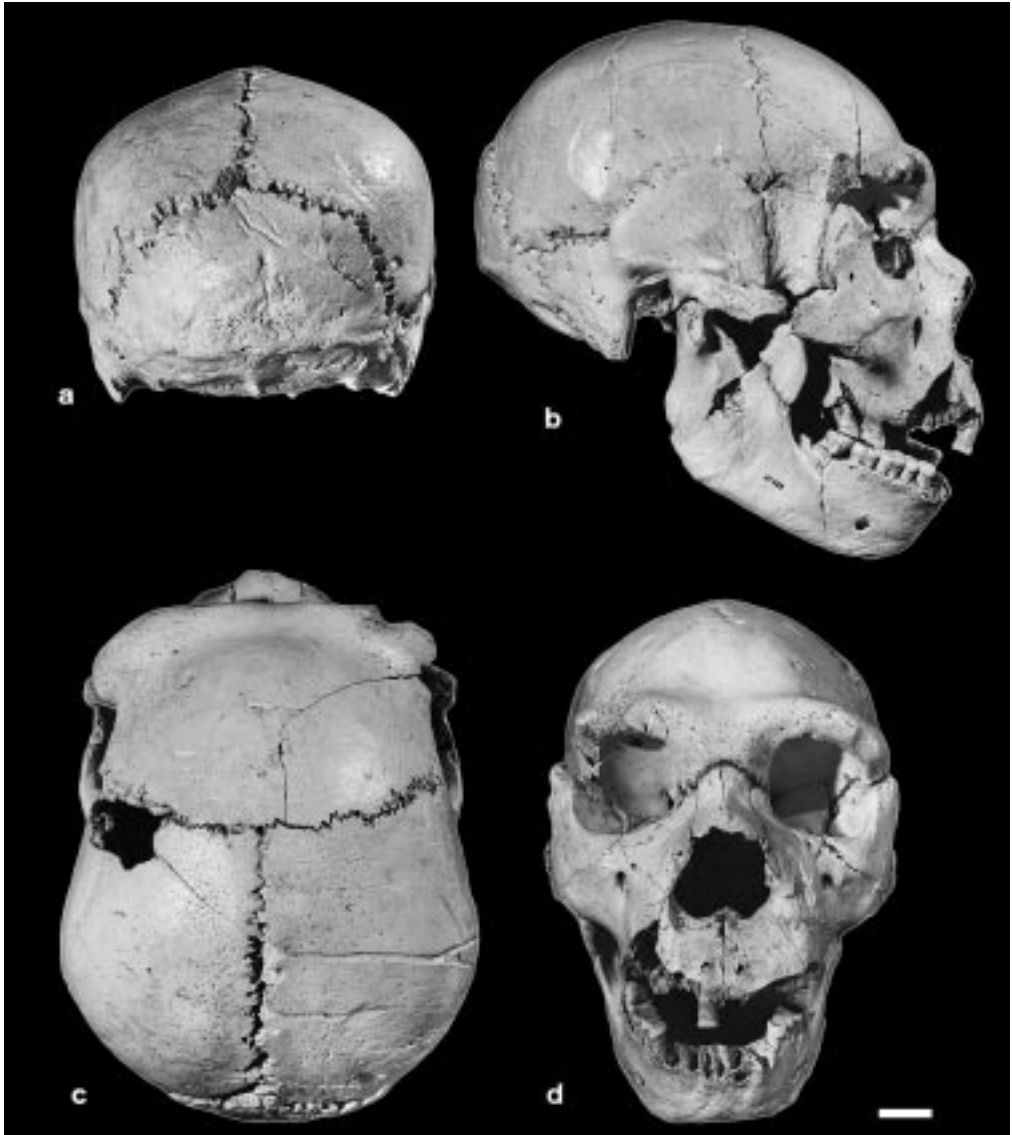


Figure 4. Atapuerca SH Cranium 5. The cranial side walls are vertical in rear view. Scale bar represents 2 cm.

Cranium 8. (AT-17a-c, AT-31a-b, AT-32a-b, AT-130, AT-173a-b, AT-433, AT-568, AT-569, AT-724, AT-1543, AT-1547, AT-1548, AT-1549, AT-1551, AT-1552, AT-1613, AT-1615) [Figures 8(c) and (d)]. Most of a left parietal bone of an adult specimen, with articulated fragments of frontal bone, right parietal bone and two lambdoidal ossicles plus most of the petrous, tympanic and mastoid regions of a left temporal bone. Parietal I, described as an isolated cranial bone in *Arsuaga et al.* (1991), belongs to this skull.

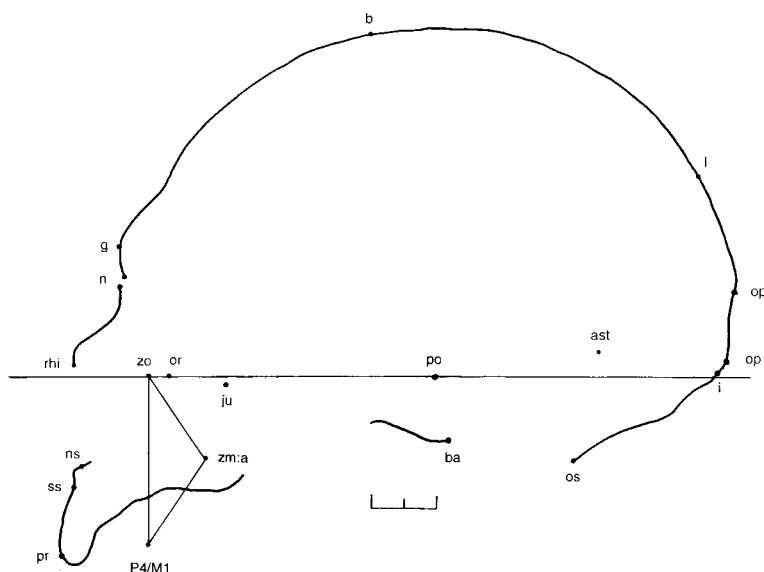


Figure 5. Sagittal profile of Atapuerca SH Cranium 5. This profile was drawn with the dioptograph and later checked with sagittal tomographic images. In the reconstruction of the cranium, the frontal and nasal sides of the nasofrontal suture are slightly apart at nasion. Opisthocranium can be located in two different positions on the occipital bone, both equidistant from glabella. Zygoorbitale, zygomaxillare anterior and the P4/M1 septum are connected by lines to indicate their relative positions. Martin's definition of inion was used (Martin & Saller, 1957; Hublin, 1978a). Scale bar represents 2 cm.

Cranium 9. (AT-621, AT-779, AT-782, AT-1158) [Figure 8(b)]. This set consists of the posterior superior quadrant of a right parietal bone, with lambda and segments of sagittal and lambdoidal borders, a rhomboidal lambdatic bone and a large part of the occipital plane, mostly of the right side. This specimen seems to be adolescent, according to the occipital morphology (see below).

Parietal bones

AT-619+AT-778 [Figure 9(a)]. Central part of a right adult parietal bone, with lambdoidal and coronal sutures missing.

AT-785+AT-803+AT-1196 [Figure 9(b)]. A right juvenile parietal bone almost complete, only lacking bregma.

Occipital bones

Occipital II. (AT-45a-b, AT-56, AT-181, AT-201a-c, AT-202a-c, AT-725) [Figure 9(c)]. Both lambdoidal borders are complete, as well as the right occipitomastoid suture and a segment of the left one, but a portion of the central part of the occipital plane and most of the nuchal plane are lacking. It corresponds to an adult individual.

Occipital IV. (AT-361a-b, AT-493) [Figure 9(d)]. Most of the squamous portion of an occipital bone, lacking the right asterionic region and a segment of the left lambdoidal suture. This specimen looks juvenile, and probably belongs to a late adolescent.

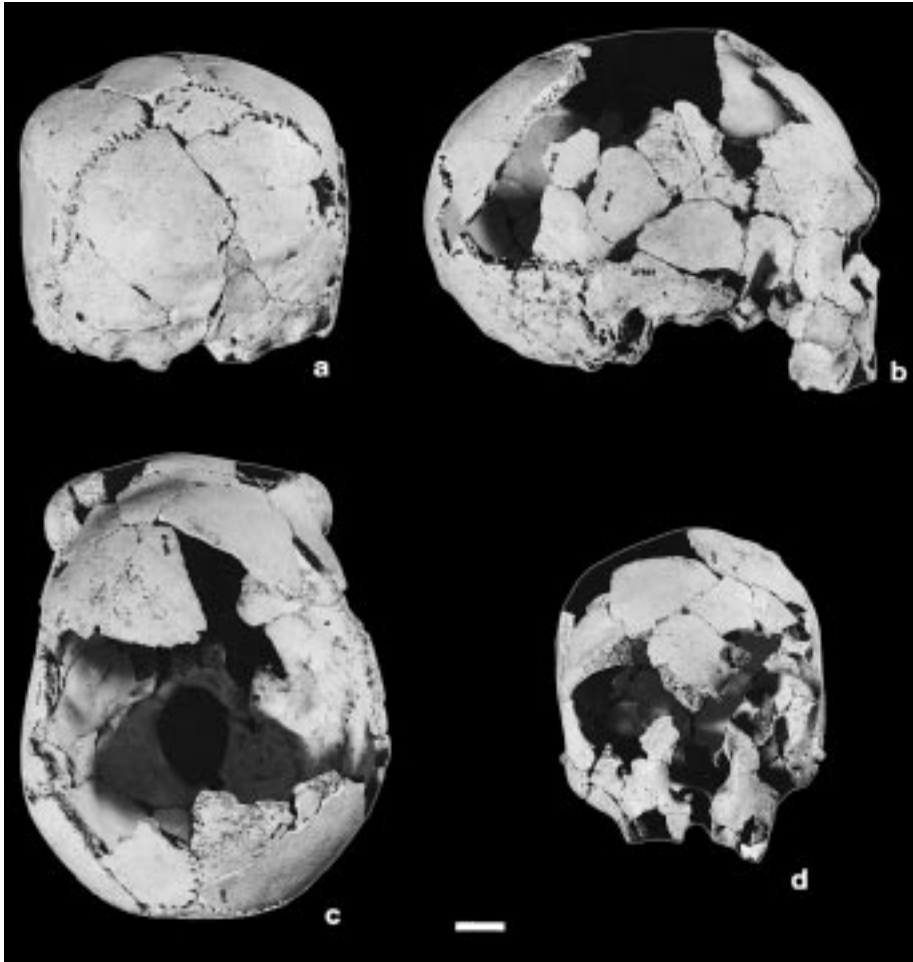


Figure 6. Atapuerca SH cranium 6. Note the oval area of irregular surface above the occipital torus. Scale bar represents 2 cm.

AT-39+AT-224+AT-1594+AT-1662. These four fragments of an adult occipital bone preserve the right side of the occipital torus as well as the asterion and the temporo-occipital border.

AT-1600. A fragment of an adult occipital bone with the right asterion and the right occipito-mastoid suture, articulated with a small fragment of the adjacent right temporal bone.

Temporal bones

In the Sima de los Huesos collection there are 19 isolated temporal bone remains. Three of them are very complete (*AT-84*, *AT-643* and *AT-644*). The Sima de los Huesos temporal bones are studied in greater detail in a separate paper ([Martínez & Arsuaga, 1997](#)).

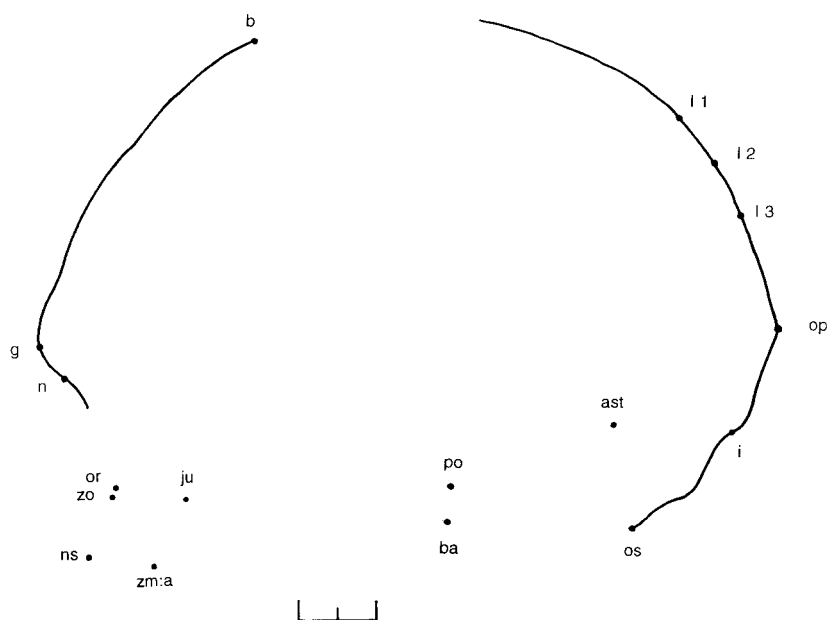


Figure 7. Sagittal profile of Atapuerca SH Cranium 6. This profile was drawn with the diptograph. Nasospinale (ns) and orbitale (or) are approximated. Since there is a large lambdatic bone, lambda 1 corresponds to the upper point of the lambdatic bone, lambda 3 corresponds to the lower point and lambda 2 is placed inside the bregmatic bone, following Howells' (1973) technique. Scale bar represents 2 cm.

Frontal bones

AT-200 [Figure 10(e)]. This adult frontal fragment is preserved from approximately the right midorbit position past the midline, including a portion of the nasofrontal region plus a small part of the adjacent central squama.

AT-237+AT-499+AT-1155+AT-1156 [Figure 10(c)]. Three fragments of an adult frontal bone representing most of a supraorbital torus lacking the lateral half of the right side. A big portion of left and central squama is also preserved. The apophysis crista galli (AT-237) was found separately, in a different campaign.

AT-400+AT-1050 [Figure 10(d)]. A very complete adult supraorbital torus only lacking small portions of bone exo- and endocranially in the medial region of the left orbit. Most of the right side of the squama is also preserved.

AT-620+AT-783. Corresponds to a big portion of a right frontal squama preserving the coronal border from the right temporal line past to the midline.

AT-630+AT-777+AT-1168+AT-1550 [Figure 10(b)]. This set consists of the complete right supraorbital torus and glabellar region from the frontomalar suture to left dacryon plus a large portion of the right and central squama plus a big fragment of the right greater wing and pterygoid process of the sphenoid. It corresponds to an adult individual. AT-1550, an isolated



Figure 8. (a) and (e) Atapuerca SH Cranium 7. (b) Atapuerca SH Cranium 9. (c) and (d) Atapuerca SH Cranium 8. Scale bar represents 2 cm.

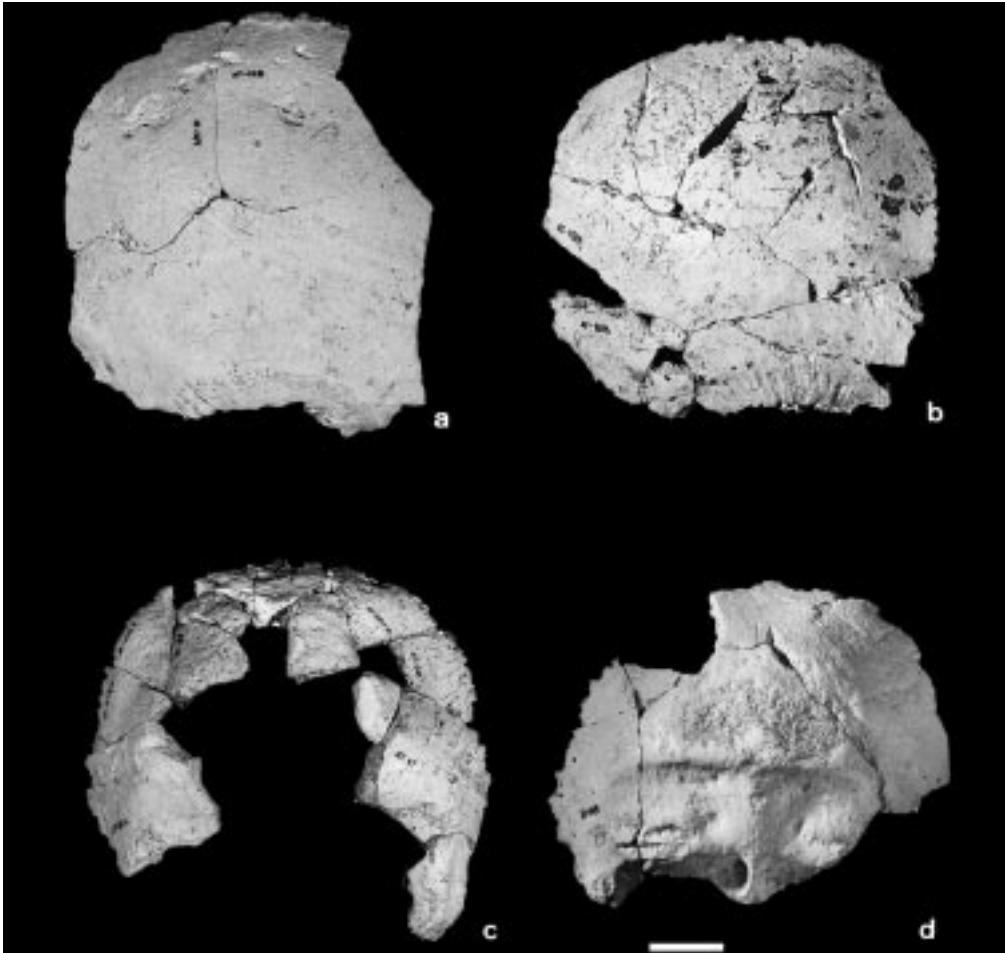


Figure 9. (a) AT-619+AT-778. (b) AT-785+AT-803+AT-1196. (c) Atapuerca SH Occipital II. (d) Atapuerca SH Occipital IV. Note the absence of an occipital crest between the superior and inferior nuchal lines and the very separated attachments of the semispinalis capitis muscles. Scale bar represents 2 cm.

large fragment of a frontal bone left side is associated with this set based on morphological and metrical criteria.

Zygomatic bones

AT-628. This fossil represents an adult left zygomatic bone lacking the temporal process.

AT-711. Frontal process of an adult right zygomatic bone with part of the maxillary process.

AT-768. Left zygomatic bone of a juvenile specimen, lacking the temporal process and attached to a small portion of the left maxilla.

AT-1170. Similar region than in AT-768 but on the right side. Probably corresponds to the same individual than AT-768.

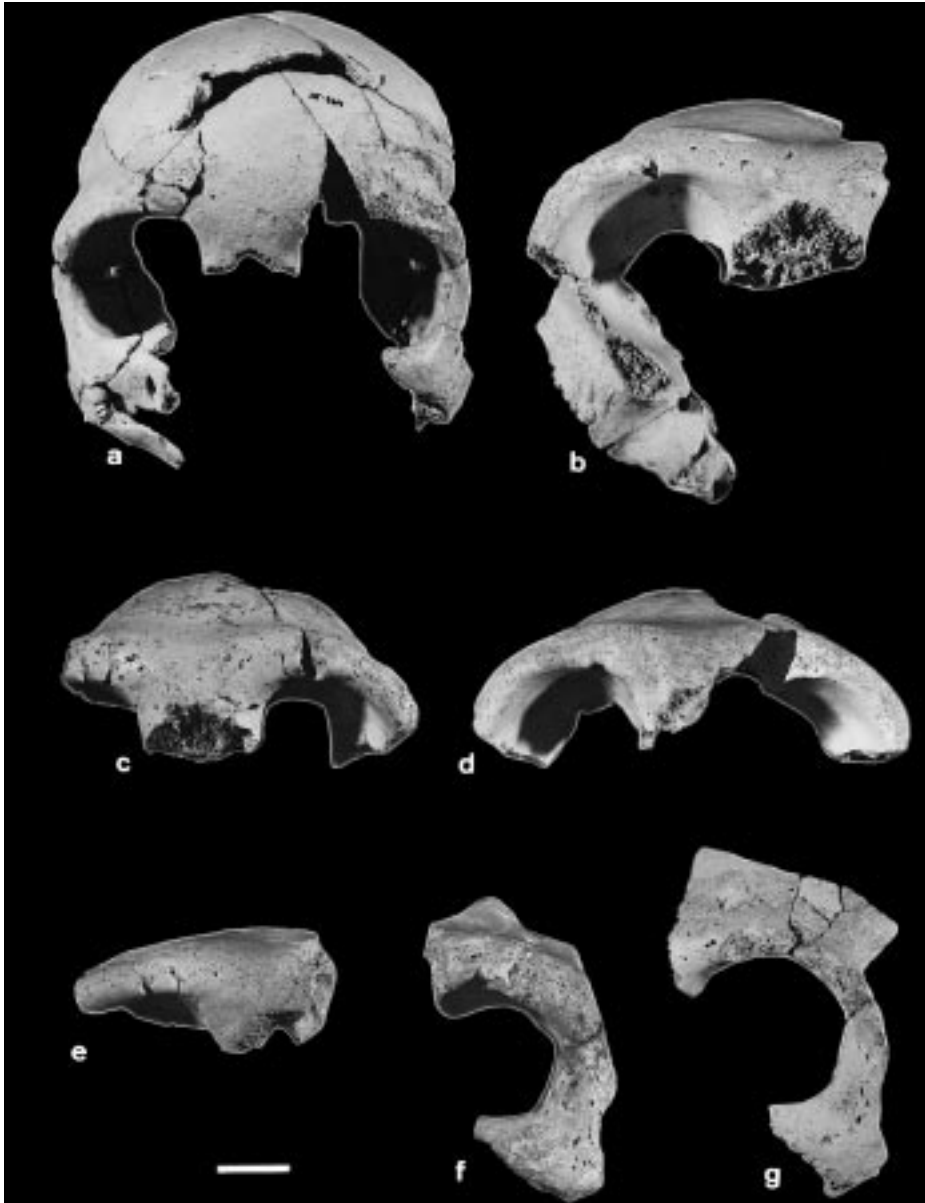


Figure 10. (a) AT-465+AT-624+AT-764+AT-765+AT-766+AT-1159. (b) AT-630+AT-777+AT-1168+AT-1550. (c) AT-237+AT-499+AT-1155+AT-1156. (d) AT-400+AT-1050. (e) AT-200. (f) AT-121+AT-1545. (g) AT-626+AT-1150. Scale bar represents 2 cm.

AT-931. Left frontal process of an adult zygomatic bone.

Maxillae

AT-638+AT-772 [Figure 11(f)]. Right maxilla preserving the alveolar process from the canine to the third molar plus the maxillary body adjacent to the margin of the nasal aperture. It fits



Figure 11. (a) AT-629. (b) AT-404. (c) and (e) AT-767+AT-963. (d) AT-1100+AT-1111+AT-1197+AT-1198. (f) AT-638+AT-772. Scale bar represents 2 cm.

with AT-792 mandible and belongs to individual dentition XXVII. Based on dental and mandibular evidence [Bermúdez de Castro \(1995\)](#) and [Bermúdez de Castro & Nicolás \(1997\)](#) sex this adult individual as a male.

AT-780. A fragmentary palate preserving some alveoli.

AT-1130. Small fragment of right maxillary alveolar process extending from M1 to M3. It corresponds to individual dentition V (an adult individual; [Bermúdez de Castro & Nicolás, 1997](#)).

Faces

AT-121+AT-1545 [Figure 10(f)]. A left supraorbital torus comprising from a point short of the midorbit to the frontomalar suture, articulated to the frontal process of the left zygomatic bone with part of the maxillary process. It corresponds to an adult individual.

AT-404 [Figure 11(b)]. An almost complete adult left zygomatic bone, lacking a small part of the temporal process plus part of the left maxilla including the infraorbital foramen and the canine fossa region.

AT-465+AT-624+AT-764+AT-765+AT-766+AT-1159 [Figure 10(a)]. Most of a juvenile face preserving the whole frontal bone except for a small fragment of the left superior orbital border plus both pterionic regions of the sphenoid greater wings plus both zygomatic bones only lacking the left temporal process plus a small part of the right maxilla including the infraorbital foramen and zygomaticoalveolar margin. Using supraorbital torus development as a criterion (see below), this individual seems to be a late child or an early adolescent. Childhood is defined here as post-M1 emergence and pre-M2 emergence (Smith, 1993).

AT-626+AT-1150 [Figure 10(g)]. A complete left supraorbital torus preserving 11 mm of frontal squama plus the complete left zygomatic bone except for the temporal process. Based on supraorbital torus development (see below), this individual could be a child.

AT-629 [Figure 11(a)]. A complete right zygomatic bone plus parts of the right maxilla including the inferior orbital border, the frontal process and a small fragment that preserves the masseter insertion on the zygomaxillary border. It corresponds to an adult individual.

AT-767+AT-963 [Figures 11(c) and (e)]. A very complete left maxilla lacking a great portion of the zygomatic process and the frontal process plus the right maxillary palatine process and anterior part of the alveolar process plus both palatine horizontal plates and pterygoid processes. Based on the state of dental maturation its age at death would be around 14 years (Bermúdez de Castro, pers. comm.).

AT-1100+AT-1111+AT-1197+AT-1198 [Figure 11(d)]. This set comprises the right alveolar process of maxilla extending from the midline to M1, the complete right margin of the nasal aperture and the right frontal process plus the superior half of the left nasal bone plus the left maxilla, lacking most of the zygomatic process. Bermúdez de Castro (pers. comm.) estimates the age at death of this individual at 16–18 years because, based on the alveolus, the left last molar (missing) of this individual could be starting to emerge (i.e., cutting the gingiva; as in the other Atapuerca SH fossils, age at death is calculated according to dental aging standards for modern humans). It is likely that this fossil fits with mandible AT-607 (individual dentition XXIII) sexed as female by Bermúdez de Castro (1995) and Bermúdez de Castro & Nicolás (1997) and as a male by Rosas (1995, 1997).

Besides the above-mentioned fossils, many fragments of a probably very complete facial skeleton (with M3 erupted) were found in 1995 (AT-1625+AT-1626+AT-1627+AT-1628+AT-1629+AT-1630+AT-1631+AT-1632+AT-1633+AT-1634+AT-1635). This specimen is currently under restoration and is not included in the present study.

Table 1 Craniometric variables of the Sima de los Huesos crania

	NEUROCRANIAL VARIABLES									
	Cr.1	Cr.2	Cr.3	Cr.4	Cr.5	Cr.6	Cr.7	Cr.8	Occ.II	Occ.IV
1. GOL. Maximum cranial length	—	—	—	(201)	185	186	—	—	—	—
1d. NOL. Nasio-occipital length	—	—	—	199	185	181	—	—	—	—
5. BNL. Basion-Nasion length	—	—	—	108.6	109	104	—	—	—	—
7. Foramen magnum length	—	—	—	42	38	44	—	—	—	—
8. XCB. Maximum cranial breadth	—	—	—	164	146	136	—	—	—	—
9. Minimum frontal breadth	—	—	102.1	117	105.7	100	—	—	—	—
10. XFB. Maximum frontal breadth	—	—	115	126	(118.5)	—	—	—	—	—
10b. STB. Bistephanic breadth	—	—	113.5	119.5	(110.8)	(116)	—	—	—	—
11. Biauricular breadth	—	—	—	155.5	139	122	—	—	—	—
11(1). Interporial breadth	—	—	—	134	120	106.5	—	—	—	—
12. ASB. Basterionic breadth	120	((136))	113.5	132	116.5	117.6	112	((441))	112.6	((112.5))
17. BBH. Basion-bregma height	—	—	—	131	125	130	—	—	—	—
20. Auriculo-bregmatic height	—	—	—	121	107.5	121	—	—	—	—
26. Frontal sagittal arc	—	—	—	(126)	114	109	—	122	—	—
27. Parietal sagittal arc	—	((120))	107	118	112	—	—	—	—	—
28. Occipital sagittal arc	—	—	—	125	114	109	—	—	—	((115))
28(1). Lambda-inion arc	75	—	84	77	65	75	—	—	—	((72))
29. FRC. Frontal sagittal chord	—	—	—	115	106	98	—	—	—	—
30. PAC. Parietal sagittal chord	—	((113))	96.5	111	104.6	119	—	110.5	—	—
30c. Bregma-astension chord	—	((133)) (0)	128 (0)	143.5 (0)	129.4 (0)	137.5 (0)	—	141.5 (0)	—	—
30(3). Lambda-astension chord	85.5 (0)	89.8 (0)	92.7 (0)	95.6 (0)	82.2 (0)	86.2 (0)	82.5 (0)	89 (0)	88.6 (0)	87.5 (0)
	85.5 (r)	—	88.5 (r)	95.5 (r)	85.5 (r)	89.6 (r)	74.5 (r)	—	87.3 (r)	—
31. OCC. Occipital sagittal chord	—	—	—	94.3	92.4	91.5	—	—	—	(91)
31(1). Lambda-inion chord	64	—	74	67.1	61	66	—	—	—	((64.5))
31(2). Inion-opisthion chord	—	—	—	46.2	49.5	35	—	—	—	39.3
32b. NBA. Nasion angle (ba-n-br)	—	—	—	71.7	71.1	80.1	—	—	—	—
32c. BBA. Basion angle	—	—	—	56.4	53.3	48	—	—	—	—
32(5). FFA. Frontal angle	—	—	—	139.8	144.7	145.8	—	—	—	—
33e. PAA. Parietal angle	—	((147))	150.5	145.7	143	144	—	145.7	—	—
33d. OCA. Occipital angle	—	—	—	106.5	113.9	126.1	—	—	—	((113.9))
33(4). Occipital curvature angle (l-i-o)	—	—	—	110.5	116.3	129.1	—	—	—	((119.5))

Table 1 continued on next page

Table 1 *Continued from previous page*

	FACIAL VARIABLES				
	Cranium 4	Cranium 5	Cranium 6	AT-767+ AT-963	AT-1100+AT-1111+ AT-1197+AT-1198
40. BPL. Basion-prosthion length	—	121.2	—	—	—
41b. IML. Inferior malar length	—	36.4 (l)	—	—	—
41c. XML. Maximum malar length	—	61 (l)	—	—	—
41d. MLS. Malar subtense	—	15.2 (l)	—	—	—
43. Outer biorbital breadth	—	129.3	111	—	—
43a. FMB. Internal biorbital breadth	115	112	103.5	—	—
43b. NAS. Nasio-frontal subtense	22	22	20	—	—
44. Biorbital breadth	—	113	100	—	—
45. ZYB. Bizygomatic breadth	—	144	—	—	—
45(1). JUB. Bijugal breadth	—	131.5	108	—	—
46b. ZMB. Bimaxillary breadth	—	118.4	93	((110))	((102))
47. Total facial height	—	132	—	—	—
48. NPH. Upper facial height	—	85	—	—	67.1
48d. WMH. Check height	—	33.5 (l)	(26.7) (r)	—	—
		34 (r)			
48(1). Alveolar height	—	28.7	—	20	19.1
49(a). DKB. Interorbital breadth	(38)	33	—	—	—
50. Anterior interorbital breadth	(31.2)	30	—	—	—
51. Orbital breadth (mf)	—	44.4 (l)	—	—	—
		44 (r)			
51a. OBB. Orbital breadth (d)	—	42.7 (l)	(39.4) (l)	—	—
		41.7 (r)			
52. OBH. Orbital height	—	33 (l)	—	—	—
54. NLB. Nasbreadth	—	38.5	((26))	37	32
55. NLH. Nasal height	—	57.3	(49.2)	—	—
55(1). Height of pirif. aperture	—	31.2	—	—	—
56. Length of nasal bones	—	28.8	—	—	—
57. WNB. Simotic chord	—	19.4	—	—	—
57(1). Greatest breadth of nasal bones	—	27.1	—	—	—
57(2). Superior breadth of nasal bones	—	20	—	—	—
57(3). Inferior breadth of nasal bones	—	25	—	—	—
60. Maxillo-alveolar length	—	70	—	—	—
61. MAB. Maxillo-alveolar breadth	—	76	—	—	—
62. Internal palate length	—	55	—	—	—
63. Internal palate breadth	—	44	—	—	—
72. Facial sagittal angle	—	79.0	—	—	—
72(5). PRA. Prosthion angle (ba-pr-n)	—	60.9	—	—	—
72b. NAA. Nasion angle (ba-n-pr)	—	76.2	—	—	—
72c. BAA. Basion angle (n-ba-pr)	—	42.9	—	—	—
74. Alveolar sagittal angle	—	78	—	—	—
76a. SSA. Zygomaxillary angle	—	111.2	—	((121.7))	((107))
77a. NFA. Nasio-frontal angle	138.1	137.1	139.7	—	—

*Table 1 continued on next page**Minimum number of individuals*

The minimum number of calvaria is 13, calculated using the following crania, occipital bones and parietal bones: from Crania 1–9, Occipital II and Occipital IV, parietal bones + AT-619, AT-778 and AT-785+AT-803+AT-1196. For the temporal bone, the minimum number of

Table 1 *Continued from previous page*

	RADII		
	Cranium 4	Cranium 5	Cranium 6
VVR. Vertex radius	121	108.5	—
NAR. Nasion radius	106	99.5	100
SSR. Subspinale radius	—	114	—
PRR. Prosthion radius	—	125	—
DKR. Dacryon radius	—	88 (l)	90.5 (l)
ZOR. Zygoorbitale radius	—	86 (l)	(86) (r)
FMR. Frontomalare radius	—	76 (l)	82 (r)
EKR. Ectoconchion radius	—	74 (l)	—
ZMR. Zygomaxillare radius	—	72.5 (l)	76 (r)
AVR. Molar alveolus radius	—	101 (l)	—
Bregma radius	121	107.5	121
Lambda radius	110.5	101	108
Asterion radius	47 (l)	50.5 (l)	47.5 (l)
Inion radius	87.5	85	77.5
Opisthocranion radius	105	94.5	98

All measures in millimetres or degrees. Since there is one or more lambdatic wormian bones in SH Crania 2, 3, 6, 7 and 8, lambda was located following [Howells \(1973: p. 168\)](#): "... extending the general curving course of each half of the lambdoid suture to their intersections with the midline", although it is not easy when both lambdatic sutures are not totally preserved. Numbers of variables according to [Bräuer \(1988\)](#). Martin's definition of inion was used ([Martin & Saller, 1957](#); [Hublin, 1978a](#)). Maximum cranial breadth was taken on the supramastoid crests. Radii were taken as perpendiculars to the transmeatal axis, following [Howells \(1973\)](#). Outer biorbital breadth and internal biorbital breadth of Cranium 5 were taken on the malar side of the frontomalar suture. In Cranium 2, bregma was reconstructed. Biasterionic breadth in Crania 2 and 8, and bimaxillary breadth in AT-767+AT-963 and AT-1100+AT-1111+AT-1197+AT-1198, were estimated by doubling the distance from the preserved terminus to the sagittal plane. In Occipital IV, opisthion was located at the most inferior sagittal point of the preserved occipital squama. If this point is not the real opisthion, it must be very close.

individuals (MNI) is 13 ([Martínez & Arsuaga, 1997](#)). For the frontal bone, the MNI is 11: from Crania 3–6, AT-121+AT-1545, AT-400+AT-1050, AT-465+AT-624+AT-764+AT-765+AT-766+AT-1159, AT-237+AT-499+AT-1155+AT-1156, AT-626+AT-1150, AT-630+AT-777+AT-1168+AT-1550, and the facial skeleton under restoration. For the facial skeleton the MNI is 10, calculated as the number of left malar bones in the sample: AT-404, AT-465+AT-624+AT-764+AT-765+AT-766+AT-1159, AT-628, AT-768, AT-931, AT-626+AT-1550, AT-121+AT-1545, Cranium 5, Cranium 6 and the facial skeleton under restoration. So the total minimum number of calvaria in the sample is 13, calculated from the calvaria or the temporal bones; the facial remains that can be associated to the calvaria (i.e., the crania) are included in the counting of calvaria.

Comparative sample and methods

In this study we compare the Atapuerca sample with other fossil skulls. The standard measurements (to nearest 0.1 mm) of the most complete Sima de los Huesos (SH) cranial remains are shown in [Table 1](#). We have also studied the original fossils of SK 847, Bodo, Broken Hill 1 and 2, Petralona, Swanscombe, Gibraltar 1, Tabun 1, Saccopastore 1 and 2, the Krapina and Vindija samples, La Chapelle-aux-Saints, La Quina 5, Guattari 1 (Monte Circeo), Omo Kibish 1 and 2, and Mladeč 1, although in the cases of Broken Hill,

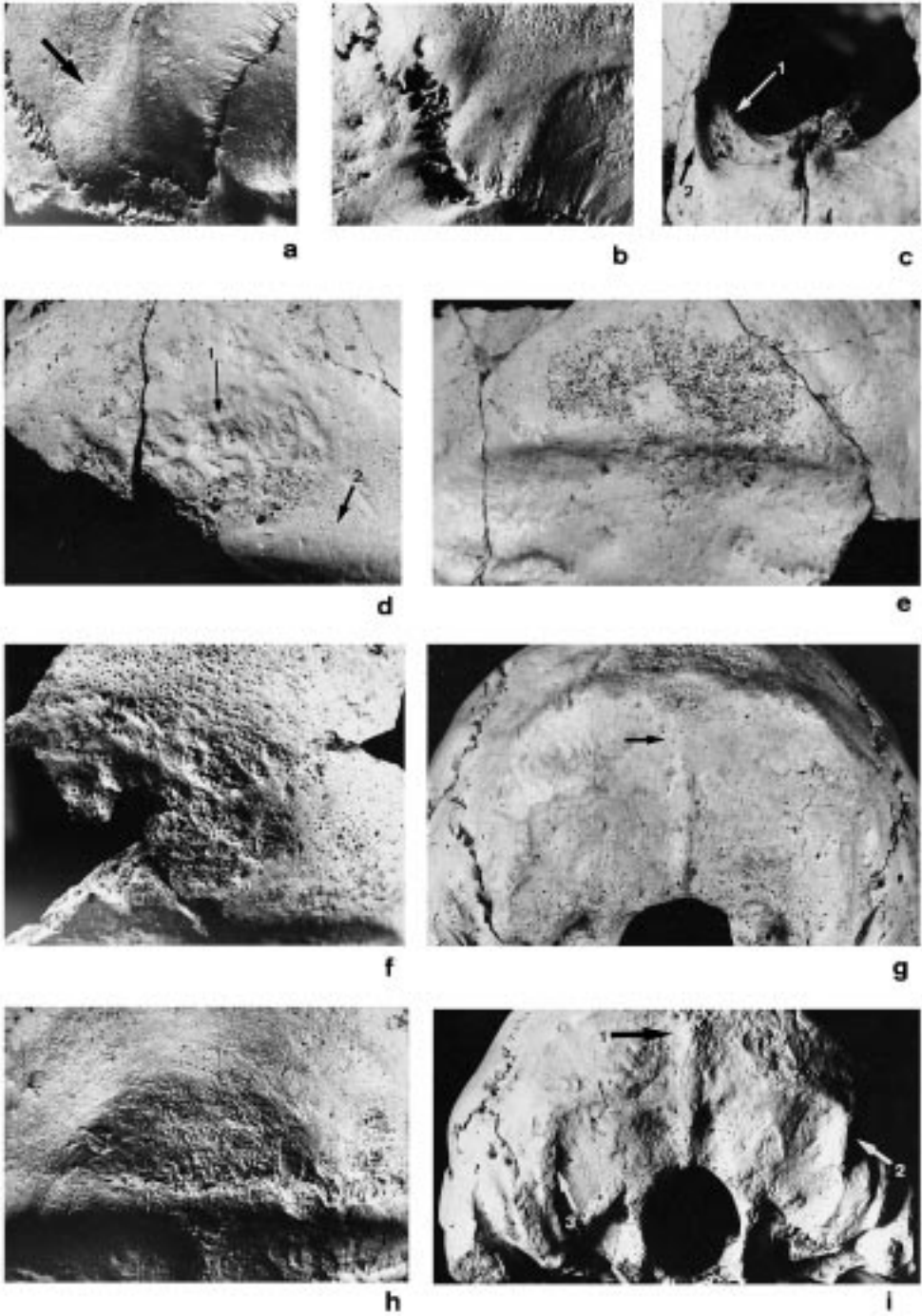


Figure 12.

Swanscombe, Gibraltar 1, Tabun 1, La Chapelle-aux-Saints, Guattari 1 (Monte Circeo), and La Quina 5, our measurements were supplemented with measurements published by other authors on the original specimens. We have also measured casts of the rest of the fossils considered in the article, but the craniometric variables used for comparisons were, whenever possible, measurements that have been published on the original fossils, supplemented by our own measurements on casts. For Steinheim and ER 3733, we recorded measures of the skull base on stereophotographs of the original fossils, using the microscope especially designed for that purpose at the Department of Human Anatomy and Cell Biology of the Liverpool University. Since the Saccopastore specimens are well-preserved last interglacial Neandertals, likely corresponding to isotope stage 5e (Manzi & Passarello, 1991), special attention is paid in this paper to comparisons with them.

To measure fragmentary fossils (especially facial remains), we benefited from a mechanical device designed to record three dimensional coordinates of the selected landmarks (Martínez, 1995). With this technique, it is possible to estimate bilateral diameters or angles with great accuracy when one of the terminus of the measure is lacking, reconstructing the lost landmark by doubling the distance from the preserved terminus to the midsagittal plane.

Univariate calvarial comparative analysis

For a better characterization of the individual neurocranial variables, the raw data of the Atapuerca SH and other European and African Middle Pleistocene fossils have been standardized to Z-scores using Neandertal statistics (i.e., by subtracting the Neandertal mean and dividing by the Neandertal standard deviation for each variable).

Atapuerca SH Cranium 5 is not unusual by the standard of Neandertal raw variables (Figure 13), but Atapuerca SH Cranium 4 displays an extraordinarily large maximum cranial breadth (M8), minimum frontal breadth (M9), biauricular breadth (M11), biasteronic breadth (M12), and remarkably low occipital angles (M33(4) and M33d). In other words, the Atapuerca SH Cranium 4 braincase is very broad and its occiput too angled for the Neandertal standards.

Petralona (Figure 14) also has a broad braincase (M8) and cranial base [M11(1) and M11], as well as a long nuchal plane (M31(2)), projected inion (INR) and angled occipital bone (M33(4) and M33d), and Broken Hill deviates from Neandertals mainly in the low occipital

Figure 12. (a) Angular torus in Atapuerca SH Cranium 4 (right side). The torus is demarcated superiorly by a sulcus (arrow) more distinct than in SH Cranium 5. (b) Slight angular swelling in Atapuerca SH Cranium 5 (right side). (c) Cranium 5 nasal aperture. Note the spinal crest (1) and lateral crest (2) in the right side and the prenasal fossa between them. (d) Cranium 9 suprainiac area. Note the excavated oval area (1), with bowl-shaped depressions above the occipital torus (2). (e) Occipital IV suprainiac area of dense pitted surface. In this individual, the pitted bone surface only represents a very thin layer, as can be observed in the patch of missing surface. (f) Cranium 3 suprainiac oval area of irregular ("cratered") surface similar to that of Cranium 9 but with many more small pits. (g) SH Cranium 5 nuchal plane. Note the absence of an occipital crest between the superior and inferior nuchal lines (arrow). The attachments of the semiespinalis capitis muscles are separated by a flat and broad surface. The Waldeyer's crests are conspicuous on both sides (anteroinferior arms of the inferior nuchal line between the attachments of m. rectus capitis posticus major and m. obliquus capitis superior). (h) Cranium 4 posterior view. Note the straight, horizontal occipital torus, and above it the flat triangular area of irregular surface circumscribed by uplifted bone. To the right there is a smaller round area of rough surface. (i) Nuchal plane of Atapuerca SH Cranium 4. Note the presence of external occipital crest (1) between the superior and inferior nuchal lines, separating the attachments of the right and left semiespinalis capitis muscles. In the right side there is a well-developed Waldeyer's crest (2); in the left side the crest was present but it is eroded (3).

angle (M33d). Bodo exhibits a long frontal bone (M26 and M29) and a large basion angle (M32c), compared with Neandertals.

The ratio auriculo-bregmatic height/maximum cranial length (M20/M1) is very high in the Atapuerca SH skulls (both look high in lateral view) (Figure 15). Atapuerca SH Cranium 5 also exhibits an outstanding basion-bregma height relative to cranial length (M17/M1), and although the Z-score of Cranium 4 is only 1.3, all the Neandertals of our sample yield lower

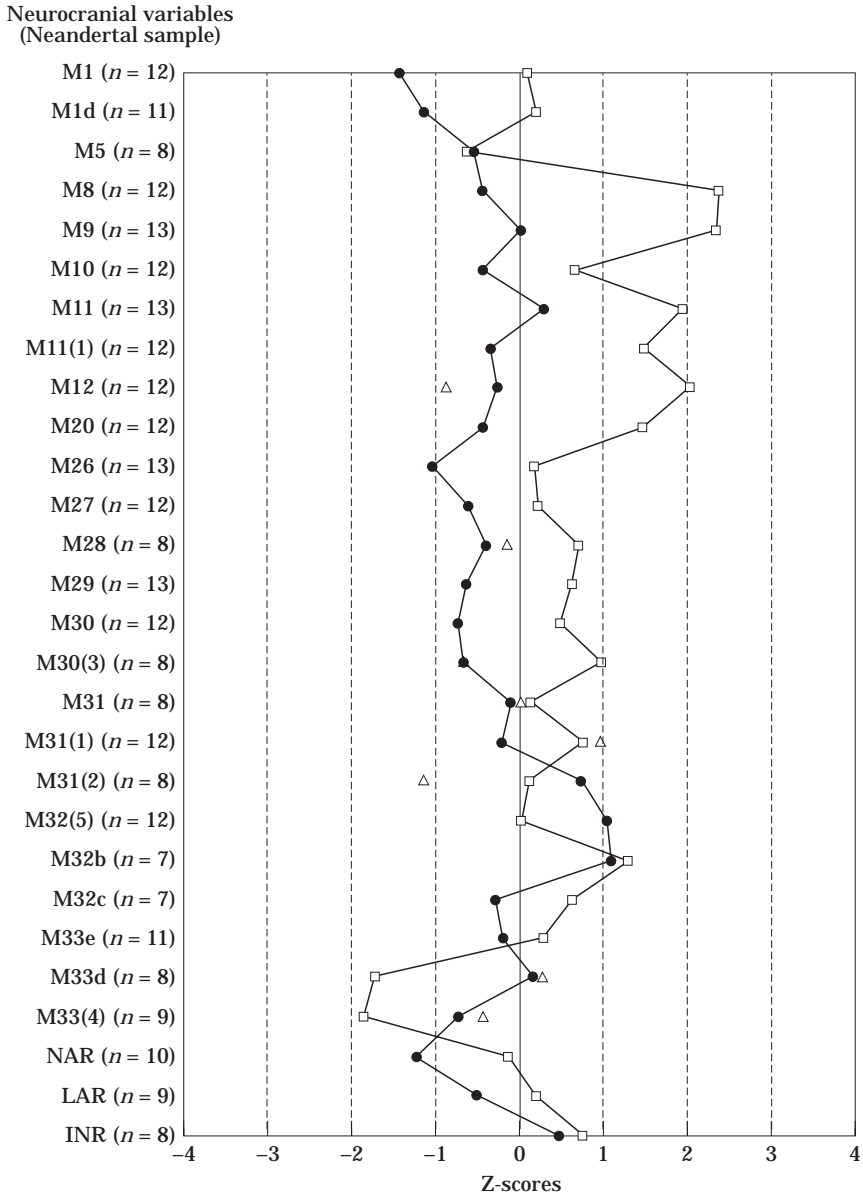


Figure 13.

values. Atapuerca SH Cranium 4 has an extraordinarily large maximum cranial breadth relative to maximum cranial length (M8/M1) (it looks very broad in superior view); in this index Cranium 5 is also above the upper end of the Neandertal range in our sample (although its Z-score is 1.47). The basion–nasion distance is short relative to maximum cranial length (M5/M1) in Atapuerca SH Cranium 4, Petralona and Broken Hill (Figure 16), but not in Atapuerca SH Cranium 5 (actually it is relatively longer than in any Neandertal, although the sample is small). The occipital sagittal chord relative to biasterionic breadth (M31/M12) is below the lower end of the Neandertal range in Cranium 4 and Broken Hill.

Compared with Neandertals, the braincase is broad in Petralona (Figure 16) with respect to cranial length (M8/M1), and in Petralona and Broken Hill the minimum frontal breadth is narrow in relation to the maximum cranial breadth (M9/M8) (i.e., divergent sides in superior view). In Petralona the occipital curvature index (M31/M28) is more than two standard deviations below the Neandertal average (reflecting an angulated occiput).

Neither Atapuerca SH Occipital IV nor Swanscombe deviate from Neandertals in absolute or in relative measures.

Parietal arch shape and cranial vault outline

Relative to modern humans, Neandertals and other archaic fossils show a parietal arch shorter sagittally (bregma–lambda) and broader inferiorly (biasterionic breadth), with lower values of the ratio bregma–asterion chord $\times 100$ /biasterionic breadth (BAC/ASB). Stringer (1983) yields a Neandertal average of 113 (± 3), and a modern human average of 124 (± 4). In *Homo ergaster* and Asian *Homo erectus* the ratios for BAC/ASB are close to 100.

In Atapuerca SH, the index values are: Cranium 4=108.3, Cranium 5=111.3, Cranium 3=113.7 and Cranium 6=117.2, although the biasterionic breadth, like other basicranial breadths (Martínez, 1995), probably would have increased after the age at death of Cranium 6 (around 14 years based on dental maturation) and Cranium 3 (also adolescent). The very tentative estimates of the ratio in Atapuerca SH Cranium 2 and Cranium 8 are very low, around 100 (but the biasterionic breadths were calculated by doubling the distance from left asterion to the sagittal plane, and bregma has been reconstructed in Cranium 2).

Figure 13. Z-scores profiles for Atapuerca SH Cranium 4 and Cranium 5 calvaria and Occipital IV. Each Atapuerca individual measurement was put in standard form: the Neandertal mean is subtracted from it and it is divided by the Neandertal standard deviation. In the graph the central vertical line represents the Neandertal average and the vertical lines to the right and to the left represent Neandertal standard deviations. The Neandertal sample used for calvarial and facial z-scores profiles includes Shanidar 1, Shanidar 5, Tabun 1, Amud 1, La Chapelle-aux-Saints, La Ferrassie 1, Neandertal, Monte Circeo, Saccopastore 1, Saccopastore 2, Gibraltar 1, Spy 1, Spy 2 and La Quina 5. Numbers of variables according to Bräuer (1988). Maximum cranial breadth is taken wherever it is found (on the parietal bones in Neandertals and on the supramastoid crests in Atapuerca SH Crania 4 and 5). Radii are taken as perpendiculars to the transmeatal axis from nasion, lambda and inion. M1 (GOL)=maximum cranial length; M1d (NOL)=nasio–occipital length; M5 (BNL)=basion–nasion length; M8=maximum cranial breadth; M9=minimum cranial breadth; M10 (XFB)=maximum frontal breadth; M11=biauricular breadth; M11(1)=interporial breadth; M12 (ASB)=biasterionic breadth; M20=auriculo–bregmatic height; M26=frontal sagittal arc; M27=parietal sagittal arc; M28=occipital sagittal arc; M29 (FRC)=frontal sagittal chord; M30 (PAC)=parietal sagittal chord; M30(3)=lambda–asterion chord; M31 (OCC)=occipital sagittal chord; M31(1)=lambda–inion chord; M31(2)=inion–opisthion chord; M32(5) (FRA)=frontal angle; M32b (NBA)=nasion angle; M32c (BBA)=basion angle; M33e (PAA)=parietal angle; M33d (OCA)=occipital angle; M33(4)=occipital curvature angle (l–i–o); NAR=nasion radius; LAR=lambda radius; INR=inion radius. In parentheses code abbreviations in the system of Howells (1973). (□) AT Cranium 4; (●) AT Cranium 5; (△) AT Occipital IV.

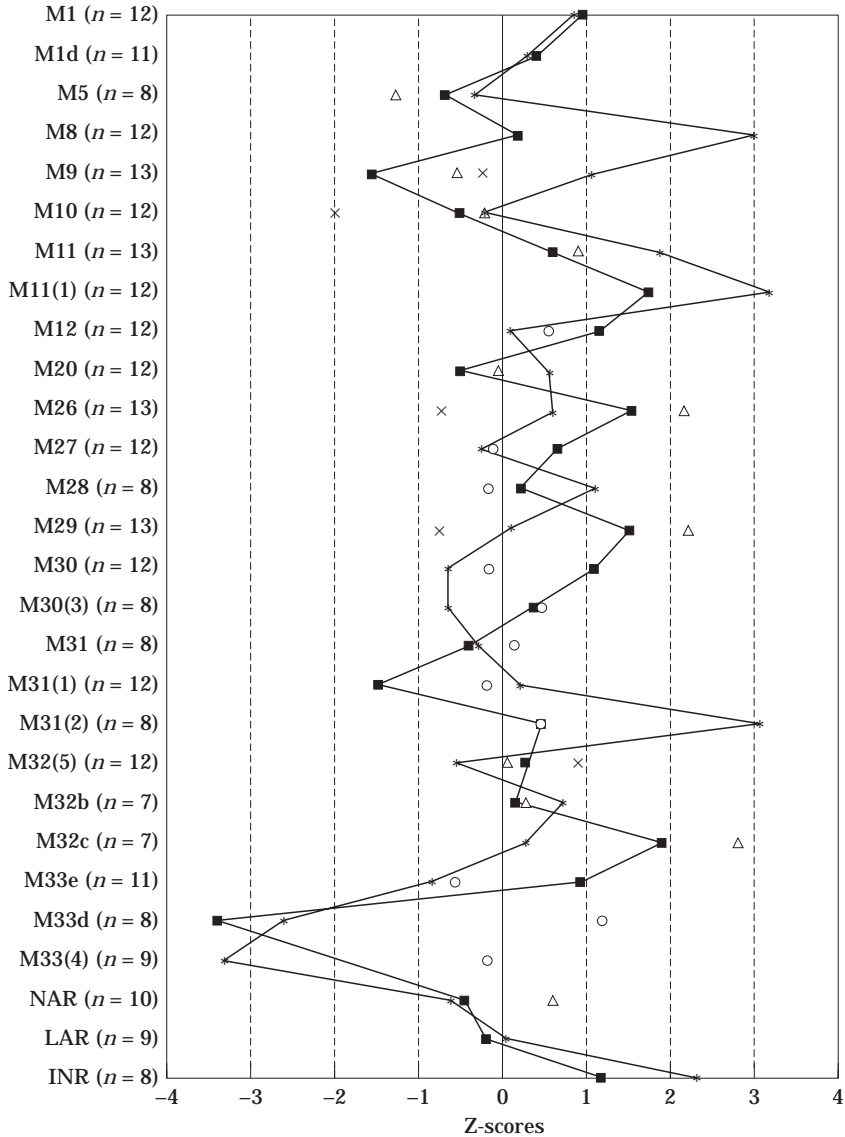
Neurocranial variables
(Neandertal sample)

Figure 14. Z-scores profiles of calvarial variables for Petralona, Broken Hill, Arago 21, Bodo and Swanscombe. Transformations of data and variable numbers as in Figure 13. (*) Petralona; (■) Broken Hill; (x) Arago; (Δ) Bodo; (○) Swanscombe.

The ratio for BAC/ASB in Swanscombe is 109 and in Petralona depends on the location of the asterion among extrasutural bones (112.9 or 103.3; 109 or 106 to Stringer, 1983). In Broken Hill our estimation of the ratio is 107.1, although Stringer (1983) obtains a value of 113. Values well below the modern average reported by Stringer (1983) can also be found in Omo Kibish 2 (113.3) and Eliye Springs (116.3; Bräuer & Leakey, 1986), but the earliest

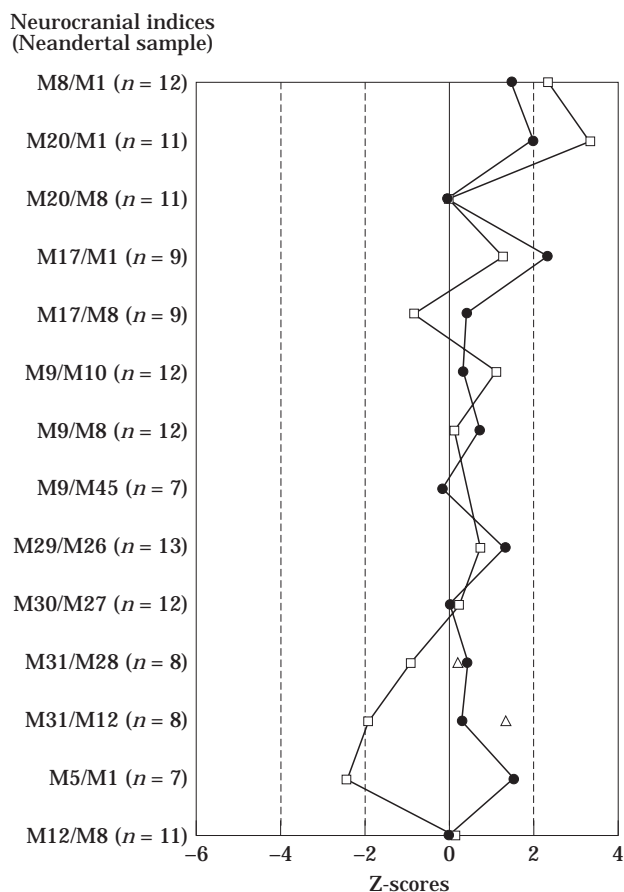


Figure 15. Z-scores profiles of calvarial indices for Atapuerca SH Cranium 4, Cranium 5 and Occipital IV. Data standardized as explained in Figure 3. Numbers of variables according to Bräuer (1988). M8/M1 = max. cranial breadth/max. cranial length; M20/M1 = Au-Br height/max. cranial length; M20/M8 = Po-B height/max. cranial breadth; M17/M1 = Ba-B height/max. cranial length; M17/M8 = Ba-B height/max. cranial breadth; M9/M10 = min. frontal breadth/max. frontal breadth; M9/M8 = min. frontal breadth/max. cranial breadth; M9/M45 = min. frontal breadth/bi-zygomatic breadth; M29/M26 = frontal sag. chord/frontal sag. arc; M30/M27 = parietal sag. chord/parietal sag. arc; M31/M28 = occipital sag. chord/occipital sag. arc; M31/M12 = occipital sag. chord/biasterionic breadth; M5/M1 = Ba-N length/max. cranial length; M12/M8 = biasterionic breadth/max. cranial breadth. (□) AT Cranium H; (●) AT Cranium 5; (△) AT Occipital IV.

modern humans from Africa like Omo Kibish 1 (with a BAC/ASB value around 123) or from Europe as Mladeč 1 (122·4), exhibit a modern-like parietal arch shape.

The maximum cranial breadth is situated on the supramastoid crests in Crania 4, 5, and 8, as well as in the juvenile Crania 6 and 7. This is a plesiomorphous trait, and Neandertals show the derived condition of a maximum cranial breadth that coincides with the maximum biparietal breadth.

When viewed from behind, the parietal wall sides are slightly convergent towards the top in Crania 2, 4, and 8 [Figures 2(c) and 8(d)], and the sides are more parallel in Atapuerca SH Cranium 7 [Figure 8(e)], in Cranium 5, which is reminiscent of Swanscombe in this trait [Figure 4(a)], and in Cranium 6 [Figure 6(a)] and Cranium 3 [Figure 1(d)], although the

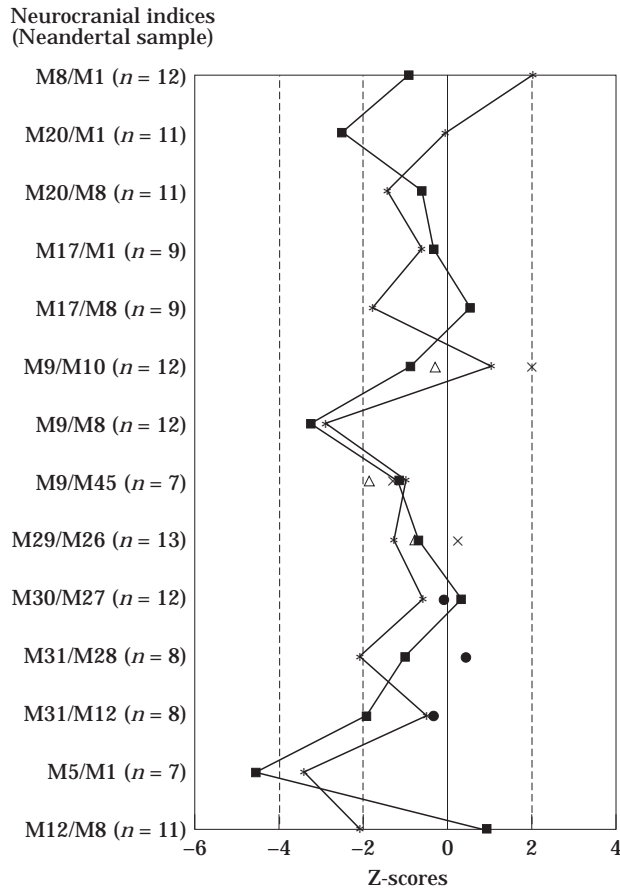


Figure 16. Z-scores profiles of calvarial indices for Petralona, Broken Hill, Arago, Bodo and Swanscombe. Indices as in Figure 15. (*) Petralona; (■) Broken Hill; (x) Arago; (Δ) Bodo; (●) Swanscombe.

cranial bases of these two young specimens could become wider when adult (Martínez, 1995), and thus the parietal wall sides become more convergent superiorly. Anyway, the Atapuerca cranial vault outlines in posterior view are not circular as in Neandertals (an autapomorphic feature), although the “house-like” contour (i.e., vertical sides) could be considered intermediate between the “tent-like” profile (convergent sides) and the Neandertal “bomb-like” (round) contour (Hublin, 1982, 1996). The Neandertal characteristic contour appears in the late Middle Pleistocene fossil from Biache-Saint-Vaast and in the last interglacial Saccopastore 1. The Cova Negra parietal bone, once thought to be Middle Pleistocene (Lumley, 1970), also shows a circular profile, but this fossil (together with new discoveries including another parietal bone with the same type of contour) actually corresponds to the Upper Pleistocene (Arsuaga *et al.*, 1989; Gracia *et al.*, 1992).

The adult braincase outline when viewed from behind seems to develop early in life, because it is “en maison” in Skhül 1 (around 3–4 years old) and “en bombe” in the same age Neandertal specimens Roc de Marsal and Subalyuk 2 according to Tillier (1992), and in the less than 2 years old Dederiyeh skeleton (Akazawa *et al.*, 1995).

Angular torus and sagittal keeling

In the Sima de los Huesos Cranium 6 the superior and inferior temporal lines diverge posteriorly, so that the smooth and polished bone surface that is found between the temporal lines occupies the whole area of parietal bone adjoining the parietomastoid border. In Cranium 4, this area is raised, forming an angular swelling or torus, bordered superiorly by a deep sulcus that demarcates the angular torus from the rest of the parietal bone [Figure 12(a)]. Among the considerable diversity found in *Homo* (Bräuer & Mbua, 1992), the morphology of Cranium 4 angular torus most resembles that of Arago 47. Cranium 5 [Figure 12(b)] exhibits an attenuated version (but still recognizable) of the Cranium 4 angular torus, and on the other hand, there is no indication of a real swelling of the mastoid angle in the rest of the Atapuerca SH sample: AT-619+AT-778, AT-785+AT-803+AT-1196, Cranium 8, Cranium 1, and the juvenile Crania 3, 6 and 7.

Cranium 4 exhibits a distinct frontal keeling that begins at the supraglabellar region, fading out in the bregma region. On Cranium 5 the keel is restricted to the anterior half of the frontal squama (as in Arago 21). Both Atapuerca skulls [Figures 2(c) and 4(a)], as well as Cranium 8 also exhibit real parietal keeling behind the bregma region. Frontal keelings are observed in the preserved frontal regions of AT-200, AT-400+AT-1050, AT-630+AT-777+AT-1168+AT-1550 and AT-237+AT-499+AT-1155+AT-1156. On the juvenile Cranium 6, a less pronounced metopic ridge extends from behind the supraorbital torus up to the fracture edge. There is also a sagittal bulging in the frontal squama AT-620+AT-783. Even in the very young specimen AT-465+AT-624+AT-764+AT-765+AT-766+AT-1159 there is a slight frontal sagittal prominence. Hence, all specimens of the Atapuerca SH sample show a mid-sagittal elevation on the frontal squama. Thus, although the frontal and parietal keelings were once considered apomorphic characters of Asian *H. erectus* (Andrews, 1984; Stringer, 1984; Wood, 1984), it is now clear that these traits also occur in the Atapuerca sample, as well as in other European and African Middle Pleistocene fossils (Bräuer & Mbua, 1992; Wu & Bräuer, 1993). Nevertheless these keelings are lacking in Neandertals. The undated Altamura fossil, with clear Neandertal features in the facial skeleton show a metopic ridge (Pesce Delfino & Vacca, 1993).

Morphological analysis of the occipital bone

Neandertals show a distinctive set of traits in the occipital bone. Some of the features are apomorphies:

(1) A large suprainiac fossa with an uneven (porous/rough) floor. This more or less elliptical depression is generally surrounded by a triangular uplifted area of bone with apex in the midline and the base on the occipital torus (Santa Luca, 1978; Hublin, 1978*b*, *d*).

(2) A weak occipital torus only developed in the central region of the occipital bone, straight (horizontal) in a posterior view but with two points of lateral projection and a depressed middle part in superior or inferior views.

The characteristic Neandertal occipital transverse torus and suprainiac fossa are discernible in very young Neandertal specimens as Engis 2 and La Quina H 18 (Hublin, 1980*a*), Roc de Marsal and Subalyuk 2 (Tillier, 1992) and even in the less than 2 years old Dederiyeh infant (Akazawa *et al.*, 1995).

Other characters are primitive in Neandertals: absence of external occipital protuberance and presence of a linear tubercle; endinion located well below inion.

Finally, some features are usually found in classic Neandertals but also sometimes in other fossils: lambdoidal flattening and occipital bunning, well separated insertions of the semispinalis capitis (with one or two medial small pits or fossae) and absent or poorly defined external occipital crest between these insertions (Hublin, 1978*b*, *c*, 1980*b*, 1982, 1984, 1988*a*; Santa Luca, 1978, 1980).

Regarding the occipital traits that are derived for Neandertals, other character states can be defined in the European Middle Pleistocene record. Some fossils (i.e., Bilzingsleben, Vértesszöllös and Petralona) do not display a suprainiac fossa or a bilateral development of the torus. This would be a primitive condition. In particular, the occipital torus is in Vértesszöllös flat and very high, i.e., the supreme nuchal lines and the supratatorial sulcus that demarcate the upper border of the occipital torus are situated very high (close to lambda) (Hublin, 1982, 1984, 1988*a*, *b*). In other words, the Vértesszöllös torus forms a high triangle, with apex in the midline and base on the superior nuchal lines.

On the other hand, Swanscombe displays a Neandertal-like suprainiac fossa surrounded by an inverted V-shape elevation (Santa Luca, 1978; Hublin, 1978*b*, *d*). The flat and triangular occipital torus of Vértesszöllös could evolve into the morphology of Swanscombe by hollowing of the central part of the torus and formation of a large suprainiac fossa (Thoma, 1966; Hublin, 1978*b*, *c*, 1984). This way, a torus like that of Vértesszöllös might become split in two branches separated by the suprainiac fossa.

In Neandertals, the upper arm of the occipital torus is poorly separated superiorly, but it is clearly more projecting backwards than the lower arm, so that the opisthocranium lies on the upper arm, as well as the terminus of Howells' lambda-opisthion subtense (OCS). The lower arm (generally referred to simply as the occipital torus) is demarcated superiorly by the suprainiac fossa and inferiorly by the sharp edge of the superior nuchal lines. A morphology similar to Swanscombe is found in the still undated (but probably Middle Pleistocene) Reilingen (according to figures in Vlček, 1991) and perhaps in Steinheim (although the area of the torus is damaged: Santa Luca, 1978; Hublin, 1984). Finally, the late Middle Pleistocene fossils Ehringsdorf H, Biache-Saint-Vaast or La Chaise Abri Suard (and also Salzgitter-Lebenstedt, that could be of a similar age), are very close to the general pattern of the torus of classic Neandertals. The occipital morphology of Saccopastore 1 (likely dating to isotope stage 5e) illustrates the change from the Swanscombe state to the classic (late) Neandertal condition.

In this tentative character polarity (morphocline) representing different phases of reduction of the torus, the Sima de los Huesos sample should be located between Vértesszöllös and the Neandertals, and its morphology is less derived than in Swanscombe. In Atapuerca SH Cranium 4 there is a flat triangular elevation demarcated from the occipital plane by a faint supratatorial sulcus, resembling an attenuated Vértesszöllös-like torus [Figure 12(h)]. In the central part of this triangle there is an oval area of slightly more irregular surface (around 34 mm wide and 17 mm high), although not depressed as in Neandertals or in Swanscombe. To the right of the torus there is another, smaller round area of rough surface. The base of the triangle forms a thick ridge (10.5 mm high) well-delineated above and below. This ridge is horizontal in rear view and corresponds to the Neandertal torus, although there is no central depression or bilateral projection (incidentally, both traits are present in Swanscombe). Laterally, the torus continues into the ridge between the attachment areas of sterno-cleido-mastoid and the splenius capitis, which is prolonged by the mastoid crest to the apex of the mastoid process.

Cranium 4 shows a triangular linear tubercle with bony granules, and an external occipital crest (not very sharp) is present between the insertions of the semispinalis capitis (or complexus)

[Figure 12(i)], as in Petralona. In Cranium 4, the crest between the rectus capitis posterior major and the obliquus capitis superior attachments (or antero-inferior arm of the inferior nuchal line) is very developed on the right side (on the left side it is eroded) [Figure 12(i)], much more than in Swanscombe. This almost parasagittal crest is called Waldeyer's crest by Thoma (1966) in his study of the Vértesszöllös occipital bone. Waldeyer (1909) describes this ridge as "unterer (sagittaler) Nebenschenkel der Lin. nuch. inferior".

In spite of the strong prominence of Waldeyer's crest in Cranium 4, there is no retromastoid process. In his drawings, Waldeyer (1909) locates the retromastoid process in modern humans in a different position to the crest: where the superior and inferior nuchal lines meet, or in the lateral ends of the superior nuchal line. Weidenreich (1951) and Santa Luca (1980) also define the retromastoid process as a bulge in the confluence of the occipital torus and the inferior nuchal line. Hauser & De Stefano (1989: p. 107) also place the retromastoid process where the generally transverse posterosuperior branch of the inferior nuchal line "approach or converge with the superior nuchal line or even blend with it near the lateral margin of the bone".

Recently, a ridge laterally bordering the attachment of the complexus in Bilzingsleben 2 (and thus belonging to the superior nuchal crest) has been wrongly labelled the retromastoid process (Mania *et al.*, 1995). Condemi (1992) notes a well-defined but flat process in Saccopastore 1, located in the confluence of the superior branch of the inferior nuchal line and the occipital lip of the occipito-mastoid ridge. Since this region is clearly non-projecting in Saccopastore 1, it should not be named a retromastoid process. Well-developed Waldeyer's crests in Salzgitter-Lebenstedt are evident in Hublin's (1984) Figure 2. Petralona and some Neandertals also show these crests (Saccopastore 1 and La Chapelle-aux-Saints, for instance, but not Saccopastore 2).

In Cranium 5 a triangular torus distinctly separated from the occipital plane by a supratotal sulcus is not discernible, but there is some convexity of the occipital plane (instead of a regular curvature: Figure 5), so that a morphology loosely equivalent to that of Cranium 4 can be guessed [Figure 4(a)]. The occipital torus is very slightly curved in superior and inferior views (in fact it is almost straight). The torus is well delineated below, but above its surface becomes irregular and covered by an extended porosity. In Cranium 5 there is a linear tubercle with rough surface and (as in Swanscombe) there is no external occipital crest between the complexus insertions [Figure 12(g)]. The Waldeyer's crests are remarkable.

The fragmentary Cranium 1 [Figure 1(a)] shows a thick torus underneath a very slightly depressed and poorly limited pitted area, but the aforementioned triangular torus is not distinct (i.e., the suprainiac area is not superiorly circumscribed by a raised edge of bone). In AT-39+AT-224+AT-1594+AT-1662, the preserved portion of the suprainiac area is porous and apparently non-depressed, there is a triangular linear tubercle made of bone granules, and the right side of the occipital torus is undercut by a deeply excavated attachment of the semispinalis capitis.

Sima de los Huesos Occipital IV, probably a late adolescent individual, does not present a triangular elevation [Figure 9(d)]. Instead, there is an oval area with a porous surface (20 mm high and 43 mm wide) that follows the general curvature of the occipital plane (i.e., it is not flat or depressed), above a straight torus not bilaterally projecting, with a slight linear tubercle underneath. This fossil lacks an external occipital crest between the well-separated complexus impressions and there are two medial fossae. Waldeyer's crests are present in Cranium 1, Cranium 2, Occipital II, Occipital IV, AT-39+AT-224+AT-1594+AT-1662, and there is an extra-ordinary development in AT-1600.

In Cranium 6 [Figure 6(a)], an adolescent individual, and in the also adolescent Cranium 3 [Figures 1(d) and 12(f)] and Cranium 9 [Figures 8(b) and 12(d)], there are flat and large oval suprainiac areas of irregular floor above an incipient straight torus (with the linear tubercle not formed). The juvenile Cranium 7 [Figure 8(e)] shows a similar suprainiac area, but the torus below is not preserved. Cranium 6 exhibits clearly developed Waldeyer's crests, but in Cranium 7, the crests are much more slender.

In the Sima de los Huesos sample the suprainiac area shows three different types of surface, that seem to be related to the age at death. In Crania 6 and 9 [Figure 12(d)], the surface is carved by large and more or less bowl-shaped depressions (alveolar or "cratered" aspect). Since Cranium 6 is adolescent, this category corresponds to adolescence and perhaps late childhood. In Crania 3 [Figure 12(f)] and 7 [Figure 8(e)] the central part of the area is covered by very dense small pits (pitted or porous aspect), that in Occipital IV [Figure 12(e)] comprise almost the totality of the area (except in the most superior part, that shows a smooth alveolar surface). A small patch of missing outer bone in Occipital IV shows that the pitted surface only represents an extraordinarily thin layer. In the adult specimens there are only signs of this very dense pitted surface (Crania 1, 4, 5 and AT-39+AT-224+AT-1594+AT-1662). Hublin (1980a) has also noted ontogenetic changes of the suprainiac fossa surface in Neandertals, showing small cupolas in juvenile specimens and being irregular/rough/porous in adults.

In sum, in all the Atapuerca fossils (adults and juveniles), there is a suprainiac area, large and oval, with a surface different from the rest of the bone. This area can be convex, flat or only slightly depressed. In Cranium 4 it is still possible to recognize a high triangular torus. Below the suprainiac area, the occipital torus is restricted to the medial portion of the occipital bone and disappears before reaching asterion. It is straight in all views and not bilaterally developed or centrally depressed.

The Neandertal morphology of the occipital torus is only foreshadowed in Atapuerca. The external occipital protuberance is not developed in any specimen of the sample, and there is variability in the development of an external occipital crest between the complexus insertions. None of the specimens present a retromastoid process, as described by Waldeyer (1909) and Hauser & De Stefano (1989) for modern populations, or by Weidenreich (1951) or Santa Luca (1980) for the Ngandong sample. Waldeyer's crests are generally well developed and tuber-like at their origin (i.e., near the inferior nuchal crests).

On the other hand, there is no lambdoidal flattening (i.e., flattening of the occipital and/or parietal bones near lambda: Lieberman, 1995) in the Sima de los Huesos sample. In Cranium 4 the maximum cranial length is slightly greater when the rear end of the diameter (opisthocranium) lies on the apex of the triangular torus than when it lies on the base (Figure 3), but in Cranium 5 the measure is the same on the torus and on the more projecting point of the occipital plane (Figure 5). In Crania 4 and 5 the terminus of Howells' lambda-opisthion subtense lies just above inion (on the torus).

The index lambda-inion subtense ($\times 100$)/lambda-inion chord, measures the occipital plane convexity (the greater the value the more convex the occipital plane). The values in the Atapuerca SH fossils for this index are low in Occipital IV (18.6), Cranium 1 (17.19) and specially Cranium 5 (14.75), all of them clearly below the Neandertal average (22.8 ± 3.2 , $n=9$; Hublin, 1982, 1988a). Cranium 4 shows the most convex occipital plane of the Atapuerca SH sample (22.35), but as in Crania 1 and 5, the more projecting point in the midline of the isolated occipital bone (i.e., where Howells' occipital subtense is taken) is placed on the torus, instead of on a convex occipital plane like in Neandertals. The adolescent specimens Crania 3 and 6 yield indices of 18.2 and 21.6, respectively, but the occipital plane

Table 2 Principal components analysis of calvarial variables

	Factor 1	Factor 2	Factor 3
Pct of var:	44.8%	18.3%	7.6%
Cum var:	44.8%	63.0%	70.6%
Neurocranial variables:			
M1. Maximum cranial length	0.83	0.404	0.01
M1d. Nasio-occipital length	0.737	0.264	0.184
M8. Maximum cranial breadth	0.552	0.692	-0.076
M9. Minimum frontal breadth	0.847	0.094	0.172
M10. Maximum frontal breadth	0.824	-0.16	0.046
M11. Biauricular breadth	0.214	0.848	-0.077
M12. Biasterionic breadth	0.343	0.52	0.407
M20. Auriculo-bregmatic height	0.95	-0.06	-0.058
M26. Frontal sagittal arc	0.672	0.143	-0.216
M27. Parietal sagittal arc	0.824	-0.41	-0.169
M28. Occipital sagittal arc	0.721	0.036	0.143
M29. Frontal sagittal chord	0.735	0.287	-0.211
M30. Parietal sagittal chord	0.848	-0.346	-0.093
M31. Occipital sagittal chord	0.811	-0.338	0.166
M31(1). Lambda-inion chord	0.654	-0.194	0.526
M31(2). Inion-opisthion chord	-0.31	0.34	0.681
M32(5). Frontal angle	-0.344	0.614	0.207
M33e. Parietal angle	-0.521	0.465	0.533
M33d. Occipital angle	0.42	-0.72	-0.019
NAR. Nasion radius	0.563	0.326	0.181
LAR. Lambda radius	0.922	-0.101	-0.057
INR. Inion radius	0.341	0.63	-0.378

Numbers of variables according to Bräuer (1988). Martin's definition of the inion was used (Martin & Saller, 1957; Hublin, 1978a). Loadings above 0.6 are highlighted. Ptc of var: Percentage of variance; cum var: cumulative variance.

curvature could have changed had the individual matured. In Swanscombe the index is 19.7, in Saccopastore 1 it is 20.9 (placing lambda following the criterion of Howells, 1973), and in Bilzingsleben the occipital plane is very flat, yielding an index value of 13 (measurement on cast). Although very convex occipital planes (or occipital buns) are typical of Neandertals, this trait can also be found in modern humans (e.g., the convexity index is 25 in the early Upper Palaeolithic Mladeč 1).

Multivariate analysis of calvarial variables

In order to assess craniophenetic similarities between the Sima de los Huesos calvaria and other fossils, we carried out a principal component analysis (PCA) on 31 *Homo* fossils (including Sima de los Huesos Cranium 4 and Cranium 5), using 22 neurocranial variables. SPSS/PC + 4.0.1 statistical package was used (Norusis, 1990). Only complete cases were accepted in the computations. Basion-bregma height, a traditional measure of cranial height, was not used because basion is lacking in several specimens. Instead we have included the auriculo-bregmatic height. The factor matrix (Table 2) shows that Factor 1 is especially correlated with diameters and arcs that are taken in the sagittal plane, as well as with both frontal breadths. This factor accounts for almost half of the original variance. Fossils with large scores for Factor

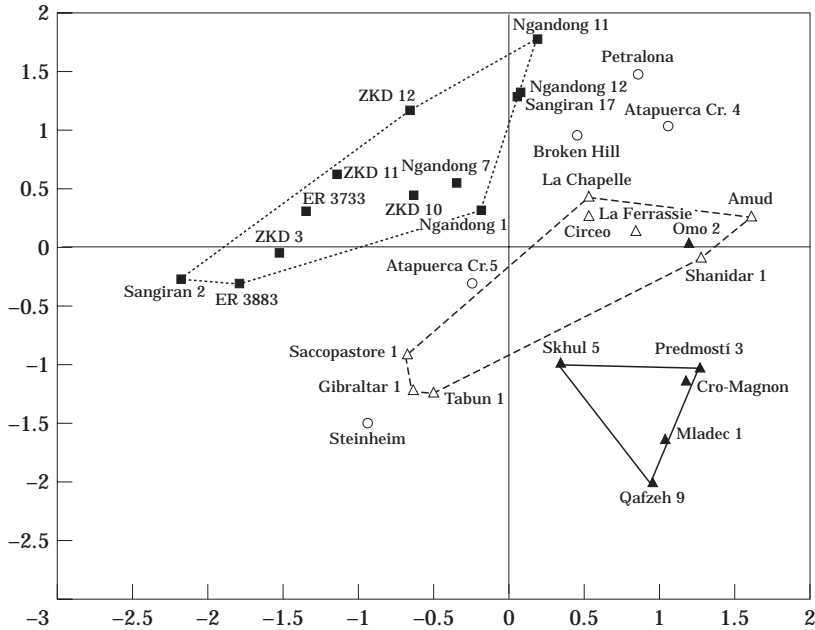


Figure 17. Scatter diagram for first and second principal components of calvarial variables. In some specimens reconstruction of the opisthion has been necessary (Zhoukoudian 3, Zhoukoudian 10, Steinheim, Tabun 1, Monte Circeo and Amud 1). Zhoukoudian 3 is not an adult individual, because the occipito-mastoidal synchondrosis is not yet fused. In Saccopastore 1, we used the lambda 3 of Sergi (1944), because it corresponds to the position of lambda according to Howells' (1973) criterion. Although the chronology and evolutionary position of Omo Kibish 2 are uncertain in the plot it has been indicated with the modern human symbol, but it is not enclosed in the envelope for the modern human sample (▲). (■) *H. erectus* broad sense (s.l.) includes the African specimens assigned to *H. ergaster* by some scholars. X axis corresponds to factor 1 and Y axis to factor 2. (△) Upper Pleistocene Neandertals. (○) Middle Pleistocene = European and African Middle Pleistocene fossils. ZKD=Zhoukoudian.

2 have large maximum cranial breadths and biauricular breadths, flat frontal bones, projected inions and angled occiputs. Length of the nuchal plane is the only variable with a loading greater (in absolute value) than 0.6 on Factor 3.

Some interesting conclusions can be drawn when the first principal component is plotted with the second one (Figure 17). The Sangiran, Zhoukoudian and Ngandong Asian *H. erectus* specimens lie all in the same trend, together with the two African *H. ergaster* fossils, that in this plot fall close to the small Sangiran 2 and Zhoukoudian 3 calvaria (although the latter is immature). So, we agree with Rightmire (1995) in that the Turkana specimens and the smallest specimens of Asian *H. erectus* cannot be distinguished at the species level based on braincase size and proportions. There are two clusters of Neandertals, the small braincases (probably females and older: Gibraltar 1, Saccopastore 1 and Tabun 1) and the big ones (probably males and more recent: La Chapelle-aux-Saints, La Ferrassie, Monte Circeo, Shanidar 1 and Amud). As a whole, Neandertals follow a trend parallel to that of *H. erectus*/*H. ergaster*. This means that for a given Factor 1 score, Neandertals show narrower braincases and cranial bases, more rounded frontal bones, less angled occipital bones and less projected inions. In modern humans (including both the Israeli and the European earliest fossils) these traits are more exaggerated. Finally, the Sima de los Huesos crania, Petralona and Broken Hill lie between

Table 3 Principal component analysis of occipital variables

	Factor 1	Factor 2	Factor 3
Pct of var:	50.5%	24.5%	12.2%
Cum var:	50.5%	75.0%	87.2%
Occipital variables:			
M12. Biasterionic breadth	0.53	− 0.655	0.229
M28. Occipital sagittal arc	0.927	0.042	− 0.259
M30.3. Lambda–asterion chord	0.83	0.072	0.29
M31. Occipital sagittal chord	0.896	0.401	0.015
M31(1). Lambda–inion chord	0.874	0.122	0.209
M31(2). Inion–opisthion chord	0.049	− 0.191	− 0.934
M33d. Occipital angle	0.208	0.88	0.295
M33(4). Occipital curvature angle	0.396	0.762	0.41

Numbers of variables according to Bräuer (1988). Martin's definition of inion was used (Martin & Saller, 1957; Hublin, 1978a). Loadings above 0.6 are highlighted. Abbreviations as in Table 2.

H. erectus and Neandertals. The extraordinarily narrow biauricular breadth estimated for Steinheim (116 mm) seems to have been reduced by distortion.

Atapuerca SH Cranium 4 clusters with Broken Hill and Petralona (these three specimens could be males), but Atapuerca SH Cranium 5 lies between them and Steinheim. Whereas Steinheim is probably a female (Wolpoff, 1980), Atapuerca SH Cranium 5 could be a female or a small male. Although in the plot Neandertals lie craniophenetically between Afro/European Middle Pleistocene fossils and modern humans, thus pointing to a possible Neandertal ancestry to European and Levant early moderns, modern humans could also stem from African specimens that are “transitional” from archaic to modern morphology, like Omo Kibish 2 (late Middle Pleistocene or early Upper Pleistocene). Unfortunately, Eliye Springs was not included in the analysis because one of the variables (biauricular breadth) cannot be taken. Finally, the third principal component (correlated with the length of the nuchal plane), does not help to discriminate between “traditional” groups.

Another different PCA has been performed, this time with eight occipital variables and 37 fossils, including three Atapuerca SH specimens. After equamax rotation the larger loadings on the first component (accounting for half the total variation) correspond to lambda–asterion chord, occipital sagittal arc and chord and occipital plane (lambda–inion) chord (Table 3). Rotation redistributes the explained variance for the individual factors. This permits the factors to be differentiated from each other. If several factors have high loadings on the same variables, it is difficult to ascertain how the factors differ. In our case, equamax rotation is the more efficient. The equamax method is a combination of the varimax method, which simplifies the factors, and the quartimax method, which simplifies variables (Norusis, 1990). Biasterionic breadth is positively correlated with the first factor and negatively correlated with the second factor. Two different measures of occipital angulation contribute to the second factor: the larger the score, the less angulated the occipital bone (and the narrower the biasterionic breadth). Inion–opisthion chord is again highly correlated to the third factor. Apparently, nuchal plane length seems to be largely independent of the other factors of occipital bone variation, but again it is not useful to separate traditional taxonomic units.

Most of the *H. erectus*/*H. ergaster* fossils have negative scores for the first two factors (bottom left quadrant), basically because of their short occipital planes and broader and angulated

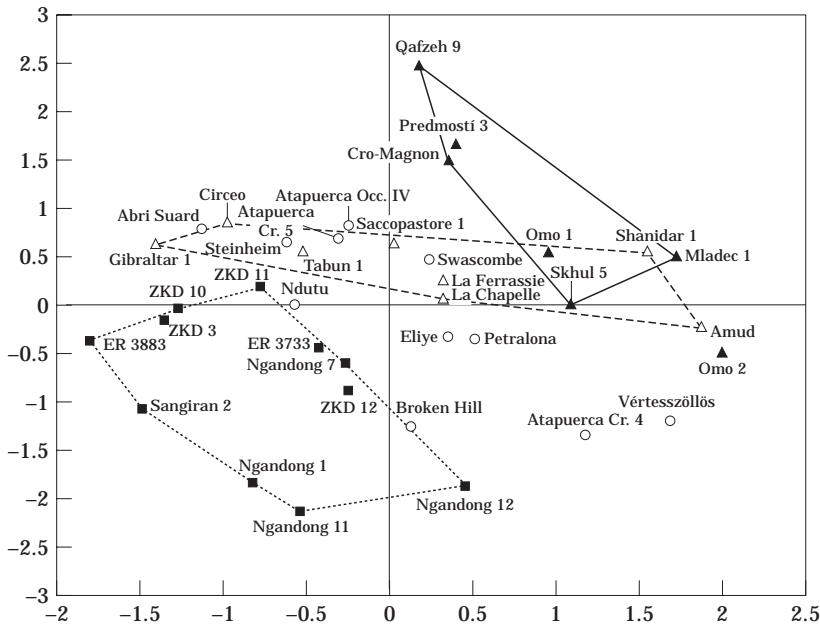


Figure 18. Scatter diagram for first and second principal components of occipital variables. In the calculations we have used Thoma's (1966) estimations for Vértesszöllös instead of those published by Wolpoff (1977). La Chaise Abri Suard is Neandertal in morphology, but it has not been enclosed in the Neandertal envelope because of its late Middle Pleistocene age. *H. erectus* broad sense (s.l.) embraces the African specimens assigned to *H. ergaster* by some scholars. X axis corresponds to factor 1 and Y axis to factor 2. (○) European and African Middle Pleistocene fossils. (■) *Homo erectus* s.l.; (△) Upper Pleistocene Neandertals; (▲) modern humans.

occiputs (Figure 18), contrary to modern humans that score positive values for both factors (top right quadrant). In particular, Cro-Magnon, Predmostí 3 and Qafzeh 9 are well separated by their large occipital angles. Shanidar 1 is the only non-modern specimen that lies within the modern human envelope. Steinheim, Swanscombe, La Chaise Abri Suard, Atapuerca SH Cranium 5 or Atapuerca SH Occipital IV fall within the Neandertal envelope or very close to it, but Eliye Springs, Petralona, Vértesszöllös, Broken Hill and Atapuerca SH Cranium 4 show broader and/or more angulated occipital bones.

Omo Kibish 2, a skull with modern *H. sapiens* affinities, yields a low value of Howells' (1973) occipital angle (OCA=106.6°), but the occipital curvature angle (l-i-o) is much higher (117.9°). Another transitional African fossil of uncertain age, Eliye Springs, yields similar values (105.9° and 116°, respectively: Bräuer & Leakey, 1986). Although the occipital shape of Omo 2 has been compared with that of Asian *H. erectus* (Stringer & Gamble, 1993), the primitive condition, as seen in *H. ergaster*/*H. erectus*, is that both occipital angles are low. On the other hand, Omo Kibish 1 (more clearly modern than Omo Kibish 2) falls within the modern human envelope.

Foramen magnum shape

To Rak et al. (1994, 1996), the foramen magnum in both juvenile and adult Neandertals tends to be more oval (anteroposteriorly elongate shape) than in modern humans. The juvenile

Atapuerca SH Cranium 6 yields an index of the foramen magnum of 68.18% (width=30 mm, length=44 mm), a low value compared with the distribution of modern human juvenile specimens measured by Rak *et al.* (1994), but yet above the values of the four immature Neandertals published by these authors: Amud 7 (57.1%), La Quina 18 (57.5%), Engis 2 (59.5%) and Teshik Tash (65% in Rak *et al.*, 1996). Creed-Miles *et al.* (1996) obtained different (greater) indices for the same juvenile Neandertals. On the other hand, these Neandertal juveniles are younger (less than 10 years old) than SH Cranium 6 (around 14 years old), and the foramen magnum index could decrease during adolescence.

With respect to adult Neandertals, published figures coming from casts, are: 65% (Rak *et al.*, 1994) or 68% (Creed-Miles *et al.*, 1996) for La Chapelle-aux-Saints; 77.4% (Creed-Miles *et al.*, 1996) for La Ferrassie 1; 90.3% (Creed-Miles *et al.*, 1996) for Saccopastore 1; and 71% for Ganovce (Rak *et al.*, 1994), obtained from the imprint of a foramen magnum in an endocast. Heim (1989) gives an index of 68% for his new reconstruction of La Chapelle-aux-Saints skull and Boule (1911–1913) calculated an index of 65.2% based on the old reconstruction. On La Ferrassie 1 original fossil, Heim (1989) obtained a value of 79%. Our own index for Saccopastore 1, taken on the original fossil, is 83.8% (width=28.9 mm, length=34.5 mm). Creed-Miles *et al.* (1996) report an average of 85.4% ($n=13$) for “adult earlier hominids”. In the Atapuerca SH Cranium 4 the index is 71.43% (width=30 mm, length=42 mm), in Cranium 5 is 73.68% (width=28 mm, length=38 mm), and in Swanscombe 75% (width=30 mm, length=40 mm).

We agree with Rak *et al.* (1996) in that after Creed-Miles *et al.* (1996) figures, the Amud 7 foramen magnum is very long compared with modern children of around its age (10 months). Interestingly, the La Chapelle-aux-Saints foramen magnum length is also extraordinary compared with other fossils and modern humans (Martínez, 1995). Nevertheless, it is not so clear that an extraordinarily long foramen magnum (and in consequence an elongate shape) is common to all (or most) Neandertals and only to them; for instance, the foramen magnum index of Ngandong 12 is 66.3% (Weidenreich, 1951). After examining a sample of 1000 modern human individuals (of all ages at death) and casts of Neandertal crania, Richards & Plourde (1995) also doubt the extreme oval-shape of the foramen magnum in Neandertals.

Univariate comparative analysis of the Atapuerca facial skeleton

Z scores relative to the Neandertal sample were computed for Atapuerca SH Cranium 5, Petralona, Arago, Broken Hill and Bodo (Figures 19 and 20). Atapuerca SH Cranium 5 differs from Neandertals in its larger outer biorbital breadth (M43) and lower orbit (M52), broader nose, absolutely (M54) and even more relative to nasal height (M54/M55), longer maxillary alveolar process (M60) and relatively larger bimaxillary breadth compared with facial height (M48/M46b) and bizygomatic breadth (M46b/M45). The late adolescent/early adult AT-1100+AT-1111+AT-1197+AT-1198 has a nasal aperture substantially narrower, absolutely (32 mm) and relative to its height (nasal index=59.3), than Atapuerca SH Cranium 5 (38.5 mm and 67.2, respectively). The fragmentary face of this fossil seems to be narrower also in the bimaxillary breadth (around 102 mm) than that of Cranium 5 (118.4 mm). AT-1100+AT-1111+AT-1197+AT-1198 has also a lower facial upper height (67 mm) than Cranium 5 (85 mm). On the contrary, the younger (around 14 years old) adolescent AT-767+AT-963 is closer to Cranium 5 in nasal breadth (37 mm) and bimaxillary breadth (estimated in 110 mm).

The immense Bodo face falls outside the 95% Neandertal range of variation (i.e., two standard deviations) for all measurements of upper, middle or lower facial breadth, absolute (M43, M43a, M44, M45(1), M46b, M61) and relative (M48/M45, M48/M46b, M46b/M45), as well as for absolute and relative nasal breadth (M54, M54/M55) and facial prognathism (M72(5), M40/M5). Although Arago 21 is severely distorted, this face seems to have an absolute and relative low orbit (M52, M52/M51a) and narrow nose (M54, M54/M55), and a

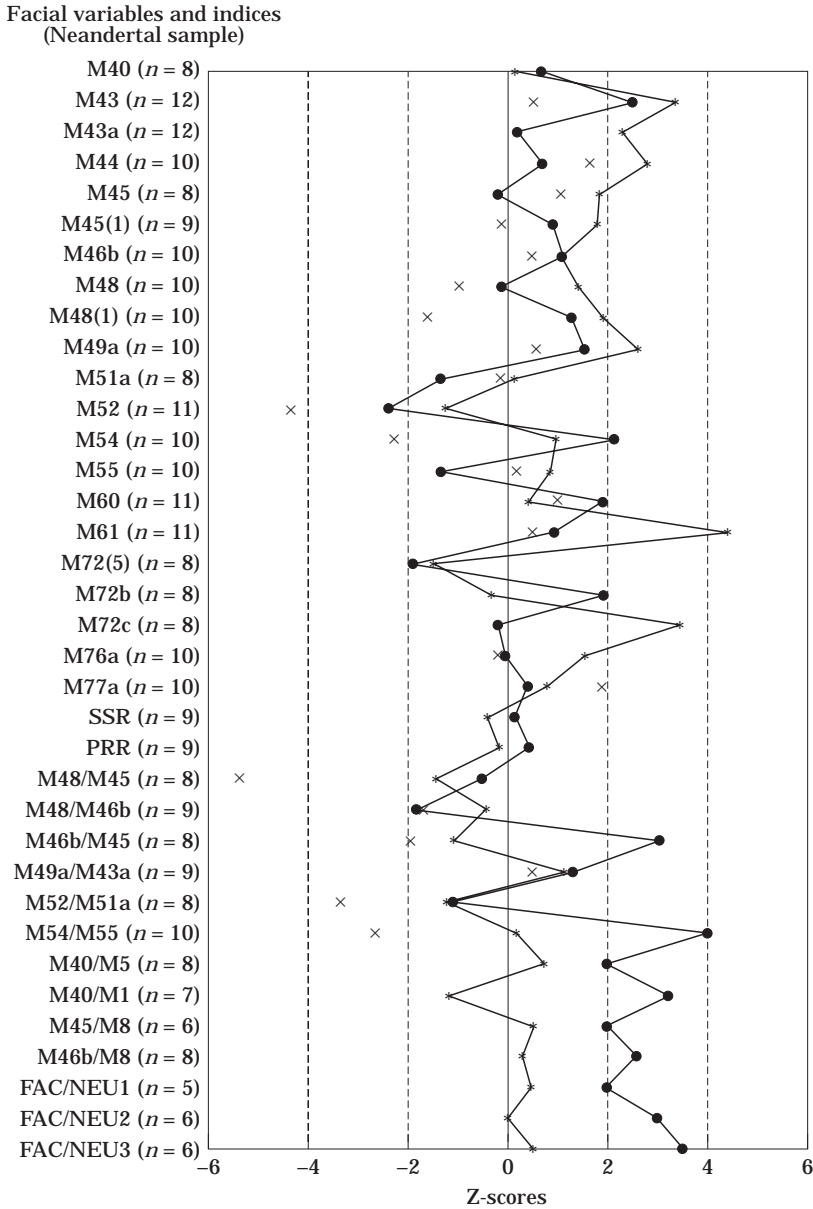


Figure 19.

relatively low face (M48/M45). Compared with Neandertals, Petralona shows a broader upper face (M43, M43a, M44) and external palate (M61, although in part due to its very developed external maxillary torus, which is included in the measure in this study), but in relative measures this fossil does not fall outside the Neandertal interval of two standard deviations. Broken Hill shows large biorbital breadths (M43, M43a), high face (M48, M48/M45) and a broad maxillary alveolar process (M61, also with an important contribution of the maxillary torus). Petralona and Bodo exhibit larger interorbital breadths (M49a) than Neandertals (i.e., Z-scores above 2), but only in absolute measures and not relative to the internal biorbital breadth (M49a/M43a). Our estimation of Atapuerca SH Cranium 4 interorbital breadth is above the upper end of the Neandertal range both in absolute and relative terms (Z-scores of 2.8 and 2.1, respectively).

Strong facial prognathism is metrically indicated by a low prosthion angle (M72(5): ba-pr-n) or profile (sagittal) facial angle (n-pr angle to Frankfurt Horizontal) and a high nasion angle (M72b: ba-n-pr). The prosthion angle of Atapuerca SH Cranium 5 (60.9°) is lower than in any Neandertal, but close to Saccopastore 1 (61.2°). Broken Hill (60.7°; 62.1° for [Stringer, 1983](#)), and Petralona (61.8°) yield similar prosthion angles, and the prognathism is more marked in Bodo (57.2°) and ER 3733 (57.6°, calculated upon measurements by Wood, 1991). Atapuerca SH Cranium 5 nasion angle (M72b=76.2°) is slightly below that of Bodo (78.1°) and ER 3733 (79.6°, and above Petralona (69.3°), Broken Hill (69.4°) or the Neandertals (although again Saccopastore 1 is very close: 74.1°). Also in facial sagittal angle, Atapuerca SH Cranium 5 is more prognathic than Neandertals (79°, Z-score = -2.3; Neandertal sample $n=9$). Finally, in Cranium 5, as well as in Bodo, the basion-prosthion distance relative to basion-nasion distance (M40/M5) is longer than in Neandertals.

The Atapuerca SH Cranium 5 face looks very big in relation to its neurocranium, and this visual impression is confirmed by its long face (basion-prosthion length) relative to the maximum cranial length (M40/M1), as well as by its large bizygomatic and bimaxillary breadths relative to maximum cranial breadth (M45/M8, M46b/M8). To compare the facial

Figure 19. Profiles of Z-scores for Atapuerca SH Cranium 5, Petralona and Arago facial skeletons. Facial measurements of these European Middle Pleistocene fossils were standardized to the Neandertal mean and standard deviation. Numbers of variables according to Bräuer (1988). M40 (BPL)=basion-prosthion length; M43=outer biorbital breadth; M43a (FMB)=internal biorbital breadth; M44=biorbital breadth; M45 (ZYB)=bizygomatic breadth; M45(1) (JUB)=bijugal breadth; M46b (ZMB)=bimaxillary breadth; M48 (NHP)=upper facial height; M48(1)=alveolar height; M49a (DKB)=interorbital breadth (d); M51a (OBB)=orbital breadth (d); M52 (OBH)=orbital height; M54 (NLB)=nasal breadth; M55 (NLH)=nasal height; M60=maxillo-alveolar length; M61 (MAB)=maxillo-alveolar breadth; M72(5) (PRA)=prosthion angle (bra-pr-n); M72b (NAA)=nasion angle (ba-n-pr); M72c (BAA)=basion angle (n-ba-pr); M76a (SSA)=zygomaxillary angle; M77a (NFA)=nasio-frontal angle; SSR=subspinal radius; PRR=prosthion radius; M48/M45=upper facial height/bizygomatic breadth; M48/M46b=upper facial height/bimaxillary breadth; M46/M45=bimaxillary breadth/bizygomatic breadth; M49a/M43a=interorbital breadth (d)/internal bioorbital breadth; M52/M51a=orbital height/orbital breadth (d); M54/M55=nasal breadth/nasal height; M40/M5=Ba-Pr length/bizygomatic breadth; M40/M1=Ba-Pr length/maximum cranial length; M45/M8=bizygomatic breadth/maximum cranial breadth; M46b/M8=bimaxillary breadth/maximum cranial breadth; FAC/NEU1= $M48 \times M40 \times M45/M1d \times M20 \times M8$ =(upper facial height \times Ba-Pr length \times bizygomatic breadth)/(nasio-occipital length \times Po-B height \times maximum cranial breadth); FAC/NEU2= $M48 \times M40 \times M46b/M1d \times M20 \times M8$ =(upper facial height \times Ba-Pr length \times bimaxillary breadth)/(nasio-occipital length \times Po-B height \times maximum cranial breadth); FAC/NEU3= $M48 \times M40 \times M46b/M1d \times M20 \times M8$ =(upper facial height \times Ba-Pr length \times bimaxillary breadth)/(nasio-occipital length \times Ba-B height \times maximum cranial breadth). In parentheses code abbreviations in the system of Howells (1973). (●) AT Cranium 5; (*) Petralona; (×) Arago.

Facial variables and indices
(Neandertal sample)

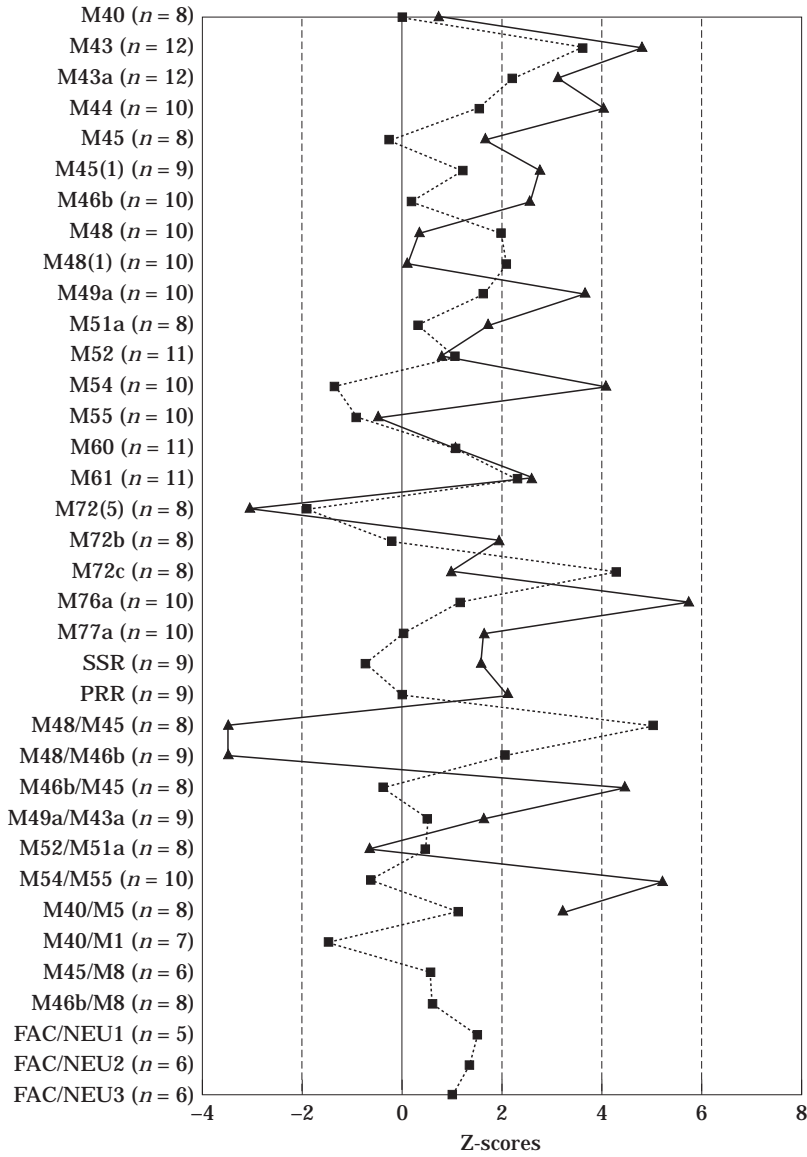


Figure 20. Z-scores profiles for (▲) Bodo and (■) Broken Hill facial variables. Variables and indices as in Figure 19.

size with the calvarial size we have designed three indices that divide the product of facial length, height and breadth by the product of calvarial length, height and breadth (Figures 19 and 20). For these three indices, Atapuerca SH Cranium 5 exhibits a relatively bigger face than Broken Hill, Petralona or any of the specimens of the small sample of Neandertals that are complete enough to make the calculations (using estimations in some instances): Shanidar 1,

La Chapelle-aux-Saints, La Ferrassie 1, Monte Circeo, Gibraltar 1 and Saccopastore 1. Cranium 5 index is still more outstanding when bimaxillary breadth replaces bizygomatic breadth. Interestingly, the “last interglacial” Saccopastore 1 is, in the two indices that can be estimated, the closest to Atapuerca SH Cranium 5 among the Neandertals of the sample. On the contrary, the indices of Petralona are near the Neandertal means.

The Atapuerca sample exhibits well-developed cheek bones, or, in other words, high infraorbital bone plates. This can be metrically illustrated by the minimum cheek height, defined by Howells (1973: p. 180) as “the minimum distance, in any direction, from the lower border of the orbit to the lower margin of the maxilla, mesial to the masseter attachment” (in fact, in most fossils the lower terminus of the measure lies in the most medial point of the masseter attachment). Among Neandertals, the highest published cheek height, as far as we know, is 32.5 mm for Shanidar 5 (Trinkaus, 1983). In Saccopastore 2, the cheek height is 33 mm and in Saccopastore 1 it is around 26.5 mm. Atapuerca SH Cranium 5 yields a cheek height of 34 mm (right side r.s.)–33.5 mm (left side l.s.). Such values are similar to those of ER 3733 (33 mm, Wood, 1991; 34 mm, Rightmire, 1990), SK 847 (32 mm) or Bodo (34 mm), but the cheek heights of AT-629 (36.3 mm) and AT-404 (37.1 mm) are close to that of Petralona (36.5) or Sangiran 17 (38 mm, Wood, 1991; 37 mm, Rightmire, 1990). On the other hand, Broken Hill (29 mm), Arago 21 (30–26.7 mm), Steinheim (26.6 mm) and Zuttiyeh (around 24 mm; the last three measures taken on casts) show substantially lower cheek heights than the Atapuerca faces.

Another indicator of infraorbital plate development is the zygomatic bone length along zygomaxillary suture or zygoorbitale (zo) to zygomaxillare anterior distance (zm:a). In Atapuerca SH Cranium 5, the length of the suture is 39.3 mm (l.s.)–38.5 mm (r.s.), in AT-629 is 38.6 mm, and that of AT-404 has been estimated in 41.4 mm. These values reflect a well-developed zygomatic bone, as in Petralona (41.4 mm), Bodo (39 mm) or Sangiran 17 (37.8 mm; Thorne & Wolpoff, 1981). Arago 21 yields a lower value for the zo-zm:a distance (32 mm, l.s.–33 mm, r.s.; Bouzat, 1982) and in Saccopastore 2 it is 34 mm.

The infraorbital foramen is in modern populations closer to the inferior orbital margin (i.e., in a higher position) than in fossil specimens in general. The minimum distance between the foramen and the orbital margin is in Atapuerca SH Cranium 5 of 15.2 mm (l.s.)–14.1 mm (r.s.) and in AT-404 of 17.7 mm. These values fall within the range of values for Middle Pleistocene fossils and Neandertals published by Condemi (1992) and Lumley & Spitey (1982). In Petralona the distance is 16.4 mm, in Saccopastore 1, the distance is 12.1 mm and 15.1 mm in Saccopastore 2.

Midfacial prognathism

The nasio-frontal angle (M77a=NFA, Howells, 1973), a measure of nasion protrusion from the lateral edges of the frontal bone, has in “classic” Neandertals (*sensu* Trinkaus, 1987; $n=9$) values inferior to 140°. Trinkaus (1983) reports values of 151° for Ehringsdorf 9, 138° for Krapina C, 142° for Krapina E and 142° for Tabun C1, and the estimation of Sergi (1944) of a similar angle (M77) for Saccopastore 1 is 140°. NFA values larger than 142°, indicating less anterior nasion projection than in any known Upper Pleistocene Neandertal (Ehringsdorf 9 could date to Middle Pleistocene; Blackwell & Schwartz, 1986), are found in ER 3733 (145° to Stringer, 1983, and 152° to us, both estimations on casts), Arago 21 (146°, Spitey, 1982), Bodo (144.1°) and Zuttiyeh (150°, Trinkaus, 1983), while other Middle Pleistocene fossils yield lower

NFA values, as Petralona (140°), AT-400+AT-1050 (141.5°), Atapuerca SH Cranium 4 (138.1°), Atapuerca SH Cranium 5 (137.1°) and Broken Hill (134.9°).

A distinctive Neandertal trait is midfacial prognathism, that can be metrically indicated by the zygomaxillary angle (M76a=SSA, [Howells, 1973](#)). For this angle, Atapuerca Cr. 5 and Arago 21 fall close to the Neandertal mean (their Z-scores are -0.05 and -0.2 respectively, although the angle of Arago 21 can be affected by postmortem distortion). The SSA angles of Broken Hill (117°) and Petralona (117.7°; 119° to [Stringer, 1983](#)) lie close to the upper end of the Neandertal range (represented by Saccopastore 2=116.7°). Interestingly, Broken Hill cannot be clearly distinguished from Neandertals in nasion (NFA) or subspinale (SSA) projection, two metrical expressions of the Neandertal facial morphology. On the contrary, the upper and midface of Bodo are flat (SSA=139°, Z score=5.67). A flat midface seems to be the condition for early *Homo*, as expressed by the zygomaxillary angle, that is 143° in OH 24 and ER 1813, and 161° in ER 1470 according to [Rightmire \(1993\)](#). We have estimated the SSA of SK 847 at 147° and that of ER 3733, on a cast, at 146°.

For the approximately 14 years old AT-767+AT-963 we have estimated a zygomaxillary angle around 122°, whereas the estimation for the late adolescent/early adult AT-1100+AT-1111+AT-1197+AT-1198, is much lower (107°), and close to that of Cranium 5 (111.2°). Apparently, midfacial prognathism develops during late adolescence in the Middle Pleistocene Sima de los Huesos population.

Midfacial prognathism can also be illustrated metrically by the difference between the distances from the transmeatal axis to the mesial edge of alveolus of upper M1 (AVR, alveolar radius) and to the lower end of zygomaxillary suture (ZMR, zygomaxillary radius) ([Howells, 1975](#)). The greater the differences (AVR-ZMR), the more anterior the position of M1 and more retracted the lower end of the zygomaxillary suture or, to sum up, the more Neandertal-like the midface. Atapuerca SH Cranium 5 and Petralona yield AVR-ZMR values (28.5 mm and 17.5 mm, respectively) that lie in the opposite extremes of the Neandertal range, with Broken Hill somewhere in between (26 mm according to [Stringer, 1983](#), and [Trinkaus, 1983](#), but only 19 mm to [Howells, 1975](#)).

The zygomaxillary angle (SSA) evaluates the projection of subspinale in front of the bi-zm:a line, that can also be measured as the difference between the subspinale radius (SSR) and the zygomaxillare radius (ZMR). Neandertals exhibit high values for this difference (between 34 mm and 45 mm). In Petralona it is 33 mm ([Stringer, 1983](#); [Stringer et al., 1979](#)), a similar value is calculated with [Howells' \(1975\)](#) estimations for Broken Hill and Cranium 5 yields a higher value of 41.5 mm.

[Howells \(1975\)](#) also noted that, as a consequence of the special topography of the midfacial region in Neandertals (with a more sagittally oriented infraorbital plate), the distance from the upper end of the zygomaticomaxillary suture to the ear opening (ZOR, zygoorbitale radius) is substantially greater than the distance from the lower end of the suture (ZMR). Actually, La Chapelle-aux-Saints (16 mm; [Howells, 1975](#)), La Ferrassie 1 (15 mm; [Howells, 1975](#)), Shanidar 1 (13.6 mm; [Trinkaus, 1983](#)) and Atapuerca SH Cranium 5 (13.5 mm) yield great values, but Shanidar 5 yields a very low ZOR-ZMR value (4 mm; [Trinkaus, 1983](#)). Comparable figures to those of Petralona (10 mm; [Stringer, 1983](#)). Broken Hill (9 mm; [Howells, 1975](#)) and Gibraltar 1 (around 10 mm) can also be found in early moderns like Predmostí 3, Zhoukoudian Upper Cave 101 or maybe Skhül 5 ([Howells, 1975](#)). In consequence, it seems that ZOR-ZMR does not clearly separate Neandertals from other fossils. From [Table 1 in Frayer \(1992\)](#) it seems that European Neandertals show considerably greater (and statistically significant) facial projections compared with the European Early

Upper Palaeolithic sample for points in the midplane (prosthion, nasospinale, nasion, glabella), in the lateral border of the nasal aperture (alare), or in the alveoli (M1/M2, P3/P4, I2/C), but that there is no difference in projection for zygomaxillare or zygoorbitale.

Visual inspection of Bodo shows that neither subspinale, nor M1 and zygoorbitale are in an advanced position with respect to zygomaxillare anterior, so that the AVR-ZMR, SSR-ZMR and ZOR-ZMR values must be low.

As noted before, associated with midfacial prognathism there is in Neandertals a relative anterior position of the posterior teeth that is manifested in the formation of the characteristic large retromolar space in the mandible or the elongation of the alveolar process behind the upper third molars. In Atapuerca SH Cranium 5, that region is broken, but the projective distance between the distal margins of the third molars and the contact between the maxillary alveolar process and the pterygoid process of the palatine is very long, around 18 mm. In Saccopastore 1, that distance is 8 mm (l.s.) and seems to be similar in Saccopastore 2. In Broken Hill, it is 7 mm, 6.2 in Petralona and only 5 mm in Arago 21 (measured on a cast). On the other hand, the maxillary dental arcade length (midsagittal distance from prosthion to a line tangential to distal margins of the third molar crowns) of Atapuerca SH Cranium 5 is reduced (56 mm) relative to Broken Hill (62 mm) and Arago 21 (64–65 mm, on a cast). Another manifestation of the advanced position of the molar series in Atapuerca SH Cr. 5 is the very anteriorly inclined roots of the upper molars, especially the third molars [Figure 4(b)], and of course the retromolar space of the mandible of this individual (AT-888+AT-721) as well as in the rest of the adult Atapuerca SH mandibles (Rosas, 1995).

Rak (1986), states that the unique facial morphology of Neandertals does not affect the position of prosthion in relation to the rest of the cranium. Although Trinkaus (1987) and Franciscus & Trinkaus (1995) consider that the “zygomatic retreat” model accounts for Neandertal facial morphology better than Rak’s “infraorbital plate” model, they believe that the total facial prognathism (defined as the distance from prosthion to the temporomandibular region) of the Neandertals was similar to that of their ancestors.

From Figure 21 it appears that Neandertals did not expand the prosthion–basion distance with respect to their European direct predecessors (Atapuerca SH Cranium 5 and Petralona) or the African fossils ER 3733, Broken Hill and Bodo. So, the maintenance of total facial length among the Neandertals (i.e., no anterior migration of prosthion) is plesiomorphous. On the contrary, there is a derived trend of reduction of total facial length in modern humans.

The projective midsagittal distance from orale to the transverse line across the middle of the glenoid fossae (a measurement close to the maximum projective length of the mandible), is longer in La Chapelle-aux-Saints, Amud 1, Shanidar 1, La Ferrassie 1, Monte Circeo, Gibraltar 1, than in Tabun 1, Saccopastore 1 and Saccopastore 2 (pointing to a diachronic trend). The group of Atapuerca SH Cranium 5, Broken Hill, Steinheim (estimated) and ER 3733, yields similar values to the smallest among Neandertals, in the upper half of the range of early modern humans and at the upper end of the range of the present day sample from Coimbra (Figure 22). Our data indicate that Neandertals kept the basion–prosthion distance constant relative to their ancestors, but the temporomandibular joint migrated backwards. For instance, the basion prosthion distance in Cranium 5 (119 mm) is similar to that of La Chapelle-aux-Saints (121 mm), but the distance orale–glenoid fossa is much longer in La Chapelle-aux-Saints (89.5 mm) than in Cranium 5 (71 mm). This migration of the temporomandibular joint was not predicted in the “zygomatic retreat” and “infraorbital plate” models, and can explain many aspects of the Neandertal morphology.

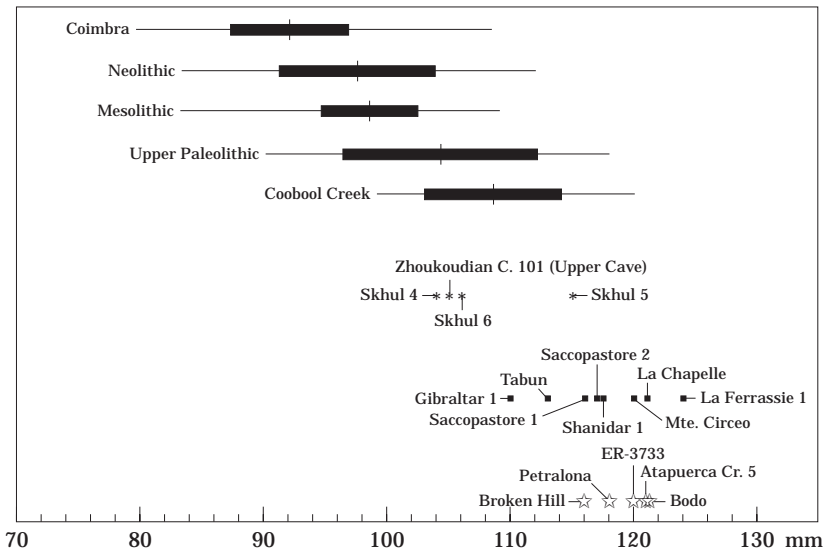


Figure 21. Basion–prosthion lengths for modern and fossil samples. Modern sample of Coimbra ($n=155$) from Martínez (1995). This sample consists of recent adult individuals of both sexes from the Instituto de Antropologia of the Coimbra University. Upper Paleolithic ($n=11$), Mesolithic ($n=33$) and Neolithic ($n=103$) samples from Frayer (1980). Coobool Creek Australian aborigines ($n=22$) from Brown (1989). Range and mean ± 1 standard deviation of the samples is indicated. Atapuerca SH Cranium 5, La Chapelle-aux-Saints, La Ferrassie 1, Monte Circeo, Gibraltar 1, Saccopastore 1 and 2, Broken Hill, Petralona, and Bodo were measured on the original specimens by the authors. Zhoukoudian (Upper Cave) C.101 was measured on a cast. Other sources: Tabun C1, Skhul 4, 5 and 6 (McCown & Keith, 1939), Shanidar 1 (Trinkaus, 1983), ER-3733 (Wood, 1991).

Multivariate analysis of facial variables

A PCA has been undertaken to assess the phenetic relationships between the Cranium 5 face and other facial fossil skeletons of *Homo*. The three first components account for 79.9% of the total variance in the data (Table 4). After oblique rotation, all the facial breadths (i.e., outer biorbital, internal biorbital, biorbital, bizygomatic, bimaxillary, interorbital and maxillo–alveolar breadths) have positive loadings higher than 0.7 on the first factor (that accounts for 57% of the sample variance), and correlations better than 0.7 with it (except for orbital breadth, with a loading of 0.59 and a correlation of 0.71 and nasal breadth with a loading 0.59 and a correlation of 0.75). The second factor represents variation in alveolar height, facial height and orbital height (loadings at least of 0.65 and correlations better than 0.7). The third component is a bipolar one, with a high positive loading for the zygomaxillary angle and a high negative loading for nasal height. The first component has a small positive correlation (0.35) with the second component and a similar negative correlation (-0.34) with the third component (Table 5).

In the three-dimensional space defined by the three first axes, Neandertals and early modern humans cluster in two well-defined and separated groups. The Lower and Middle Pleistocene specimens are scattered in the graph but none of them is particularly close to Neandertals or modern humans, except Jebel Irhoud that lies among the modern humans.

Bodo has the largest facial breadths of the sample, followed by Petralona, and SK 847 has the smallest score for the first axis (Figure 23). Saccopastore 1, Gibraltar 1 and Shanidar 1

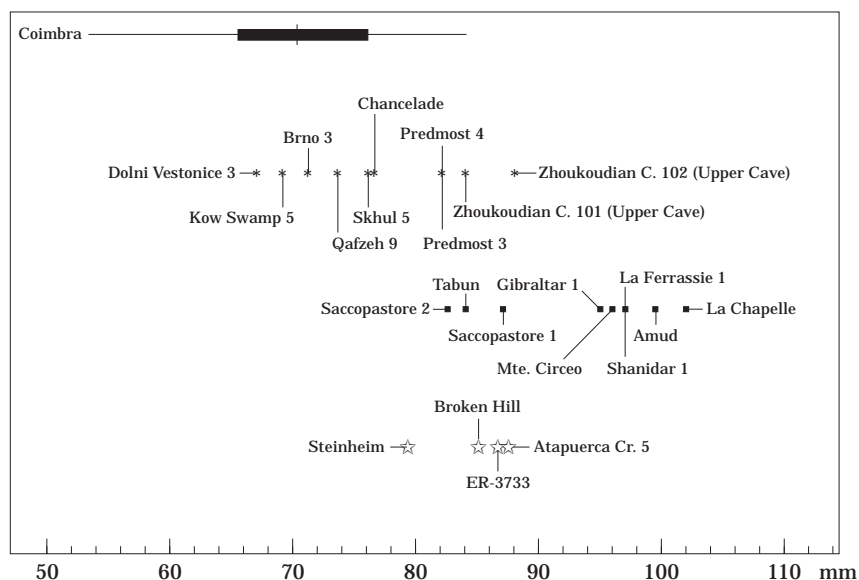


Figure 22. Projective (horizontal) midsagittal distance from orale to the transverse line across the middle of the glenoid fossae. The skulls were set in the foramen magnum plane. All measurements were taken by the authors, on casts in the cases of Dolní Vestonice 3, Brno 3, Predmost 3 and 4, Chancelade, Kow Swamp 5, Zhoukoudian (Upper Cave) C.101 and C.102, Skhul 5, Qafzeh 9, Shanidar 1, Amud 1, Steinheim and ER-3733 and on the originals in La Chapelle-aux-Saints, La Ferrassie 1, Monte Circeo, Gibraltar 1, Saccopastore 1 and 2, Tabun C1, Broken Hill and Atapuerca SH Cranium 5. ER 3733 and Steinheim (prosthion reconstructed) were measured on stereophotographs of the original fossils.

show narrower transversal facial measures than the other Neandertals of the sample. Neandertal scores for the third axis are low, reflecting subspinale protrusion and high noses. Although Atapuerca SH Cranium 5 has a low SSA, this fossil is above Neandertals for the third axis (as Broken Hill and Petralona). SK 847, ER 3733 and Bodo midfaces are very flat (probably the primitive condition for *Homo*). There is a debate over the specific attribution of SK 847 (Grine *et al.*, 1993). Our analysis shows that the main differences from *H. ergaster* (ER 3733) are in facial breadths (SK 847 is very narrow), but the phenetic distance between SK 847 and ER 3733 (Figure 23) is not greater than between some Neandertals. The modern humans in the analysis exhibit the lowest facial/alveolar/orbital heights, together with Arago 21, whose measurements are speculative due to the extensive postmortem distortion of the specimen.

Supraorbital torus thickness and morphology

The supraorbital torus is very well developed in the SH sample. We have taken the thickness of the supraorbital torus at three points following Smith & Ranyard's (1980) technique (Table 6). The torus gradually decreases in thickness from the medial point to the midorbital point except for Cranium 5 which is more even in thickness. Reaching the trigone, the thickness begins to increase slightly. The thickness at the lateral point in all the adult specimens from the Sima de los Huesos is above the Neandertal mean. Regarding the thickness at the midorbital point, three Atapuerca SH adult individuals are above the range of our Neandertal sample,

Table 4 Principal component analysis of facial variables

	Factor 1		Factor 2		Factor 3	
	Pct of var: 57.0%		12.8%		10.1%	
	Cum var: 57.0%		69.7%		79.9%	
	Pattern matrix	Structure matrix	Pattern matrix	Structure matrix	Pattern matrix	Structure matrix
Facial variables:						
M43. Outer biorbital breadth	0.91	(0.90)	0.03	(0.34)	0.06	(-0.25)
M43a. Internal biorbital breadth	0.86	(0.94)	0.16	(0.47)	-0.06	(-0.38)
M44. Biorbital breadth	0.99	(0.96)	-0.11	(0.24)	-0.01	(-0.32)
M45. Byzygomatic breadth	0.89	(0.87)	-0.26	(0.10)	-0.20	(-0.45)
M46b. Bimaxillary breadth	0.91	(0.87)	0.07	(0.35)	0.20	(-0.12)
M48. Upper facial height	0.21	(0.56)	0.72	(0.85)	-0.29	(-0.50)
M48(1). Alveolar height	-0.05	(0.23)	0.98	(0.92)	0.17	(0.01)
M49a. Interorbital breadth	0.90	(0.88)	-0.01	(0.31)	0.05	(-0.25)
M51a. Orbital breadth	0.59	(0.71)	-0.05	(0.24)	-0.43	(-0.61)
M52. Orbital height	0.04	(0.35)	0.65	(0.72)	-0.24	(-0.38)
M54. Nasal breadth	0.59	(0.75)	0.36	(0.59)	-0.09	(-0.36)
M55. Nasal height	0.25	(0.56)	0.18	(0.41)	-0.73	(-0.85)
M61. Maxillo-alveolar breadth	0.71	(0.81)	0.30	(0.55)	0.02	(-0.28)
M76a. Zygomaxillary angle	0.14	(-0.18)	-0.01	(-0.15)	0.96	(0.92)

Values of the factor pattern matrix (i.e., matrix of factor loadings) and in parentheses values of the factor structure matrix (i.e., matrix of correlations between variables and factors), after oblique rotation. Loadings above 0.6 are highlighted. Abbreviations as in Table 2.

Table 5 PCA of facial variables: factor correlation matrix after oblique rotation

	FACTOR CORRELATION MATRIX		
	Factor 1	Factor 2	Factor 3
Factor 1	1.000		
Factor 2	0.353	1.000	
Factor 3	-0.337	-0.193	1.000

and the rest of the Sima de los Huesos adult frontal bones are above the Neandertal mean. With respect to the thickness at the medial point, the Sima de los Huesos adult fossils show figures around the Neandertal mean (Figure 24).

The Middle Pleistocene specimens that we include in this analysis (Bodo, Broken Hill, Petralona, Steinheim and Arago 21) show a decrease in torus thickness from the medial point to the midorbital point, and another decrease from the midorbital point to the lateral point (except in Arago 21) (Figure 25). For the lateral point thickness, these fossils yield figures within the Neandertal range except Broken Hill which is slightly above it (Table 6). The midorbital point thicknesses of Bodo, Broken Hill and Petralona are well above the upper limit of the Neandertal range and close to some of the Atapuerca SH adult specimens. Steinheim and Arago 21 display figures close to the Neandertal mean. With respect to the medial point, the thicknesses of Broken Hill and Petralona are well above the Neandertal range and the Atapuerca SH figures. Bodo is above the Neandertal range but close to its superior limit and

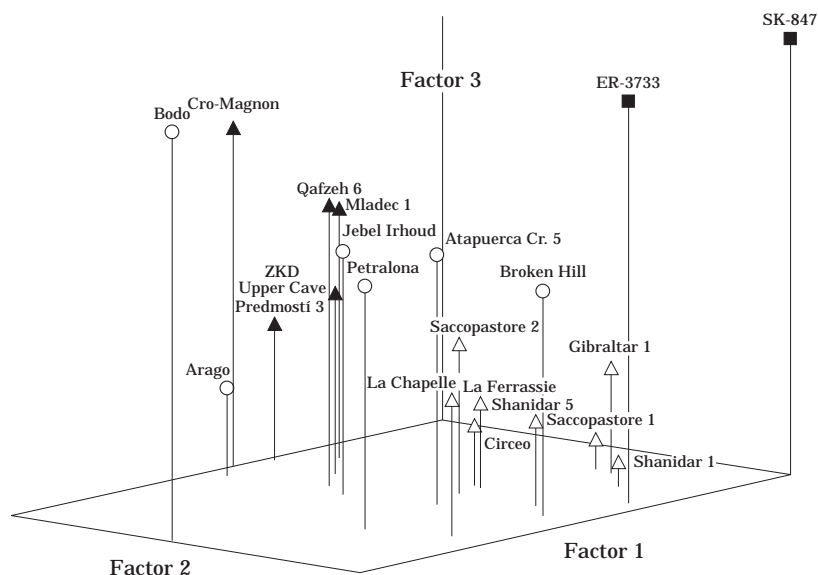


Figure 23. Scatterdiagram in the space of the first, second and third principal components of facial variables. Several bilateral diameters of SK 847 were recorded by doubling the distance from the left biometric point to the midplane. The SSA value of this fossil is estimated, but certainly the midface is transversally flat and the angle is high. (■) *Homo erectus s.l.*; (△) Upper Pleistocene Neandertals; (▲) Modern humans; (○) Middle Pleistocene.

Steinheim is within the range but at the upper end, while Arago is close to the Neandertal mean and the Atapuerca SH figures. All of them (except Arago 21) show thicknesses at the medial point above the Atapuerca SH sample.

The juvenile specimens from the Atapuerca SH sample show thickness figures (see Table 6) that clearly depart from the adult values, especially at midorbital and lateral points.

All the adult specimens from the Sima de los Huesos sample display continuity between the three elements of the supraorbital torus (lateral, orbital and glabellar segments, *sensu* Smith & Ranyard, 1980), as is characteristic of the Neandertal group. The orbital and lateral segments follow the orbital contour. A more or less developed supratatorial sulcus separates the torus from the frontal squama. In Cranium 5, AT-400+AT-1050 and AT-630+AT-777+AT-1168+AT-1550, a small supraglabellar fossa of triangular shape can be seen. In AT-200, AT-237+AT-499+AT-1155+AT-1156 and especially in the adolescent Cranium 6, the torus is more continuous through the glabellar segment, as in the Bilzingsleben frontal bone. Among Neandertals both morphologies can be found. Only in AT-200 and, particularly, in AT-630+AT-777+AT-1168+AT-1550, a slight glabellar depression extending to nasion is present, as in Arago 21, Petralona and, less pronounced, in Broken Hill (*contra* Wolpoff, 1980). This sulcus is absent in Steinheim.

Some of the frontal bones from the Sima de los Huesos (Cranium 4, AT-630+AT-777+AT-1168+AT-1550, AT-400+AT-1050) display a supraorbital morphology that is also present in the Middle Pleistocene specimens Arago 21, Bodo, Broken Hill and Dali. In these fossils, the glabellar segment faces anteriorly, the medial part of the orbital segment faces anterosuperiorly and the lateral part of the orbital segment, as well as the lateral segment, are rounded or slightly flattened. In the words of Weidenreich (1943: p. 198):

Table 6 Supraorbital torus thickness

Specimen	Side	TLP	TMOP	TMEP	Source
SH sample					
Cranium 4	l	12.0	11.5	15.4	Original, authors
	r	12.6	11.3	—	
Cranium 5	l	14.6	14.1	15.3	Original, authors
	r	—	—	15.0	
AT-121+	l	14.0	14.0	(16.0)	Original, authors
AT-1545					
AT-200	r	—	16.5	—	Original, authors
AT-400+	r	12.7	11.1	14.2	Original, authors
AT-1050	l	13.1	11.6	—	
AT-630+ . . .	r	11.3	10.9	15.0	Original, authors
AT-1550	l	11.0	10.8	(15.2)	
AT-237+ . . .	l	13.9	10.9	15.6	Original, authors
Cranium 3	l	8.2	7.9	12.2	Original, authors
	r	—	(7.8)	—	
Cranium 6	r	8.0	7.5	—	Original, authors
	l	8.0	7.4	—	
AT-465+ . . .	r	7.5	7.5	14	Original, authors
AT-626+	l	6.5	6.8	12.1	Original, authors
AT-1150					
Neandertals					
Min		8.2	6.4	12.5	La Chapelle, Gibraltar 1, Tabun, La Quina 5, Monte Circeo, Kr. 3, Kr. 4, Kr. 6, Kr. 23, Kr. 28, Kr. 37.1, Kr.
Max		15.1	13.9	18.0	37.3, Kr. 37.4, Kr. 37.5, Kr. 37.6, Kr. 37.7, Kr. 37.8,
Mean		11.0	10.1	15.0	Kr. 37.10; Vindija 261+258: Original, authors; La
S.D.		1.5	1.5	1.6	Ferrassie, Neandertal, Spy2, Amud, Shanidar 1, Spy 1,
<i>n</i>		23	24	19	Engis 1: Casts, authors.
Middle Pleistocene					
Bodo	l	13.3	14.2	18.4	Original, authors
Broken Hill	l	16.1	16.7	21.9	Original, authors
Petralona	l	12	15.6	21	Original, authors
Steinheim	r	9.8	10.1	17.1	Cast, authors
Arago 21	l	11.4	9.6	15.0	Original, Spitzery (1982)

All measurements in millimetres. Thickness at the medial point (TMEP), the lateral point (TLP) and the midorbital point (TMOP), following Smith & Ranyard (1980). To these authors, the latter point is that of minimum thickness between the first two points, and is located "on the lateral aspect of the orbital segment of the torus approximately a third of distance from the lateral to the medial point" (Smith & Ranyard, 1980: pp. 596–597). We take the thickness at that level in all the fossils where the torus is not "pinched" between the medial and the lateral points. For the comparative samples, all measurements in the table come from the left side (when possible). Sets: AT-630+AT-777+AT-1168+AT-1550; AT-237+AT-499+AT-1155+AT-1156; AT-465+AT-624+AT-764+AT-765+AT-766+AT-1159. SD=standard deviation, *n*=sample size. Crania 3 and 6, as well as AT-465+AT-624+AT-764+AT-765+AT-766+AT-1159 and AT-626+AT-1150 are juvenile specimens. Stringer *et al.* (1979) report for the Petralona original fossil a lateral thickness of torus of 15.9 mm, and a medial thickness of torus (at notch) of 20.8 mm. Kr=Krapina.

"The contours of the glabellar torus and the supraorbital tori [of *Sinanthropus*] are not rounded but show rather sharply defined surfaces. There is in particular a well developed edge where the superior and anterior surfaces meet. It is found in the Rhodesian and Ngandong skulls, whereas the other neandertalians show rounded tori"

Although Spitzery (1980) states that this morphology can also be found (less marked) in Neandertals ("apparence de torsion de la région supraorbitaire"), we cannot recognize the same morphology that is present in Arago 21 (for example) in any Neandertal fossil. Instead, Neandertals show a typical rounded aspect of the supraorbital torus, as in the Atapuerca SH

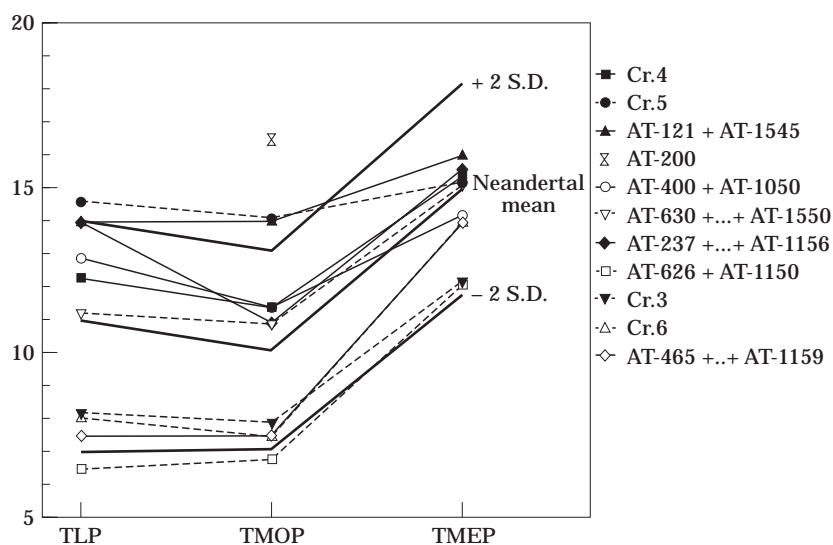


Figure 24. Supraorbital torus thickness of the Atapuerca SH sample compared with Neandertals. For the Atapuerca SH fossils we used the average between the right and left sides when both are preserved. Measurements in millimetres. S.D., standard deviation of the Neandertal sample (composed of the same specimens than in Table 6). Crania 3 and 6, as well as AT-465+AT-624+AT-764+AT-765+AT-766+AT-1159 and AT-626+AT-1150, are juvenile specimens. Sets and abbreviations as in Table 6.

Cranium 5 and AT-237+AT-499+AT-1155+AT-1156. Thus, in the Sima de los Huesos sample both character states are represented, the rounded torus of Neandertals being the apomorphic condition and the “torsioned” torus the plesiomorphic one.

In superior view the glabellar segment is the most projecting point of the supraorbital profile in all the Sima de los Huesos complete frontal bones, but in no case is there an arched profile as shown by the so-called “classic” Neandertals. On the other hand, the morphology in Atapuerca SH does not exhibit the typical *H. erectus* profile, where the lateral segments of the torus project anteriorly to the same extent as the glabellar portion, or slightly somewhat less. Thus, the Sima de los Huesos frontal bone contour in superior view display an intermediate state between the straight, shelf-like supraorbital torus and the curved one (as also occurs in Zuttiyeh, Krapina, Tabun 1 and Ehringsdorf H), showing that the lateral portion of this superstructure does not recede as much as in the curved morphology. Among the Middle Pleistocene specimens, Arago and Steinheim show more straight tori than Bodo, Broken Hill and Petralona, that present much more curved ones.

In all the frontal bones from the Sima de los Huesos sample where the central part of the superior border of the orbit is preserved, at least one supraorbital notch is well defined. Only AT-400+AT-1050, that presents the greatest notch of the sample, displays an acute lateral tubercle.

A well-vaulted roof of the orbit is present in all the frontal bones from the Sima de los Huesos, as can be seen in Neandertals and modern *H. sapiens*. This character shows another state among Asian *H. erectus*, where the orbital roof is flat (Weidenreich, 1943). Weidenreich (1943) also claims that the orbital roof is flat in Broken Hill, but in our opinion its orbits are clearly concave as well as those of Arago 21, Steinheim and Petralona. On the contrary, OH-9 displays a flat orbital roof.

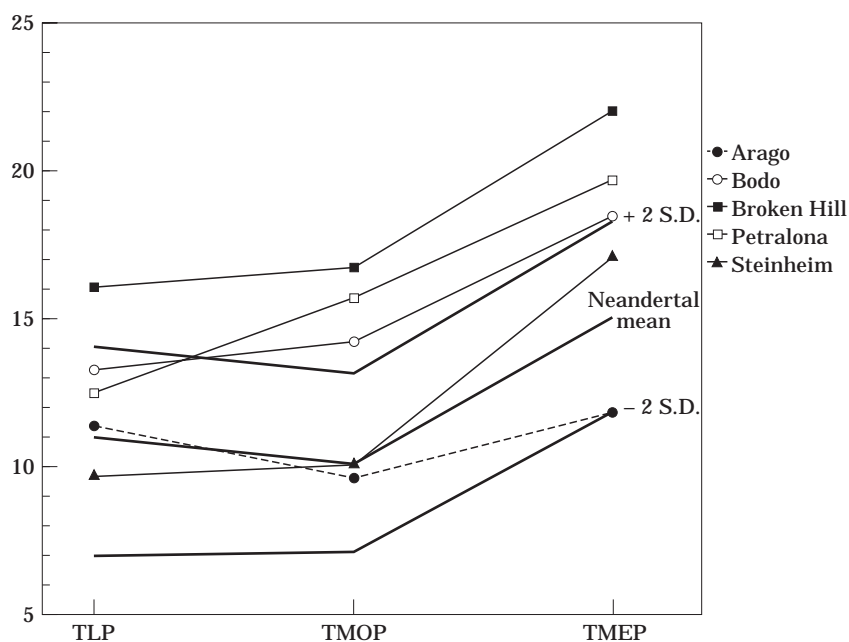


Figure 25. Supraorbital torus thickness of European and African Middle Pleistocene fossils compared with Neandertals. Measurements in millimetres. S.D., standard deviation of the Neandertal sample (composed of the same specimens as in Table 6). Abbreviations as in Table 6.

In the preserved naso-glabellar regions from the Atapuerca SH sample there is no nasal root depression, as in Neandertals. The naso-frontal suture is horizontal in the SH sample, as in the Asian *H. erectus* sample (Weidenreich, 1943). In Neandertals we can find both the Sima de los Huesos morphology and an inverted “V” shape.

Vermiculata

A vermiculate cortical surface pattern in brow ridges has been described in many fossil hominids and it is occasionally found in modern human populations and non-human primates (Tappen, 1973, 1980, 1983; Oyen *et al.*, 1979, 1981). This pattern is characterized by a worm-track surface and occasional pits. We found this cortical surface pattern in all the adult supraorbital tori recovered at the Sima de los Huesos. The distribution of the grooved and pitted areas of the brow ridges varies among the sample but some general patterns can be established. All the adult specimens from the Atapuerca SH sample display, at least, a worm-track pattern laterally to the supraorbital notch, covering the anterior and superior surfaces of the supraorbital torus. Cranium 4 shows this vermiculated pattern also on the medial orbital segments and glabella, and in AT-200 the orbital segment is pitted, but some grooves can be found in the glabellar region. The rest of the sample grades medially to a pitted pattern, sometimes restricted to the glabellar region. We found another bilateral region that always present a dense pitted pattern. These are characteristic triangular areas located behind the trigones and on the superior surface of the frontal squama, medially to the temporal lines.

In the juvenile specimens from SH only a pitted pattern is present (except for Cranium 6 that shows small ridges on the trigones) and it is quite different from the adult pitted pattern, showing a much more porous aspect that probably represents a different type of bone remodelling processes. Although in these specimens the supraorbital torus is not yet developed, this pitted pattern is seen in all the regions that will eventually form up the supratoral structure.

Frontal torus growth and pneumatization

The frontal remains AT-121+AT-1545, AT-200, AT-400+AT-1050, Cranium 4, Cranium 5, AT-630+AT-777+AT-1168+AT-1550 and AT-237+AT-499+AT-1155+AT-1156 show dimensions (Table 6), overall form and a well-developed vermiculate pattern that lead us to place them among the adult category. Regarding the juvenile individuals, there are two different stages within the Atapuerca SH sample. The adolescent category includes those specimens that have not reached the thickness dimensions of the adult stage, but already have developed a projection of the three supraorbital elements that permits us to distinguish the superstructure from the squama. Some vermiculate pattern restricted to the supraorbital trigone may also be present. Crania 3 and 6 are included in this group. In AT-626+AT-1150 and AT-465+AT-624+AT-764+AT-765+AT-766+AT-1159 there is only a slight bulging on the glabellar region and no or almost no buildup of bone laterally between the frontozygomatic suture and frontotemporale; there are no signs of vermiculate pattern in any portion. AT-626+AT-1150 corresponds to a child (before M2 emergence), but AT-465+AT-624+AT-764+AT-765+AT-766+AT-1159 is more developed and could be a late child or an early adolescent.

The Sima de los Huesos adult specimens exhibit well-developed frontal sinuses (i.e., there is neither aplasy nor hypoplasia *sensu* Tillier, 1977): Cranium 4, Cranium 5, AT-200, AT-400+AT-1050, AT-237+AT-499+AT-1155+AT-1156, AT-630+AT-777+AT-1168+AT-1550. The juvenile specimens Cranium 6 and AT-465+AT-624+AT-764+AT-765+AT-766+AT-1159 only show small fronto-ethmoidal cavities that do not reach superiorly the level of the upper orbital borders, but in the child AT-626+AT-1150, the sinus extends upwards beyond that level. Since in modern humans the main enlargement of the frontal sinus is completed at around 16 years for boys and 14 years for girls (Brown *et al.*, 1984), it is very likely that Cranium 6 would show frontal sinus hypoplasia when adult. Neandertals show well-developed frontal sinuses, as in general do Middle Pleistocene fossils, although Arago 21 display a non-pneumatized supraorbital torus (Tillier, 1977), like the Zhoukoudian skulls except Zhoukoudian 3 and, according to Day (1986), the “1966 Skull” (Zhoukoudian 5).

Midfacial topography

The Neandertal midfacial topography is characterized, among other aspects, by the “horizontal” position of the broad nasal bones, with forward projection of the “nasal apophyses of the maxillae” (*sensu* Rak, 1986) and almost horizontal nasomaxillary sutures, the “parasagittal” orientation of the infraorbital bone plate (although actually its orientation is intermediate between coronal and sagittal), the presence of a flat, convex or minimally concave infraorbital region, and the straight zygomaticoalveolar crest with absence of a notch (Rak, 1986; Trinkaus, 1987).

Rak (1986) distinguishes two topographic units in the infraorbital region. The more relevant one is vertical, “parasagittally” oriented and with a triangular shape. The smaller one is a

somewhat horizontal triangle that extends as a shelf from the medial two-thirds of the inferior orbital margin. Rak (1986: p. 161) also observes that the inferomedial corner of the orbit in some Neandertals is affected by the upward pull of the nasal apophyses, and “tapers in an unusual fashion”. Actually, the upper orbital margin is arched (as the supraorbital torus) and the lower orbital margin is very inclined (latero-inferiorly) as a consequence of the inflation of the maxillary frontal process, so that the “classic” Neandertal orbit outlines are very characteristic (as can also be seen in Rak’s representations of the idealized Neandertal face). This morphology is not found in the Sima de los Huesos faces, but it can be observed in Steinheim (although it can be affected by distortion).

The *Homo* facial topography lateral to the nasal aperture (midface) can be divided in two planes: the infraorbital plate and the lateral wall of the nasal cavity. According to Rak (1986), in the “generalized” face the infraorbital plates are coronal, and their anterior surface slopes down and slightly backwards. At the junction with the snout (or side walls of the nasal cavity), this inclination produces the depression in the face called the canine fossa. The lateral nasal plane is more evident when there is a marked nasal projection, and it becomes reduced when the nasal aperture does not protrude much. In sum, the “generalized” midface has several major components: (1) an “inflected” horizontal section of the nasomaxillary region, which is determined by (2) a coronally oriented infraorbital plate and (3) a more or less parasagittal (and developed) lateral nasal wall, and finally, (4) an anterior surface of the infraorbital plate sloping down and backwards, that in turn produces a canine fossa. Besides these structural features, the inferior margin of the infraorbital bone plate is usually curved.

Although the “generalized” morphology can be found in some fossils and in modern humans, this is certainly not the case for the first fossils of *Homo*. Actually, in early *Homo* (OH 24, ER 1813, ER 1470, WT 15000 and SK 847) the nasal projection is small or very small and lateral to the nasal aperture there is almost only one plane, that is vertical or slightly anteroinferiorly sloping, and without a proper canine fossa (or only with a shallow concavity). The infraorbital plate also slopes markedly down and forwards in australopithecines. The term canine fossa has been used with different meanings and can be misleading. Maureille (1994), terms “infraorbital depression” a general infraorbital inflection (visible in the transverse cross section of the face), and canine fossa a localized depression on the anterior face of the maxillary or zygomatic bones. We use the term canine fossa in the sense above explained (i.e., not any kind of depression but a major component of the “generalized” midfacial pattern), that is equivalent to Maureille’s “infraorbital depression”.

In Neandertals, there is a marked nasal projection and both planes (infraorbital plate and nasal wall) are continuous and face midway between anteriorly and laterally. In fact, Rak’s “parasagittal” infraorbital plate of Neandertals incorporates both planes and is not homologous with the infraorbital plate of the “generalized” face, which is strictly infraorbital, as Trinkaus (1987) points out.

To what extent Steinheim’s facial topography is affected by posthumous distortion remains uncertain, but we agree with Rak (1986) in viewing this fossil as having almost a “generalized” face (i.e., non-Neandertal). Actually Steinheim looks as if it had experienced a marked nasal projection resulting in a very large (and parasagittal) lateral nasal plane, without changing the coronal orientation of the infraorbital plane (both planes join at the infraorbital sulcus). We believe that the Steinheim morphology is somewhat exaggerated by distortion, but it represents a perfect model for the character state anterior to the Neandertal face. The Asian Middle Pleistocene skull from Dali also exhibits a marked inflexion between the infraorbital

region, facing frontally, and the lateral walls of the nasal cavity, parasagittally oriented, although again there is some post-mortem distortion of the face.

In Atapuerca SH Cranium 5 both planes (the infraorbital plate and the nasal wall) are not continuous and meet in a wide angle at the marked infraorbital sulcus. In other words, the anterior surfaces of the maxillae are not flat or convex as in Neandertals [Figures 4(b) and (d)]. Instead, the maxillae are clearly concave (in horizontal contour), more than in Petralona but still far from the “inflected” transverse cross section of the Steinheim right maxilla. In fact, Atapuerca SH Cranium 5 is a perfect example of a morphology intermediate between Steinheim in its present state and the “extended” maxillary bones of Neandertals. If the Steinheim maxillary inflection is exaggerated by post-mortem distortion, its original morphology could have been very similar to Cranium 5. This is probably not the case for Arago 21, which, although distorted, seems to correspond to a more Neandertal morphology. Spitey (1982) relate Arago 21 and Petralona to the Neandertals based on the morphology of the maxillary bone. Bodo and Petralona are similar in that both fossils only exhibit one plane lateral to the nasal aperture, but in Petralona it is more sagittally oriented than in Bodo, although clearly less than in Neandertals, except Saccopastore 2, which is in fact reminiscent of Petralona in facial morphology.

The fragmentary faces AT-1100+AT-1111+AT-1197+AT-1198 and AT-767+AT-963 show similar maxillary topography to that of Cranium 5. On the contrary, the anterior surface of the AT-404 left maxilla is very depressed [Figure 11(b)], instead of inflated as in Neandertals, but unfortunately, it is not possible to know the complete transverse cross section of AT-404, in order to establish the facial morphological pattern.

As in Petralona and apparently in Altamura (Pesce Delfino & Vacca, 1993), AT-638+AT-772 shows a marked angulation between the flat anterior surface of the maxilla (corresponding to the front teeth) and the rest of the external surface of the bone.

In Atapuerca SH Cranium 5, the inferior margin of the infraorbital bone plate (zygomaticoalveolar crest) is gently curved [Figure 4(d)], instead of being straight as is typical in Neandertals. The presence of external and/or internal maxillary tori is common among Middle Pleistocene fossils, like Arago 21 and Arago 45 (Lumley & Spitey, 1982), Petralona, Broken Hill or Steinheim. In the Atapuerca SH adult sample, Cranium 5 lacks any maxillary torus, but AT-638+AT-772 exhibits a thick internal torus at the M2 level (the M3 internal alveolar wall is abraded). The external surface of the alveolar process of this specimen is much eroded, but there are indications of an extensive external maxillary torus. In AT-1130 the external alveolar torus is reduced to a series of tubercles.

Subnasal morphology

According to Stringer (1984), Neandertals share with a majority of modern humans a raised and sharp lower rim of the nasal margin, not sharply defined in *H. erectus* or in hominoids (the primitive condition). In Atapuerca SH Cranium 5 only the right side preserves intact the original morphology [Figures 4(d) and 12(c)], the left one being affected by bone remodeling of pathological origin (Pérez *et al.*, 1997). On the right side there is a spinal crest (crista spinalis sensu Gower, 1923; McCollum *et al.*, 1993), that originates from the nasal spine and runs in a postero-lateral direction across the floor of the nose. The turbinal crest (crista turbinalis sensu Gower, 1923) is sharper at its superior extremity (near the inferior turbinal) and inferior end, which fuses with the spinal nasal crest (according to Gower, 1923, the central portion of the turbinal crest is usually flat, as in Cranium 5). It should be noted that Gower's turbinal crest is

different from the conventional crista conchalis or inferior turbinal crest, which is the root of the concha nasalis inferior or turbinatum inferior (the latter is horizontal and Gower's turbinal crest is vertical). In Cranium 5, in front of the spino-turbinal crest (fused spinal and turbinal crests), there is a lateral nasal crest (crista lateralis) that originates from the lateral margin of the nasal aperture and continues along the nasoalveolar clivus (beneath the level of the nasal spine), curving inward and fading out at the vertical between I2 and I1. Since the angle between the spinal crest and the medial palatal suture is around 45°, the spinal crest runs posteriorly and the turbinal crest (*sensu* Gower, 1923) ends at a posterior point in the inferior turbinal crest. As a consequence, there is a broad space between the spino-turbinal crest and the lateral crest, with a prenasal fossa between them in the lateral inferior corner of the nasal aperture. On the left side only the upper end of the turbinal crest can be appreciated. In AT-638+AT-772, the right side of the nasal aperture shows exactly the same pattern as Cranium 5.

Bodo and Broken Hill show a similar morphology, that seems primitive for *Homo*. Although in modern humans there are different types of lower narial margins and prenasal fossae (Lahr, 1994), the Atapuerca SH Cranium 5 pattern is very unusual in its broad separation between crests. In AT-767+AT-963 (an adolescent of around 14 years according to modern human standards), the left side lateral nasal crest and spino-turbinal nasal crest are smooth and the prenasal fossa less marked than in Cranium 5. Cranium 6 (also adolescent) seems to exhibit this configuration, but in AT-1100+AT-1111+AT-1197+AT-1198 (a late adolescent/early adult of 16–18 years) there are no crests, the nasal spine is isolated and the nasal sill is rounded.

On the contrary, in Neandertals, as in Arago 21, the lateral nasal margins continue medially as sharp inferior nasal rims that meet at the nasal spine. In Petralona, the lateral nasal border duplicates in two lateral crests that meet in the nasal spine (delineating a small fossa between them).

Schwartz & Tattersall (1996) describe among other derived traits of the Neandertal nose, an “internal nasal margin” bearing a large internal projection. The morphology of the lower border of the piriform aperture can be very clearly appreciated in the Monte Circeo (Guattari 1) fossil (specially on the left side). In this specimen the lateral crests continue as well-defined ridges curving inward and extending as far as the nasal spine, forming the lower rim of the piriform aperture. This rim does not result from spino-lateral fusion, because behind it there is also a spinal crest united to the turbinal crest (the “internal margin” of Schwartz & Tattersall, 1996, actually represents this spino-turbinal nasal crest). In Monte Circeo, the spino-turbinal nasal crest conflues superiorly with the inferior turbinal crest (the root of the concha nasalis inferior), and above it raises the medial projection observed by Schwartz & Tattersall (1996).

Atapuerca SH Crania 5 and 6, AT-767+AT-963 and AT-1217 (a small maxillary fragment) do not exhibit any medial projection, there is a light swelling in AT-1665 (another small maxillary fragment) and AT-638+AT-772, and the projection is more marked in both sides of AT-1100+AT-1111+AT-1197+AT-1198 and AT-1666 (another small maxillary fragment, where it can be appreciated that the swelling is built up of solid bone). Petralona lacks internal medial projections.

The Neandertal morphology clearly derives from that seen in Atapuerca SH Cranium 5 by (1) raising the fusion of the spinal and turbinal nasal crests forming a continuous and sharp “internal nasal margin”, (2) continuity of the lateral nasal crests that are confluent with the nasal spine and form an “external margin” of the nasal aperture (with a sulcus) between the “internal” and “external” nasal rims, and (3) raising of a bone swelling just above the inferior turbinal crest (the medial projection of Schwartz & Tattersall, 1996).

Finally, Atapuerca SH Cranium 5, AT-1100+AT-1111+AT-1197+AT-1198 and AT-767+AT-963 show a flat and horizontal nasal floor, instead of the lowered and sloping nasal floor relatively to the nasal lower rim described as a Neandertal apomorphy, also found in Petralona (Stringer, 1983; Stringer *et al.*, 1984). The nasal floor of AT-638+AT-772 is very incomplete, but it looks more lowered.

Endocranial traits

The three frontal convolutions of the brain are clearly marked on the endocranial surface of the frontal bones from the Sima de los Huesos sample. The anterior pole of the third convolution corresponding to Broca's area is very distinct from the other two convolutions. There are virtually no vascular impressions on the frontal bones. We have recovered three isolated cristae galli (AT-205, AT-237 and AT-738), AT-237 belongs to the isolated frontal bone AT-499+AT-1155+AT-1156, and Crania 4 and 5 preserve the apophysis in place. The isolated frontal bone AT-630+AT-777+AT-1168+AT-1550 preserves half of the apophysis. There are no significant differences in size and shape of these cristae from those of modern humans. In the frontal bones where the region is preserved (Cranium 6 and also the juvenile individual composed of AT-465+AT-624+AT-764+AT-765+AT-766+AT-1159) the anterior surface of the foramen caecum is present. It is important to notice that Weidenreich (1943) could not find the foramen caecum nor any crista galli apophyses among the Zhoukoudian specimens, and that he considered these structures could be absent in them, as among "anthropoids". The apophysis is present in Neandertals and Middle Pleistocene specimens such as Bodo, Arago 21, Petralona and Broken Hill, as well as in Zuttiyeh.

From a phylogenetic point of view, the most remarkable endocranial traits on the parietal bone are the presence/absence of two vascular impressions, the Breschet sinus and the lateral sulcus in the asterionic region (Gracia, 1991; Arsuaga *et al.*, 1989; Arsuaga *et al.*, 1991). Among the Sima de los Huesos specimens, only Cranium 8 shows a well-marked Breschet sinus running parallel to the coronal suture in the left parietal bone, ending in a Pacchioni's fossa. This trait is considered apomorphous for Neandertals (i.e., it is very frequent in Neandertals, but rare in modern populations and Middle Pleistocene specimens: Gracia, 1991). Regarding the lateral sulcus in the Atapuerca SH sample, in no case does the parietal bone show traces of the sinus in the asterionic region. Moreover, in the SH temporal bone sample the lateral sulcus always enters in the temporal bone from the occipital bone, without crossing the parietal bone (Martínez & Arsuaga, 1997). As we have reported elsewhere (Arsuaga *et al.*, 1989; Arsuaga *et al.*, 1991), the presence of a lateral sulcus in the parietal bone is considered a derived condition usually found in modern humans and sometimes in Neandertals.

An enlarged occipito-marginal (O-M) sinus system is present in two out of four individuals from the Atapuerca SH sample that preserve the foramen magnum region. Cranium 6 displays an enlarged O-M sinus bilaterally, but specially well pronounced and ending at the jugular foramen on the right side. The sinus sagittalis superior seems to flow down directly to the right enlarged O-M sinus, while the right and the weak left transverse sulci impressions appear to be more related to the straight sinus. AT-1661 is a very small basioccipital fragment preserving part of the foramen magnum border (probably the right side), that endocranially shows a well-enlarged O-M sinus. The other two specimens, Crania 4 and 5, do not show any atypical variation of the occipital venous sinuses.

Among the Middle Pleistocene specimens, Falk (1986) finds a right O-M sinus in Swanscombe but we consider that an enlarged O-M system is absent in this specimen, as

stated by Kimbel (1984). Falk (1986) also reports a bilateral absence of an enlarged O–M sinus system in Arago 21 (cast), but since no occipital bone has been recovered in this site, the specimen studied must be the composite skull made of Arago 21 facial skeleton, Arago 47 parietal bone, the Sangiran 17 temporal bone and the Swanscombe occipital bone! Kimbel (1984) finds evidence of a left-sided O–M sinus system in a cast of the Vértesszöllös occipital fragment. Broken Hill lacks, on the well-preserved left side, signs of presence of the O–M sinus system. Petralona shows O–M pillars bilaterally, that do not necessarily correspond to O–M drainage impressions.

Although the phylogenetic relevance of the presence/absence of an enlarged occipito-marginal sinus system is controversial (see Falk & Conroy, 1983; Falk, 1986; Falk *et al.*, 1995; Kimbel, 1984; Kimbel *et al.*, 1994), it seems that a high frequency of this trait is present in the robust australopithecine lineage (including *A. afarensis*) and low frequencies in the other hominids. The high frequency of the trait in the SH sample (in spite of the small sample size), as well as the high frequencies of some epigenetic traits, like the frequent presence of lambdatic wormian bones [Figures 1(b), (d), 6(a), 8(a), (b), (d), (e)], could be indicative of a strong kinship among the specimens recovered at the Sima de los Huesos site.

Cranial thickness

Cranial thickness is remarkable in the Sima de los Huesos sample (Arsuaga *et al.*, 1989, 1991). The SH thickness range at the parietal boss is 8.5 mm–10 mm for seven juvenile specimens. Concerning the adults, Cranium 8 is very thick at the parietal boss (13 mm), and Crania 1 and 2 lack the parietal eminence, but their thicknesses are, at least, 11 and 10 mm, respectively (the thicknesses of Crania 4 and 5 cannot be taken directly with accuracy and will be obtained in future tomographic studies). The Cranium 8 parietal boss is thicker than in Neandertals and European Middle Pleistocene fossils (Arsuaga *et al.*, 1989, 1991). The thickness at asterion of the parietal bone (taken on the suture) ranges in the SH juvenile sample from 7.5–10 mm ($n=6$), and from 8–12 mm for the adult specimens ($n=6$). The adult range falls between the Neandertal and the “*Sinanthropus*” ranges and is comparable with other European Middle Pleistocene values (Arsuaga *et al.*, 1991). Nevertheless, at the angular torus the thickness of SH Cranium 4 is remarkable, 17 mm, a figure at the upper end of the “*Sinanthropus*” range and above any other European fossil. The thickness at bregma in the SH juvenile sample ranges from 6.6–8 mm ($n=3$), and in the adult sample from 5.7–11 mm ($n=5$, Cranium 4 not included). Interestingly, in the SH sample the thickness at parietal boss (13 mm) and bregma (11 mm) are very remarkable in Cranium 8, yet it lacks an angular torus.

Discussion and conclusion

The Sima de los Huesos cranial diagnosis includes a number of features with different phylogenetic significance. Given that these remains are geographically European and chronologically Middle Pleistocene, we will concentrate on their evolutionary relationships with Neandertals and other European Middle Pleistocene fossils.

There is a great difference in cranial capacity between the only two adult specimens where it can be measured (1390 cc *vs.* 1125 cc). These brain sizes are close to the upper and lower ends of the Middle Pleistocene range for Europe and Africa. The largest braincase, Cranium 4, has a very broad calvaria and cranial base by Neandertal standards, but is comparable with Petralona.

Maximum cranial breadth is located low in the skull, at the supramastoid crests. Above them, cranial wall sides are slightly convergent upwards or vertical (parallel) in rear view. This character state is intermediate between the low pentagonal shape (primitive condition) and the round contour that Neandertals exhibit or the high pentagonal shape displayed by modern humans.

The occipital torus is centrally developed and horizontal, but not bilaterally projecting and depressed in the middle as in Neandertals. Above the torus there is a suprainiac area of irregular surface, which is convex, flat or only very slightly depressed (but less than in Swanscombe). This occipital pattern could be viewed as derived from a high triangular torus (with the apex pointing away from the nuchal plane) as in Vértesszöllös, and foreshadows the Neandertal morphology. Inion is located on the linear tubercle, a non-modern feature also found in Neandertals. In the Atapuerca SH sample the attachment of superior oblique muscle is bordered medially by a generally raised Waldeyer's crest. There is variation inside the Sima de los Huesos hypodigm in occipital sagittal angulation, but Cranium 4 occipital angles, although higher than in Petralona, fall below the Neandertal range.

In side view the Sima de los Huesos braincases are not elongated as in Neandertals and lack their typical lambdoidal flattening and occipital bun. In the adult Crania 1, 4 and 5, as well as in the probably late adolescent Occipital IV, the most projecting point of the isolated occipital bone (i.e., the terminus of Howells' lambda-opisthion subtense) lies on the occipital torus, just above inion. This is the primitive character state, also found in Bilzingsleben, Petralona, Vértesszöllös and in Asian and African counterparts. On the other hand, in Neandertals and modern humans the most projecting point lies on the occipital squama, above the suprainiac fossa, and far from inion. Swanscombe is transitional between the Sima de los Huesos and Neandertal occipital morphologies. A strong convexity of the occipital squama (a bun) is also found in modern humans, including some European early Upper Palaeolithic fossils (some of them even show occipital bunning e.g. Mladeč 1), but in Skhül 5 the most projecting point of the occipital bone lies on the superior nuchal crest. Thus, Neandertals and modern humans share a derived condition, that can be regarded as an apomorphy or as a homoplasy (if gene exchange is not considered). This condition cannot be inherited from the last common ancestor of both Neandertals and modern humans, because the European Middle Pleistocene ancestors of Neandertals show the primitive condition as well as some early modern humans. In consequence, we believe that it is a homoplasy.

The foramen magnum in the Sima de los Huesos sample does not exhibit the extremely elongated shape reported for some Neandertals by Rak *et al.* (1994).

The multivariate analysis of calvarial variables shows three well-defined craniophenetic groups: Asian *H. erectus/H. ergaster*, Neandertals (with Omo Kibish 2) and early Levantine and European modern humans. Atapuerca SH Crania 4 and 5, Petralona and Broken Hill lie between *H. erectus/H. ergaster* and Neandertals, as would do Steinheim if, as we suspect, the biauricular breadth had not been reduced posthumously. Another multivariate analysis, only with occipital variables, discriminate very well the *H. erectus/H. ergaster* from early modern humans, but the latter group and Neandertals partially overlap. Broken Hill, Eliye Springs, Petralona, Atapuerca SH Cranium 4 and Vértesszöllös are well separated from Neandertals and modern humans, but Atapuerca SH Cranium 5 and Occipital IV, Steinheim and Swanscombe lie among Neandertals.

In the Sima de los Huesos skulls there are more or less developed frontal and parietal keelings, as well as a true angular torus in Cranium 4. These are primitive traits absent in Neandertals.

The facial skeleton of Cranium 5 is extraordinarily large relative to the braincase (a primitive trait not found in Petralona), and with a facial prognathism more marked than in Neandertals. In these two features the last interglacial Saccopastore 1 is the closest Neandertal specimen to Sima de los Huesos Cranium 5.

In the Sima de los Huesos hypodigm, the supraorbital torus is always double arched (probably the primitive condition for *Homo*), instead of shelf-like as in Asian *H. erectus*. Although there are different degrees of continuity of the supraorbital torus through the glabellar region, the Sima de los Huesos morphology is reminiscent of Neandertals. As in Neandertals, nasion is not depressed in the SH sample.

Sima de los Huesos Cranium 5 shows many of the traits associated with Neandertal midfacial prognathism, such as broad and projecting nasal bones or an advanced position of subspinale and upper dentition in front of the bi-zygomaxillare chord (Figure 5), but the infraorbital plate (*sensu* Rak, 1986) is neither convex nor flat. Instead, it is concave in horizontal contour, and its lower margin (the zygomaticoalveolar crest) is gently curved, and not straight as in Neandertals. So, the typical Neandertal facial pattern is not fully developed in Cranium 5, although this specimen's morphology is clearly transitional. There is a marked depression in AT-404 maxilla, indicating variability in mid-facial topography in the Sima de los Huesos sample.

Cranium 5 exhibits a very wide nasal aperture (in absolute and relative terms). Broad noses are common in Neandertals but also in ER 3733 and Bodo (probably the broadest one in the fossil record). The Sima de los Huesos subnasal morphology clearly deviates from the sharp lower rim of the nasal margin seen in Neandertals, showing a more primitive condition.

The temporal bone traits of phylogenetic interest of the SH sample can be separated into three groups (Martínez & Arsuaga, 1997): (1) there is only one Neandertal derived trait: inclined anterior wall of the glenoid fossa; (2) a derived trait shared by Neandertals and modern humans: high temporal squama; (3) plesiomorphies for *Homo*: developed postglenoid process, low frequency of contribution of the sphenoid bone to the medial wall of the glenoid fossa, tympanic plate coronally orientated, presence of styloid process, absence of anterior mastoid tubercle, mastoid processes well developed and projecting in the adults, low juxtamastoid eminence, less projected than the mastoid process, and digastric groove not closed anteriorly.

In sum, together with a number of primitive features not found in Neandertals, the Sima de los Huesos crania show incipient Neandertal traits in the occipital bone, a generally plesiomorphous temporal bone with only one Neandertal derived trait, and a more developed Neandertal morphology in the supraorbital torus and facial skeleton. So, our conclusion is that the Sima de los Huesos population is evolutionarily related to Neandertals as a sister group.

It is clear for all scholars that the late European Middle Pleistocene fossils (as Ehringsdorf, Biache-Saint-Vaast or La Chaise-Suard) are very close to the Upper Pleistocene Neandertals. But Vandermeersch (1985) included older European Middle Pleistocene fossils as Arago, Petralona, Steinheim or Swanscombe in the Neandertal clade and Vértesszöllös at its base, so that, in their view, only the Bilzingsleben fragments and the Mauer mandible would not show Neandertal characteristics. More important, according to Vandermeersch (1985), no African or Asian Middle Pleistocene fossils can be considered as directly linked to Neandertals. Bräuer's (1984) "Afro-European *sapiens*-hypothesis" regards all the European Middle Pleistocene fossils as one line, characterized by a considerable variability, which led to the Neandertals of the last glaciation, whereas the African Middle Pleistocene contemporaries evolved into modern humans. To Hublin (1988a, b), all the European Middle Pleistocene

fossils are related to Neandertals, except Mauer, Vértesszöllös and Bilzingsleben, considered *incertae sedis*, although, according to him, the absence of Neandertal apomorphies in very fragmentary specimens is not a criterion to exclude them from the Neandertal lineage. His conclusion is that the period between 500,000 and 400,000 B.P. could well be the beginning of Neandertal history (Hublin, 1996).

On several occasions, Stringer (1983, 1985) has stated that Mauer, Vértesszöllös, Bilzingsleben, Arago and Petralona, together with Broken Hill 1, Bodo and perhaps Dali, form the stem group for Neandertals and modern humans and could be classified as a distinct species (*Homo heidelbergensis*). After discussing several possible evolutionary models and taxonomic alternatives (Stringer, 1991), he finally concluded that the Neandertal lineage seems to have its roots deep in the Middle Pleistocene, and that the Sima de los Huesos evidence favours a scheme where all the European Middle Pleistocene fossils are Neandertal ancestors (Stringer, 1993). Nevertheless, he came back to the concept of *H. heidelbergensis* as a Middle Pleistocene common ancestor for Neandertals and modern humans in a more recent publication (Stringer & McKie, 1996), a notion shared with Tattersall (1996). Rightmire (1996) also links Bodo with Broken Hill, Elandsfontein, Ndutu, Mauer, Arago and Petralona in *H. heidelbergensis*, a species that would have originated in Africa or Western Eurasia and that could be ancestral to modern humans and Neandertals or to both and late Middle Pleistocene archaic Asians as Yunxian, Dali and Jinniushan.

We have previously stated that all the European Middle Pleistocene fossils are, without exceptions, ancestors (only) of the Late Pleistocene Neandertals (Arsuaga *et al.*, 1993, 1996*a,b*; Carbonell *et al.*, 1995). Although our own cladistic analysis (Arsuaga *et al.*, 1995) points to an exclusive Neandertals/modern humans common ancestor, we believe that it is not represented in the currently available European Middle Pleistocene record because that ancestor should be more primitive (and, thus, older). So, we agree with the concept of *H. heidelbergensis* as a stem species, but not with the content (nor with the name, see below).

Anyway, as the debate on the existence of a Middle Pleistocene Afro-European (and maybe also Asian) stem species (or “Neandertal deep roots” *vs.* “Neandertal short roots” controversy) cannot be considered over, in the following lines we will review the European and African Middle Pleistocene evidence.

The facial morphology is very important for this argument, because Petralona, Arago, Bodo and Broken Hill have been grouped in *H. heidelbergensis* based on their phenetic facial similarities. Lumley & Spitory (1982) observed that the faces of *Homo erectus*, the “Anteneandertals” and the Neandertals were smooth, with low or gentle relief (with the unexplained exception of Steinheim). Thus, these fossils would share a plesiomorphy.

In our opinion, a flat face, with not much nasal projection, and absence of a well-defined canine fossa, is the primitive condition for *Homo* (*H. habilis*, *H. rudolfensis*, *H. ergaster*). In this condition, the infraorbital plates are coronal and vertical or anterior–inferior sloping.

But in our view, the morphotype of the last common ancestor of Neandertals and modern humans includes a “generalized” midface, a face with more nasal projection, a flexed maxilla (in transverse cross section), a canine fossa (or in other words, a down and backwards sloping infraorbital plane), and a curved zygomaticoalveolar crest, with a high root. Of course, a “generalized” or more sculptured face (with high relief) is more likely to be found in smaller, more delicate faces (i.e., especially in juveniles or females), than in large, massive faces, with attenuated relief.

In the European lineage there was a marked increase in nasal projection, together with maxillary pneumatization. The resultant face shows a maxilla oriented midway between

coronally and sagittally (in Neandertals), and a straight zygomaticoalveolar crest. Although the ideal “generalized” face has not been found in a European Middle Pleistocene fossil, transitional examples between this and fully Neandertal morphologies can be found in Steinheim and AT-404, and less distinctly in Atapuerca SH Cranium 5. On the contrary, Arago 21 exhibits a Neandertal face, with midfacial projection, an extended maxilla and a Neandertal-like nasal lower rim. Although mid-facial projection is less marked in Petralona (metrically it is at the limit of the Neandertal range of variation), the morphology of the face is reminiscent of Neandertals. In fact, it resembles (metrically and morphologically) that of Saccopastore 2, a scaled-down version of the Petralona face, according to [Stringer & Gamble \(1993\)](#). A recent re-analysis of ESR dating of Petralona, suggesting an age of 150–250 ka ([Grün, 1996](#)), does not favour the placement of this fossil in the stem group for Neandertals and modern humans.

A “generalized” midface can be found in early and present-day modern humans, as well as in a number of Middle Pleistocene African specimens as Jebel Irhoud 1, Laetoli H 18 or Florisbad (recently dated with an experimental method around 260 ka: [Grün et al., 1996](#)). Bodo does not show the “generalized” model, but the extensive pneumatization of this face obscures the facial relief, as happens in Arago 21, Petralona or the Neandertals. What differentiates Bodo from them is the absence of midfacial prognathism. Broken Hill 1 is midway between the Neandertal and the “generalized” midface. It could be an example of gene exchange between the European and African lineages, as the “multiregional model” predicts (see for instance [Wolpoff & Caspari, 1996](#)), or it could represent the limit of the African range of variation, just as Petralona is at the limit of the European range. In the absence of other “European” traits in the Broken Hill 1 skull, we prefer the latter explanation. On the other hand, the more fragmentary Broken Hill 2 exhibits the “generalized” condition and resembles Laetoli H 18. These specimens could have a different chronology, however. The very fragmentary Nduvu face has also been described as having an infraorbital concavity ([Bräuer, 1991](#)).

Anyway, when comparing fossil faces such as Atapuerca SH Cranium 5, Arago 21, Petralona or Broken Hill 1 with Neandertals, focusing on incipient traits or vague resemblances, it should be made clear that craniophenetically (in the multivariate analysis) none of them cluster with Neandertals.

Some components of the “generalized” face have been recognized in the record of Asian *H. erectus* ([Pope, 1992](#)), but it is not clear if the complete pattern was present. This morphology is more clear in Dali. In this case it could represent a pattern already present in *H. erectus s.s.*, or it could point to a Middle Pleistocene migration from Africa.

As mentioned before, a morphocline has been proposed with the Vérteszöllös–Sima de los Huesos–Swanscombe–Neandertal occipital bone morphologies. Steinheim and Reilingen could be more or less close to Swanscombe in this character state polarity. More problematic are the Bilzingsleben remains. The new discoveries provide a more complete picture of the braincase of one individual ([Mania et al., 1995](#)), that has been reconstructed following OH 9. The occipital bone is angulated and without any sign of Neandertal features, but the supraorbital torus, although very thick and projecting, is continuous at the glabella as in Neandertals, and the trigone is unlike OH 9 or Asian *H. erectus* ([Arsuaga et al., 1991](#)). The remains are too fragmentary anyway as to be positioned in any evolutionary tree.

The phylogenetic analysis of the facial and occipital traits can be supplemented with the analysis of the temporal bone features (a more extensive description and discussion of the temporal bone evolutionary morphology can be found in [Martínez & Arsuaga, 1997](#)). The

pictures of the Bilzingsleben right temporal bone in Mania *et al.* (1995) show an inclined anterior wall of the glenoid fossa, a derived trait also found in Neandertals and Steinheim, Petralona, Castel di Guido (Mallegni & Radmilli, 1988), Reilingen and all the cases in the Sima de los Huesos sample. La Chaise Suard, Biache-Saint-Vaast and Ehringsdorf H exhibit, besides this trait, an occipitomastoid region derived as in Neandertals (i.e., reduced mastoid processes and anteriorly obliterated digastric grooves). In the evolution of the Neandertal lineage in Europe there are three different stages in the changes of the temporal bone (Martínez, 1995; Martínez & Arsuaga, 1997). The oldest is a generally primitive condition with an inclined anterior wall of the glenoid fossa. In late Middle Pleistocene fossils and early Upper Pleistocene fossils (i.e., Saccopastore and Krapina) the occipitomastoid region typical of Neandertals can be found. Finally, "classic" Upper Pleistocene Neandertals also display a true anterior mastoid tubercle.

The still only preliminary reported Ceprano braincase (Ascenzi *et al.*, 1996) could be older than Mauer and has been described as primitive in a number of features (e.g., supraorbital torus and occiput). This fossil, together with the sample of Gran Dolina in Sierra de Atapuerca (Carbonell *et al.*, 1995), can help to establish the origin and antiquity of the Neandertal clade.

Neandertals evolved in Europe during the Middle Pleistocene in conditions of geographic and genetic isolation (allopatry), whereas modern humans evolved outside of Europe. In allopatric speciation (the most common speciation type) a new species arises from a peripherally isolated population, as did the European Middle Pleistocene humans. Thus, Neandertals and modern humans represent separate evolutionary lineages and there is enough morphological divergence between them to name Neandertals as a different species (*Homo neanderthalensis*), even if Neandertals and modern humans could have potentially interbred and therefore was a limited gene exchange.

According to Eldredge & Cracraft (1980) when one species is ancestral to another, the plesiomorphous species is diagnosable only in terms of the absence of apomorphies, or in a more positive fashion, the unique retention of plesiomorphies. In other words, the ancestral species would exhibit a unique combination of plesiomorphies and apomorphies, without any autapomorphy. When the plesiomorphous species is only known from an earlier period of time than that of the apomorphous species, then the two species could be samples from a single reproductive continuum, and thus the same evolutionary species, but Eldredge & Cracraft (1980) recognize that methodologically there is no way to establish the existence of the continuum. To these authors, splitting of a portion of the ancestral species is the only real mode of speciation, implying disruption of the within-species reproductive cohesion.

Nevertheless, we believe that there is a way to establish if two samples represent an example of continuous change within a lineage (phyletic evolution) by the mechanisms of natural selection and genetic drift. If this were the case it should be expected that evolutionary novelties (apomorphies) that are fixed (present in all members of the species) in a time period, will be inconstant (not always present) in a sample from an earlier period of the same. If the characters are more or less independent of each other, different combinations of primitive and derived traits should be expected for the fossils of the earlier sample.

This is exactly what we found in the European fossil record. While Upper Pleistocene Neandertals exhibit a suite of derived traits, the European Middle Pleistocene fossils show different combinations of primitive and derived features (e.g., Petralona shows a Neandertal face and a primitive occipital bone, whereas Steinheim shows derived features in the occiput and a primitive face). Diversity in such combinations is found also inside the Sima de los Huesos sample.

Middle Pleistocene Europeans and Neandertals represent the same “evolutionary” species, an ancestral-descendant sequence of populations without rupture of the reproductive continuity (Eldredge & Cracraft, 1980). Nevertheless, European Middle Pleistocene fossils and Neandertals (including the very derived late Middle Pleistocene fossils), are morphologically distinct enough as to name them differently, but only for practical reasons, because the two chrono-species are samples from a single reproductive continuum. In other words, the European human Middle Pleistocene chrono-species would be equivalent to other mammal chrono-species such as the bear *Ursus deningeri* (the proposed Lower and Middle Pleistocene ancestor of the late Middle and Upper Pleistocene species *Ursus spelaeus*). Many other lineages are known in the European Pleistocene such as the rhinoceroses *Stephanorhinus etruscus*–*Stephanorhinus hundsheimensis*, the proboscidean lineage *Mammuthus meridionalis*–*Mammuthus trogontherii*–*Mammuthus primigenius*, or the rodentian lineages *Mimomys savini*–*Arvicola cantiana*–*Arvicola terrestris*, and *Alophaiomys*–*Microtus* (Kolfschoten, 1996). Certainly, other examples could be given of anagenetic evolutions, and in all cases there are problems with the chronological and morphological limits and the taxonomic status (genus, species, subspecies) of the different segments of these evolutionary continua.

Only terminal species or species without any descendants (such as Neandertals in our opinion) are diagnosable in terms of uniquely derived traits. But in the European Middle Pleistocene sample each single fossil (even within the Sima de los Huesos sample) exhibits a unique combination of plesiomorphies and Neandertal apomorphies, because these traits were polymorphic and more or less independent in the Middle Pleistocene. The fossils included in the European Middle Pleistocene species could show any combination of some derived traits shared with Neandertals, together with many primitive traits not present in Neandertals. Incipient Neandertal-like traits (i.e., not the plesiomorphy nor the apomorphy, but intermediate character states that may be called “mesiomorphies”), could also be used.

One possible name for this exclusively European Middle Pleistocene species is *H. heidelbergensis* Schoetensack, 1908, but the problem is that it is difficult to say if the Mauer mandible (the holotype) belongs to a human population that shared derived features with Neandertals. We consider this possibility very likely, because Mauer is closer to other European Middle Pleistocene fossils, as the Sima de los Huesos sample, than to the Lower Pleistocene fossils from the Gran Dolina site, also in the Sierra de Atapuerca (Carbonell *et al.*, 1995). So, the redefined *H. heidelbergensis* species would include all the known European Middle Pleistocene fossils (including the Sima de los Huesos sample), with the exception (provisional) of Ceprano and that of the very Neandertal-like fossils of the end of this period, as Biache-Saint-Vaast or La Chaise Suard.

Acknowledgements

We are indebted to many persons that gave us access to the fossils under their care and provided their kindly help: C. B. Stringer and R. Kruszynski (Natural History Museum, London), B. Vandermeersch (Université de Bordeaux), J.-L. Heim (Musée de l’Homme, Paris), Ato Jara Haile Mariam (National Museum of Ethiopia, Addis Ababa), J. F. Thackeray (Transvaal Museum, Pretoria), G. Manzi and P. Passarelli (Università di Roma), L. Bondioli (Museo “L. Pigorini”, Rome), H. Seidler (Universität Wien), G. D. Koufos (Aristotle University of Thessaloniki) and J. Radović (Croatian National History Museum, Zagreb). Access to the modern skeletal collection of Instituto de Antropologia of the Universidade de Coimbra and facilities for the study were provided by M. Laranjeira and E. Cunha. Special

thanks are given to T. White (University of California, Berkeley) and B. Asfaw for their invaluable help in Ethiopia. We also thank Leslie Aiello and the three anonymous reviewers, who made very helpful suggestions for the improvement of the paper. Field work in the Atapuerca sites is supported by Consejería de Cultura y Turismo de Junta de Castilla y León and this research was funded by Dirección General de Investigación Científica y Técnica of Spain, Projects PB86-0615-C03-02, PB90-0126-C03-02 and PB93-0066-C03-01.

References

- Aguirre, E., Basabe, J. M. & Torres, T. (1976). Los fósiles humanos de Atapuerca. *Zephyrus* **26-27**, 489-511.
- Aguirre, E. & Lumley, M. A. (1977). Fossil Men from Atapuerca, Spain: their bearing on human evolution in the Middle Pleistocene. *J. hum. Evol.* **6**, 681-688.
- Aguirre, E., Arsuaga, J. L., Bermúdez de Castro, J. M., Martínez, I. & Rosas, A. (1986). Los fósiles humanos de Ibeas (Sierra de Atapuerca, Burgos). Inventario y determinación del número mínimo de individuos. *Estudios geol.* **42**, 511-519.
- Aguirre, E., Arsuaga, J. L., Bermúdez de Castro, J. M., Gracia, A., Martínez, I. & Rosas, A. (1989). Human remains from Atapuerca-Ibeas (Burgos, Spain). In (G. Giacobini, Ed.) *Hominidae. Proceedings of the 2nd International Congress of Human Palaeontology*, pp. 251-255. Milano: Jaca Book.
- Aguirre, E., Arsuaga, J. L., Bermúdez de Castro, J. M., Carretero, J. M., Gracia, A., Martínez, I., Pérez, P. J. & Rosas, A. (1991). Les hominidés fossiles d'Ibeas, mise à jour de l'inventaire. *L'Anthropologie (Paris)* **95**, 473-500.
- Aguirre, E. & Bermúdez de Castro, J. M. (1991). Ibeas (Atapuerca). In (R. Orban, Ed.) *Hominid Remains. An Up-Date. Spain*, pp. 42-51. Bruxelles: Department of Anthropology and Human Genetics, Université Libre de Bruxelles.
- Akazawa, T., Muhesen, S., Dodo, Y., Kondo, O. & Mizoguchi, Y. (1995). Neanderthal infant burial. *Nature* **377**, 585-586.
- Andrews, P. (1984). An alternative interpretation of the characters used to define *Homo erectus*. *Cour. Forsch. Inst. Senckenberg* **69**, 167-171.
- Arsuaga, J. L. (1993). Les Hommes fossiles de la Sierra de Atapuerca. *La Recherche* **24**, 1399-1400.
- Arsuaga, J. L., Gracia, A., Martínez, I., Bermúdez de Castro, J. M., Rosas, A., Villaverde, V. & Fumanal, M. P. (1989). The human remains from Cova Negra (Valencia, Spain) and their place in European Pleistocene human evolution. *J. hum. Evol.* **18**, 55-92.
- Arsuaga, J. L., Carretero, J. M., Martínez, I. & Gracia, A. (1991). Cranial remains and long bones from Atapuerca/Ibeas (Spain). *J. hum. Evol.* **20**, 191-230.
- Arsuaga, J. L., Martínez, I., Gracia, A., Carretero, J. M. & Carbonell, E. (1993). Three new human skulls from the Sima de los Huesos site in Sierra de Atapuerca, Spain. *Nature* **362**, 534-537.
- Arsuaga, J. L., Martínez, I., Gracia, A. & Carretero, J. M. (1995). Cranial and postcranial remains at the Sima de los Huesos (Sierra de Atapuerca) and human evolution during the Middle Pleistocene. In (J. M. Bermúdez, J. L. Arsuaga & E. Carbonell, Eds) *Human Evolution in Europe and the Atapuerca Evidence I*, pp. 283-303. Valladolid: Junta de Castilla y León.
- Arsuaga, J. L., Martínez, I., Carretero, J. M., Gracia, A., Lorenzo, C. & Bermúdez de Castro, J. M. (1996a). Evolución humana en Europa: Registro y debates. *Rev. Esp. Paleontol.* **nº Extraord.** 269-277.
- Arsuaga, J. L., Gracia, A., Martínez, I. & Lorenzo, C. (1996b). The Sima de los Huesos (Sierra de Atapuerca, Spain) cranial evidence and the origin of Neanderthals. In (E. Carbonell & M. Vaquero, Eds) *The Last Neanderthals, the First Anatomically Modern Humans: A Tale About the Human Diversity*, pp. 39-49. Barcelona: Universitat Rovira i Virgili. (In press.)
- Ascenzi, A., Segre, A. G., Biddittu, I., Cassoli, P. F. & Segre, E. (1996). Human calvaria of the middle Pleistocene of Campo Grande di Ceprano (Ceprano, Frosinone). *XIII International Congress of Prehistoric and Protohistoric Sciences. Forlì (Italia) 8-14 September 1996. Abstracts 2*, pp. 193-194.
- Bermúdez de Castro, J. M. (1995). The hominids from the Sima de los Huesos of the Sierra de Atapuerca karst: Minimum number of individuals, age at death and sex. In (J. M. Bermúdez, J. L. Arsuaga & E. Carbonell, Eds) *Human Evolution in Europe and the Atapuerca Evidence I*, pp. 263-281. Valladolid: Junta de Castilla y León.
- Bermúdez de Castro, J. M. & Nicolás, E. (1997). Palaeodemography of the Atapuerca-SH hominid Middle Pleistocene sample. *J. hum. Evol.* **33**, 333-355.
- Bischoff, J. L., Fitzpatrick, J. A., León, L., Arsuaga, J. L., Falgueres, C., Bahain, J. J. & Bullen, T. (1997). Geology and preliminary dating of the hominid-bearing sedimentary fill of the Sima de los Huesos, Sierra de Atapuerca, Burgos, Spain. *J. hum. Evol.* **33**, 129-154.
- Blackwell, B. & Schwartz, H. P. (1986). U-series analysis of the lower travertine at Ehringsdorf, DDR. *Quat. Res.* **25**, 215-222.
- Bocquet-Appel, J. P. & Masset, C. (1995). L'âge au décès dans les populations inhumées: comparaison de méthodes et de résultats. *Antrop. Port.* **13**, 39-48.

- Boule, M. (1911–1913). L'Homme fossile de la La Chapelle-aux-Saints. *Ann. de Paléontol.* **6**, 111–172; **7**, 21–56, 85–192; **8**, 1–70.
- Bouzat, J. L. (1982). Le malaire de l'Homme de Tautavel. *1er Congrès International de Paléontologie Humaine (Nice, 1982). Prétirage*, pp. 137–153.
- Bräuer, G. (1984). The “Afro-European sapiens”, and hominid evolution in East Asia during the late Middle and Upper Pleistocene. *Cour. Forsch. Inst. Senckenberg* **69**, 145–165.
- Bräuer, G. (1988). Osteometrie. In (R. Knussmann, Ed.) *Anthropologie* (4th edition of Martin's textbook), vol. 1, part 1, pp. 160–232. Stuttgart: G. Fischer.
- Bräuer, G. (1991). L'hypothèse africaine de l'origine des hommes modernes. In (J. J. Hublin & A. M. Tillier, Eds) *Aux Origines d'Homo sapiens*, pp. 181–215. Paris: Puf.
- Bräuer, G. & Leakey, R. E. (1986). The ES-11693 Cranium from Eliye Springs, West Turkana, Kenya. *J. hum. Evol.* **15**, 289–312.
- Bräuer, G. & Mbua, E. (1992). *Homo erectus* features used in cladistics and their variability in Asian and African hominids. *J. hum. Evol.* **22**, 79–108.
- Brown, W. A., Mollison, T. I. & Chinn, S. (1984). Enlargement of the frontal sinus. *Ann. Hum. Biol.* **11**, 221–226.
- Brown, P. (1989). Coobool Creek. *Terra Australis* **13**, 1–205.
- Carbonell, E., Bermúdez de Castro, J. M., Arsuaga, J. L., Díez, J. C., Cuenca-Bescós, G., Sala, R., Mosquera, M. & Rodríguez, X. P. (1995). Lower Pleistocene hominids and artifacts from Atapuerca-TD6 (Spain). *Science* **269**, 826–830.
- Condemni, S. (1992). *Les Hommes Fossiles de Saccopastore et leurs Relations Phylogénétiques*. Cahiers de Paléoanthropologie. Paris: CNRS.
- Creed-Miles, M., Rosas, A. & Kruszynski, R. (1996). Issues in the identification of Neandertal derivative traits at early postnatal stages. *J. hum. Evol.* **30**, 147–153.
- Cuenca-Bescós, G., Laplana Conesa, C., Canudo, J. I. & Arsuaga, J. L. (1997). Small mammals from Sima de los Huesos (Sierra de Atapuerca, Spain). *J. hum. Evol.* **33**, 175–190.
- Day, M. H. (1986). *Guide to Fossil Man*. Eastbourne: Cassell.
- Eldredge, N. & Cracraft, J. (1980). *Phylogenetic patterns and Evolutionary process*. New York: Columbia University Press.
- Falk, D. (1986). Evolution of cranial blood drainage in hominids: enlarged occipital/marginal sinuses and emissary foramina. *Am. J. phys. Anthropol.* **70**, 311–324.
- Falk, D. & Conroy, G. (1983). The cranial venous sinus system in *Australopithecus afarensis*. *Nature* **306**, 779–781.
- Falk, D., Gage, T. B., Dudek, B. & Olson, T. R. (1995). Did more than one species of hominid coexist before 3 Ma?: Evidence from blood and teeth. *J. hum. Evol.* **29**, 591–600.
- Franciscus, R. G. & Trinkaus, E. (1995). Determinants of retromolar space presence in Pleistocene *Homo* mandibles. *J. hum. Evol.* **28**, 577–595.
- Frayser, D. W. (1980). Sexual dimorphism and cultural evolution in the late Pleistocene and Holocene of Europe. *J. hum. Evol.* **9**, 399–415.
- Frayser, D. W. (1992). Evolution at the European edge: Neanderthal and Upper Paleolithic relationships. *Préhist. Européenne* **2**, 9–69.
- García, N., Arsuaga, J. L. & Torres, T. (1997). The carnivore remains from the Sima de los Huesos Middle Pleistocene site (Sierra de Atapuerca, Spain). *J. hum. Evol.* **33**, 155–174.
- Gower, C. D. (1923). A contribution to the morphology of the apertura piriformis. *Am. J. phys. Anthropol.* **6**, 26–36.
- Gracia, A. (1991). Impresiones endocraneales del hombre de Ibeas. In (E. Rebató & R. Calderón, Eds). *VI Congreso de Antropología*, pp. 351–360. Bilbao: Universidad del País Vasco.
- Gracia, A., Arsuaga, J. L. & Martínez, I. (1992). Los restos humanos craneales de Cova Negra, Valencia. *Rev. Esp. Paleontol.* **Extra** 77–81.
- Grine, F. E., Demes, B., Jungers, W. L. & Cole, T. M. (1993). Taxonomic affinity of the early *Homo* cranium from Swartkrans, South Africa. *Am. J. phys. Anthropol.* **92**, 411–426.
- Grün, R. (1996). A re-analysis of electron spin resonance dating results associated with the Petralona hominid. *J. hum. Evol.* **30**, 227–241.
- Grün, R., Brink, J. S., Spooner, N. A., Taylor, L., Stringer, C. B., Franciscus, R. G. & Murray, A. S. (1996). Direct dating of Florisbad hominid. *Nature* **382**, 500–501.
- Hauser, G. & De Stefano, G. F. (1989). *Epigenetic Variants of the Human Skull*. Stuttgart: Schweizerbart.
- Heim, J. L. (1989). La nouvelle reconstitution du crâne néandertalien de La Chapelle-aux-Saints. Méthode et résultats. *Bull. et Mém. de la Soc. d'Anthrop. de Paris n.s.* **1**, 95–118.
- Howells, W. W. (1973). Cranial variation in man: a study by multivariate analysis of patterns of difference among recent human populations. *Peabody Mus. Pap. No. 67*.
- Howells, W. W. (1975). Neanderthal Man: Facts and figures. In (R. H. Tuttle, Ed.) *Paleoanthropology: Morphology and Paleocology*, pp. 389–408. The Hague: Mouton.
- Hublin, J. J. (1978a). Anatomie du centre de l'écaillé de l'occipital. Le problème de l'inion. *Cahiers d'Anthropol. (Paris)* **2**, 65–83.
- Hublin, J. J. (1978b). Quelques caractères apomorphes du Crâne néandertalien et leur interprétation phylogénétique. *C.R. Acad. Sc. de Paris 287 (sér. D)* 923–926.

- Hublin, J. J. (1978*d*). Le Torus Occipital Transverse et les Structures Associées. Evolution dans le genre *Homo*. Ph.D. Dissertation, Université de Paris VI.
- Hublin, J. J. (1980*a*). La Chaise Suard, Engis 2 et La Quina H 18: développement de la morphologie occipitale externe chez l'enfant préneandertalien et néandertalien. *C.R. Acad. Sci. Paris* **291**, 669–672.
- Hublin, J. J. (1980*b*). A propos de restes inédites du gisement de La Quina (Charente): un trait méconnu des néandertaliens et des préneandertaliens. *L'Anthropologie (Paris)* **84**, 81–88.
- Hublin, J. J. (1982). Les anténéandertaliens: présapiens ou préneandertaliens. *Geobios. mémoire spécial* **6**, 345–357.
- Hublin, J. J. (1984). The fossil man from Salzgitter-Lebenstedt (FRG) and its place in human evolution during the Pleistocene in Europe. *Z. Morph. Anthropol.* **75**, 45–56.
- Hublin, J. J. (1988*a*). Caractères dérivés de la région occipito-mastoidienne chez les néandertaliens. In (E. Trinkaus, Ed.) *L'Homme de Néandertal, 3: L'Anatomie*, pp. 67–73. Liège: Eral.
- Hublin, J. J. (1988*b*). Les plus anciens représentants de la lignée préneandertalienne. In (E. Trinkaus, Ed.) *L'Homme de Néandertal, 3: L'Anatomie*, pp. 81–94. Liège: Eral.
- Hublin, J. J. (1996). The first Europeans. *Archaeology* **49**, 36–44.
- Kimbel, W. H. (1984). Variation in the pattern of cranial venous sinuses and hominid phylogeny. *Am. J. phys. Anthropol.* **63**, 243–263.
- Kimbel, W. H., Johanson, D. C. & Rak, Y. (1994). The first skull and other new discoveries of *Australopithecus afarensis* at Hadar, Ethiopia. *Nature* **368**, 449–451.
- Kolfschoten, T. van (1996). Mammalian remains in a Palaeolithic context. In (S. Milliken & C. Peretto, Eds) *Archaeology, Methodology and the Organisation of Research*, pp. 19–35. Forlì: ABACO.
- Lahr, M. M. (1994). The multiregional model of modern human origins: a reassessment of its morphological basis. *J. hum. Evol.* **26**, 23–56.
- Lieberman, D. E. (1995). Testing hypotheses about recent human evolution from skulls. *Curr. Anthropol.* **36**, 159–197.
- Lumley, M. A. de (1970). La pariétal humain anténéandertalien de Cova Negra (Jativa, Espagne). *C.R. Acad. Sci. Paris* **270**, 39–41.
- Lumley, M. A. de & Spitz, J. (1982). Le maxillaire de l'homme de Tautavel. *1er Congrès International de Paléontologie Humaine (Nice, 1982). Prétrirage* 154–177.
- Mallegni, F. & Radmilli, A. M. (1988). Human temporal bone from the Lower Palaeolithic site of Castel di Guido, near Rome, Italy. *Am. J. phys. Anthropol.* **76**, 176–182.
- Mania, D., Mania, U. & Vlček, E. (1995). Dernières découvertes de restes humaines dans le travertin du pléistocène moyen de Bilzingsleben. État actuel des recherches. *L'Anthropologie (Paris)* **99**, 42–54.
- Manzi, G. & Passarello, P. (1991). Il campione fossile del Lazio e l'evoluzione dell'uomo di Neandertal in Italia. *Anthropol. Contemporanea* **14**, 129–138.
- Martin, R. & Saller, K. (1957). *Lehrbuch der Anthropologie*, 3rd ed. Stuttgart: G. Fischer.
- Martínez, I. (1995). La Base del Cráneo el Hueso Temporal en la Evolucion de los Hominidos, con Especial Referencia a los Fosiles de Atapuerca (Burgos). Ph.D. Dissertation, Universidad Complutense de Madrid.
- Martínez, I. & Arsuaga, J. L. (1985). Restos humanos neurocraneales del yacimiento de Atapuerca. *Actas IV Congr. Esp. Antrop. Biol. (Barcelona, 1985)*, pp. 513–522.
- Martínez, I. & Arsuaga, J. L. (1987). Estudio antropológico de los fragmentos de parietal. In (E. Aguirre, E. Carbonell & J. M. Bermúdez de Castro, Eds) *El Hombre Fósil de Ibeas y el Pleistoceno de la Sierra de Atapuerca I*, pp. 369–376. Valladolid: Junta de Castilla y León, Consejería de Cultura y Bienestar Social.
- Martínez, I. & Arsuaga, J. L. (1997). The temporal bones from Sima de los Huesos site (1984–1994). *J. hum. Evol.* **33**, 283–318.
- Maureille, B. (1994). La face chez *Homo erectus* et *Homo sapiens*: recherche sur la variabilité morphologique et métrique. Ph.D. Dissertation, Université de Bordeaux I.
- McCollom, M. A., Grine, F. E., Ward, S. C. & Kimbel, W. H. (1993). Subnasal morphological variation in extant hominoids and fossil hominids. *J. hum. Evol.* **24**, 87–111.
- McCown, T. D. & Keith, A. (1939). *The Stone Age of Mt. Carmel II. The fossil human remains from the Levallois-Mousterian*. Oxford: Clarendon Press.
- Norusis, M. J. (1990). *SPSS Base System User's Guide*. Chicago: SPSS Inc.
- Oyen, O. J., Rice, R. W. & Cannon, M. S. (1979). Browridge structure and function in extant primates and Neanderthals. *Am. J. phys. Anthropol.* **51**, 83–96.
- Oyen, O. J., Rice, R. W. & Enlow, D. H. (1981). Cortical surface patterns in human and non human primates. *Am. J. phys. Anthropol.* **54**, 415–419.
- Pérez, P. J., Gracia, A., Martínez, I. & Arsuaga, J. L. (1997). Paleopathological evidences of the cranial remains from the Sima de los Huesos Middle Pleistocene site (Sierra de Atapuerca, Spain). *J. hum. Evol.* **33**, 409–421.
- Pesce Delfino, V. & Vacca, E. (1993). An archaic human skeleton discovered in Altamura (Bari, Italy). *Riv. Antropol.* **71**, 249–257.
- Pope, G. G. (1992). Craniofacial evidence for the origin of modern humans in China. *Yearb. Phys. Anthropol.* **35**, 243–298.
- Rak, Y. (1986). The Neanderthal: A new look at an old face. *J. hum. Evol.* **15**, 151–164.
- Rak, Y., Kimbel, W. H. & Hovers, E. (1994). A Neandertal infant from Amud Cave, Israel. *J. hum. Evol.* **26**, 313–324.

- Rak, Y., Kimbel, W. H. & Hovers, E. (1996). On Neandertal autapomorphies discernible in Neandertal infants: a response to Creed-Miles *et al.* *J. hum. Evol.* **30**, 155–158.
- Richards, G. D. & Plourde, A. M. (1995). Reconsideration of the 'Infant', Amud-7. *Am. J. phys. Anthropol.* **20** (Suppl.), 180–181.
- Rightmire, G. P. (1990). *The Evolution of Homo Erectus. Comparative anatomical studies of an extinct human species*. Cambridge: University Press.
- Rightmire, G. P. (1993). Variation among early *Homo* crania from Olduvai Gorge and the Koobi Fora region. *Am. J. phys. Anthropol.* **90**, 1–33.
- Rightmire, G. P. (1995). Geography, time and speciation in Pleistocene *Homo*. *S. Afr. J. Sci.* **91**, 450–454.
- Rightmire, G. P. (1996). The human cranium from Bodo, Ethiopia: evidence for speciation in the Middle Pleistocene? *J. hum. Evol.* **31**, 21–39.
- Rosas, A. (1995). Seventeen new mandibular specimens from the Atapuerca/Ibeas Middle Pleistocene hominids sample (1985–1992). *J. hum. Evol.* **28**, 533–559.
- Rosas, A. (1997). A gradient of somatic maturation for the Atapuerca sample and Middle Pleistocene hominid variability. *J. hum. Evol.* **33**, 319–331.
- Santa Luca, A. P. (1978). A re-examination of presumed Neandertal-like fossils. *J. hum. Evol.* **7**, 619–636.
- Santa Luca, A. P. (1980). *The Ngandong Fossil Hominids. A comparative study of a Far Eastern Homo erectus group*. New Haven: Yale University Publications in Anthropology 78.
- Schwartz, J. H. & Tattersall, I. (1996). Significance of some previously unrecognized apomorphies in the nasal region of *Homo neanderthalensis*. *Proc. Natl. Acad. Sci. USA* **93**, 10,852–10,854.
- Sergi, S. (1944). Craniometria e craniografia del primo paleantropo di Saccopastore. *Ricerche di Morphologia* **20–21**, 733–791.
- Smith, B. H. (1993). The physiological age of KNM-WT 15000. In (A. Walker & R. Leakey, Eds) *The Nariokotome Homo erectus skeleton*, pp. 195–220. Cambridge: Harvard.
- Smith, F. H. & Ranyard, G. C. (1980). Evolution of the supraorbital region in Upper Pleistocene hominids from South-Central Europe. *Am. J. phys. Anthropol.* **53**, 589–610.
- Spitery, J. (1980). Etude comparée de l'os frontal chez *Homo erectus*. D.E.A. Museum National d'Histoire Naturelle.
- Spitery, J. (1982). La face de L'Homme de Tautavel. *1er Congrès International de Paléontologie Humaine (Nice, 1982). Prétirage*, 110–136.
- Stringer, C. B. (1983). Some further notes on the morphology and dating of the Petralona hominid. *J. hum. Evol.* **12**, 731–742.
- Stringer, C. B. (1984). The definition of *Homo erectus* and the existence of the species in Africa and Europe. *Cour. Forsch. Inst. Senckenberg* **69**, 131–143.
- Stringer, C. B. (1985). Middle Pleistocene hominid variability and the origin of Late Pleistocene humans. In (E. Delson, Ed.) *Ancestors: The Hard Evidence*, pp. 289–295. New York: Alan R. Liss.
- Stringer, C. B. (1991). *Homo erectus* et "*Homo sapiens* archaïque". Peut-on définir *Homo erectus*? In (J. J. Hublin & A. M. Tillier, Eds) *Aux Origines des Homo sapiens*, pp. 49–74. Paris: Presses Universitaires de France.
- Stringer, C. B. (1993). Secrets of the Pit of the Bones. *Nature* **362**, 501–502.
- Stringer, C. B., Howell, F. C. & Melentis, J. K. (1979). The significance of the fossil hominid skull from Petralona, Greece. *J. Archeol. Sci.* **6**, 235–253.
- Stringer, C. B., Hublin, J. J., Vandermeersch, B. (1984). The origin of anatomically modern humans in Western Europe. In (F. H. Smith & Spencer, Eds) *The Origins of Modern Humans: A World Survey of the Fossil Evidence*, pp. 51–135. New York: Alan R. Liss.
- Stringer, C. B. & Gamble, C. (1993). *In Search of the Neanderthals*. London: Thames and Hudson.
- Stringer, C. B. & McKie, R. (1996). *African Exodus. The Origin of Modern Humanity*. London: Jonathan Cape.
- Tappen, N. C. (1973). Structure of bone in skulls of Neandertal fossils. *Am. J. phys. Anthropol.* **38**, 93–98.
- Tappen, N. C. (1980). The vermiculate surface pattern in brow ridges of australopithecines and other very ancient hominids. *Am. J. phys. Anthropol.* **52**, 515–528.
- Tappen, N. C. (1983). The development of the vermiculate pattern in the brow region of crania from Indian Knoll, Kentucky. *Am. J. phys. Anthropol.* **60**, 523–537.
- Tattersall, I. (1986). *The Last Neanderthal*. New York: Macmillan.
- Thoma, A. (1966). L'occipital de l'Homme mindélien de Vértesszöllös. *L'Anthropologie (Paris)* **70**, 495–534.
- Thorne, A. G. & Wolpoff, M. (1981). Regional continuity in Australasian Pleistocene hominid evolution. *J. hum. Evol.* **55**, 337–349.
- Tillier, A. M. (1977). La pneumatisation du massif cranio-facial chez les hommes actuels et fossiles. *Bull. et Mém. de la Soc. d'Anthrop. de Paris* **4**, 177–189, 287–316.
- Tillier, A. M. (1992). The origins of Modern Humans in Southwest Asia: Ontogenetic aspects. In (T. Akazawa, K. Aoki & T. Kimura, Eds) *The Evolution and Dispersal of Modern Humans in Asia*, pp. 16–28. Tokyo: Hokusen-sha.
- Trinkaus, E. (1983). *The Shanidar Neanderthals*. New York: Academic Press.
- Trinkaus, E. (1987). The Neandertal face: evolutionary and functional perspectives on a recent hominid face. *J. hum. Evol.* **16**, 429–443.

- Vandermeersch, B. (1985). The origin of Neandertals. In (E. Delson, Ed.) *Ancestors: The Hard Evidence*, pp. 306–309. New York: Alan R. Liss.
- Vlček, E. (1991). L'homme fossile en Europe central. *L'Anthropologie (Paris)* **95**, 409–472.
- Waldeyer, W. (1909). Der Processus retromastoideus. *Abhandlungen der Königlich-Preussischen Akademie der Wissenschaften, Phys. math. Klasse. Abh.* **1**, 1–32.
- Weidenreich, F. (1943). The skull of *Sinanthropus pekinensis*; a comparative study on a primitive hominid skull. *Paleontologia Sinica, Series D* **5**, 1–150.
- Weidenreich, F. (1951). Morphology of Solo Man. *Anthropol. Papers Am. Mus. Nat. Hist.* **43**, 205–290.
- Wolpoff, M. H. (1977). Some notes on the Vértesszöllös Occipital. *Am. J. phys. Anthropol.* **47**, 357–364.
- Wolpoff, M. H. (1980). Cranial remains of Middle Pleistocene European hominids. *J. hum. Evol.* **9**, 339–359.
- Wolpoff, M. H. & Caspari, R. (1996). Why aren't Neandertals humans? In (O. Bar-Yosef, L. Cavalli-Sforza, R. J. March & M. Piperno, Eds) *The Lower and Middle Palaeolithic*. The Colloquia of XIII International Congress of Prehistoric and Protohistoric Sciences 5, pp. 133–156. Forli: ABACO.
- Wood, B. (1984). The origin of *Homo erectus*. *Cour. Forsch. Inst. Senckenberg* **69**, 99–111.
- Wood, B. (1991). *Koobi Fora Research Project. Volume 4. Hominid Cranial Remains*. Oxford: Clarendon Press.
- Wu, X. & Bräuer, G. (1993). Morphological comparison of archaic *Homo sapiens* crania from China and Africa. *Z. Morph. Anthropol.* **79**, 241–259.